

INFRARED PHOTOMETRY OF ECLIPSING BINARY STARS

A THESIS SUBMITTED FOR

THE DEGREE OF DOCTOR OF PHILOSOPHY

by

R. AKINCI

Department of Astronomy

University of Leicester

1978

UMI Number: U435637

All rights reserved

INFORMATION TO ALL USERS

The quality of this reproduction is dependent upon the quality of the copy submitted.

In the unlikely event that the author did not send a complete manuscript and there are missing pages, these will be noted. Also, if material had to be removed, a note will indicate the deletion.



UMI U435637

Published by ProQuest LLC 2015. Copyright in the Dissertation held by the Author.  
Microform Edition © ProQuest LLC.

All rights reserved. This work is protected against  
unauthorized copying under Title 17, United States Code.



ProQuest LLC  
789 East Eisenhower Parkway  
P.O. Box 1346  
Ann Arbor, MI 48106-1346

THESIS  
556344  
8 8 78



x753005319

### Acknowledgements

I am very grateful to many people who generously gave me their assistance throughout this investigation. Firstly, I wish to thank Professor A.J. Meadows for accepting me into the department and Professor A. Kizilirmak for suggesting and arranging my study in England. Next I particularly wish to thank my supervisor Dr. R.F. Jameson for all his help, encouragement and invaluable guidance during the course of this study. I thank Dr. D.J. Adams, Dr. J. Hough, Dr. A.J. Longmore, J. Abolins, A. McCall and A.B. Giles for assistance with the observing in Tenerife. I must thank V. Brooksbank and D.P. Goodrich for their technical help in modifying the apparatus, mechanically and electronically respectively.

I would also like to thank Dr. A.R. King and Dr. D.J. Raine for useful discussions.

I am specially grateful to Mrs. N. Corby for her excellent typing of the manuscript. My thanks go to S. Hughes, P.A. Lawson and M.R. Sherrington for their kind help with my English.

I thank the Education Ministry of the Turkish Government for financial support.

Finally, I specially thank my wife Sevil for moral support, encouragement and also useful help with the observing.

## CONTENTS

	Page	
<b>CHAPTER 1</b>	<b>INTRODUCTION</b>	<b>1.1</b>
	Sources of Line Radiation, Sources of Band Spectra, Sources of Infrared Continuum Radiation	1.2
	Infrared Excesses in Stars	1.5
	Late-Type Stars	1.6
	Intermediate and Early-Type Stars	1.8
	Infrared Emission from Binary Stars	1.13
	Cataclysmic Variables, Eclipsing Binary Stars	1.16
<b>CHAPTER 2</b>	<b>INSTRUMENTATION</b>	<b>2.1</b>
	Infrared Detectors	2.1
	The Photometer	2.21
	The Cryostat	2.23
	Choppers	2.24
	Filters, Windows and Lenses	2.27
	Electronics	2.31
<b>CHAPTER 3</b>	<b>OBSERVING TECHNIQUES</b>	<b>3.1</b>
	Observing Program	3.1
	Selecting Standard Stars	3.2
	Observing, Data Reduction and Errors	3.3
	Atmospheric Corrections	3.5
<b>CHAPTER 4</b>	<b>OBSERVATIONS AND DISCUSSION OF W URSAE MAJORIS-TYPE STARS</b>	<b>4.1</b>
	AB Andromedae	4.1



## CHAPTER 1

## INTRODUCTION

Close binary stars, both semi-detached and contact, have gas streams and disk-like envelopes. Such gas flow will tend to show up in the infrared by virtue of its free-free radiation. The problem of asymmetry of the light curves of several eclipsing binaries has been examined on the assumption that gas streams are primarily responsible. However, a more interesting feature, such as an envelope surrounding one or both components with a gas flow as a supplying source could have explained the observed peculiarities in some systems. Recently, infrared photometry has become an important tool in studies of circumstellar material in close binary systems.

The aim of this thesis is to obtain infrared light curves of eclipsing binaries which are thought to have gas streaming in order to gain information about gas streams and other features.

Infrared astronomy has now been studied seriously for about fifteen years, and so much has been written that it is inappropriate to try to review the whole subject in this thesis. Probably the best review of infrared astronomy to be found is *Infrared The New Astronomy* by Allen (1975). Neugebauer et al. (1971) have published the review relating to photometric infrared astronomy. They divided the topics up into sections based on types of infrared object.

In this chapter the types of stars of interest to infrared astronomers will briefly be mentioned in similar sections, concentrating especially on binary stars; however, in order to understand the infrared radiative mechanism a brief discussion will initially be given on the sources of infrared radiation.

A. Sources of Line Radiation

Lines are formed by electron transitions between energy levels in a neutral or ionized atom. The radiation may be seen in absorption against a continuum background or in emission. In the emission spectra of stars some of the important atoms responsible for infrared line emission are HeI, HeII, CII, CIII and CIV. Atoms which appear in absorption include H, He, C, Na, Mg, Si, Fe and Sr.

B. Sources of Band Spectra

The broad and deep absorption bands of water vapour and carbon dioxide molecules exist throughout the infrared region. This absorption is due to the fact that the energy of stretching and bending vibrations of the molecular bands of H<sub>2</sub>O and CO<sub>2</sub>, and the quantum transitions coincide with the infrared photon energy range. Rotation-vibration bands always lie in the infrared. The more common bands include CO, CN, SiO, TiO and H<sub>2</sub>.

A list of important atoms and molecules responsible for infrared lines and bands respectively is given in the review by Spinrad and Wing (1969) on the infrared spectra of stars.

C. Sources of Infrared Continuum Radiation

(a) Blackbody Radiation

A blackbody absorbs all electromagnetic energy incident on it. Such a body must emit energy at exactly the same rate as it absorbs energy in order to be in perfect thermal equilibrium. A blackbody has been defined as one which emits the maximum possible amount of energy for all wavelengths at a characteristic temperature T. The most useful mathematical formulation of blackbody emission is the Planck function which relates the radiant energy flux,  $F_{\lambda}$ , to

the wavelength,  $\lambda$ , and the temperature, T. Max Planck derived theoretically the equation which describes the spectral energy distribution from a blackbody at temperature T K:

$$F_{\lambda} = \frac{c_1}{\lambda^5} \left[ \exp(c_2/\lambda T) - 1 \right]^{-1} \quad (1.1)$$

where  $c_1 = 2\pi hc^2$  and  $c_2 = hc/k$ ; h is Planck's constant, c is the velocity of light and k is Boltzmann's constant.  $F_{\lambda}$  is measured in Watts  $\text{cm}^{-2} \mu\text{m}^{-1}$ .

Planck's expression shows that the hotter the body, the greater the radiant energy emitted and the shorter the wavelength of peak emission. This latter property is best described by Wien's displacement law which can be expressed as

$$\lambda_{\text{max}} T = \text{constant} \quad (1.2)$$

( $\lambda$  in microns, T in K)

where  $\lambda_{\text{max}}$  is the wavelength of peak emission. Thus, the cooler the body the longer the wavelength of peak emission.

#### (b) Free-free Emission

Ionized and kinetically hot gases, known as plasmas, consist of neutral and ionized atoms, and the free electrons associated with the ionization. In such a plasma, Coulomb scattering of the electrons by the ions results in the acceleration of charged particles. This acceleration of charged particles is accompanied by a resultant emission of radiation known as free-free emission. Spectra due to free-free emission in such plasmas are flat with a high frequency cut-off, corresponding to the maximum kinetic energy of the electrons. When the plasma becomes optically thick there is also a long wavelength cut-off, and the spectrum slope then becomes that

of a blackbody.

For an optically thin plasma, the free-free emission unit solid angle, volume, and time at a given frequency is given by

$$j\nu = 5.443 \times 10^{-39} Z^2 g \exp[-c_2/\lambda T] T^{-\frac{1}{2}} N_e N_i$$

in erg cm<sup>-3</sup> sec<sup>-1</sup> sr<sup>-1</sup> Hz<sup>-1</sup> [ T in K, N<sub>i</sub> and N<sub>e</sub> in cm<sup>-3</sup> ]

(1.3)

where Z is the ionic charge  
 g is the Gaunt factor  
 N<sub>e</sub> is the electron density  
 N<sub>i</sub> is the ion density.

(c) Cyclotron and Synchrotron Radiation

The electrons moving in a magnetic field are accelerated into a circular or spiral path around the magnetic field and therefore, according to classical electrodynamics, they must emit electromagnetic radiation. This process of emission is nonthermal, as opposed to (a) and (b) above, which are thermal processes. At low electron velocities radiation is emitted in all directions, with the same frequency as that of the electrons about the magnetic field. Such emission is known as cyclotron radiation. However, at relativistic electron velocities the nature of the emitted radiation changes. A relativistic electron spirals a magnetic line of force, and the orbital acceleration causes the electron to emit plane-polarised radiation known as synchrotron radiation. This radiation is extremely directional, nearly all of the energy is emitted in a very small angle [  $\theta \sim mc^2/E = 1/\gamma$ ,  $\gamma = 1/\sqrt{1 - (v^2/c^2)}$  ] along the direction of the particle's motion. The spectra of synchrotron radiation are essentially a continuum in appearance. The radiation energy spectrum

is determined by the energy distribution of the particles (usually electrons) and the strength of the magnetic field.

(d) Compton Scattering

When a photon undergoes a collision with an electron, the photon energy may be reduced and part of the photon's energy is transferred to the electron as a gain in kinetic energy.

All the continuum processes that have been mentioned above may also produce absorption effects, e.g. synchrotron self absorption.

D. Infrared Excesses in Stars

Geisel (1970) listed the seventy stars known to radiate excess infrared energy. For the purposes of constructing this list, she defined the term "infrared excess" in terms of the difference between the observed K( $2.2 \mu\text{m}$ ) - N( $10.2 \mu\text{m}$ ) colour and the K - N colour corresponding to the star's spectral type. She also noted that this definition only provides an observational distinction between stars with infrared excesses and those without. Neugebauer et al. (1971) defined a stellar infrared excess as the radiation emitted, within a given infrared wavelength interval, greater than would be expected from a star radiating like a blackbody of effective temperature appropriate to its spectral type.

Infrared excesses in stars are now nearly always associated with some extra mechanism which makes the star brighter in the infrared. The excess material can be gas or dust, each producing a characteristic energy spectrum.

E. Late-Type Stars

Many strong infrared sources are, according to their spectral characteristics, classified as late-type, cool, stars. Since cool stars are so bright at infrared wavelengths, they were extensively studied in the infrared sky surveys. Because of their low colour temperatures the supergiant stars of classes M and later are strong infrared emitters in the 1 - 2  $\mu\text{m}$  region. Almost all observed M supergiants are among the brightest objects at 5  $\mu\text{m}$  and 10  $\mu\text{m}$ . Most of the stars in the Two-Micron Sky Survey by Neugebauer and Leighton (1969) are K and M stars. The well known objects are  $\alpha$  Ori,  $\mu$  Cep, NML Cyg, VY CMa, NML Tau and  $\alpha$  Her.

$\alpha$  Ori was the brightest one of 25 stars observed at 10  $\mu\text{m}$  by Wildey and Murray (1964). A photometer with a liquid hydrogen-cooled mercury-doped Germanium photoconductor, the spectral response of which is limited to 8 - 14  $\mu\text{m}$  region, was used for these observations. They suggested from these observations that 8 - 14  $\mu\text{m}$  stellar radiation is only of thermal origin.

Gillett et al. (1968) discussed the results of observations of the spectra of seven late-type stars, including the supergiants  $\alpha$  Ori and  $\mu$  Cep in the wavelength region from 2.8 to 14  $\mu\text{m}$ . A broad emission peak near 10  $\mu\text{m}$  in the spectra of  $\alpha$  Ori and  $\mu$  Cep was the most definite feature observed. Woolf and Ney (1969) suggested that this emission peak corresponds to a peak in the emittance of silicate materials and that the silicate dust produces the excess emission by thermal reradiation. In 1970, Low and Swamy (1970) published the Narrow-band infrared photometry of  $\alpha$  Ori, extending out to 24.5  $\mu\text{m}$ . They found that the agreement between the observed spectrum of silicate material and the observed spectrum of the infrared excess in  $\alpha$  Ori was consistent with the silicate dust

hypothesis. Gillett et al. (1971) have concluded that the majority of the cool stars observed have excess radiation at long wavelengths  $\lambda \approx 10 \mu\text{m}$  that can be from solid particles which surround the stars. Lambert and Snell (1975) constructed the infrared energy distributions from observations of  $\alpha$  Ori and W Hya reported in the literature in order to explore the possible contribution to the infrared excess from a stellar chromosphere. They interpreted the spectrum of these stars between 8 and  $30 \mu\text{m}$  in terms of three components: a photosphere, a silicate dust cloud and a cool chromosphere. They also found that the chromospheric temperature for W Hya is higher than that for  $\alpha$  Ori.

NML Cyg is a very faint object, being fainter than 18 mag. visually. However, it is one of the brightest stars observed at infrared wavelengths [Neugebauer et al. (1965), Johnson et al. (1965)]. This star was the subject of a number of investigations by various authors [see Ford and Rubin (1965), Wing et al. (1967), Johnson (1968), Herbig and Zappala (1970), Herbig (1974), Herbig and Lorre (1974)]. Wilson and Barrett (1968) reported the detection of intense, nonthermal, OH emission from NML Cyg and weaker emission from several other infrared stars. Herbig and Lorre (1974) obtained the direct photographs of the image of NML Cyg at an effective wavelength of about  $0.8 \mu\text{m}$  and concluded that the image of NML Cyg is entirely stellar at  $0.8 \mu\text{m}$ . Several spectral classifications of NML Cyg appear in the literature. Johnson (1966) classified it as M6 Ia. Herbig and Zappala (1970) concluded that the luminosity of NML Cyg is closer to that of a giant than a supergiant.

Humphreys (1974) reported strong absorption-line weakening in the near infrared spectra of three M supergiants, S Per, VY CMa, and VX Sgr with large infrared excesses. She argued that the near

infrared photometry of these stars indicated large infrared excesses as the cause of the veiling. She interpreted these excesses in terms of optically thin chromospheric  $H^-$  free-bound emission and suggested that optically thin free-free emission may be responsible for the 3 - 8  $\mu m$  infrared emission. Fawley (1977) made spectroscopic and narrow-band infrared observations of 15 G, K and M supergiants with large infrared excesses. He searched for line weakening and chromospheric near infrared emission in the peculiar M stars S Per, VY CMa and VX Sgr. However, his results suggested that the line weakening of S Per and VX Sgr is variable and is probably photospheric in origin, while that of VY CMa may be constant. He concluded that the 3 - 8  $\mu m$  infrared excesses cannot be free-free emission and are probably thermal radiation from the circumstellar shells.

NML Tau and IRC+10011 which emit most of their energy in the infrared are extensively studied Mira-type variables. Most of the Mira variables have infrared excesses which peak around 10 - 11  $\mu m$  wavelengths (Gillett et al. 1971). NML Tau varies by more than 2 mag. with a period of greater than 532 days and has been classified as an M8e spectral type (Wing et al. 1967). Both NML Tau and IRC+10011 are OH radio emission sources (Wilson et al. 1970).

#### F. Intermediate and Early-Type Stars

The early-type stars to be discussed briefly in this section are hot stars. The peak of their energy is observed in the short wavelengths (visible or ultraviolet). Their stellar continuum emission decreases in the infrared wavelengths. However, some hot stars have infrared excesses which can be interpreted in terms of material around the star which will give rise to this excess radiation. The existence of infrared excesses from some early-type stars was

shown by the data of Johnson (1965) and Johnson et al. (1966). Johnson (1967) investigated the relationship between spectral type and intrinsic K - L colour index for early-type stars. He concluded from his review of infrared data on 85 early-type stars that most early-type stars, dwarfs and supergiants, do not have significant infrared excesses and their intrinsic infrared colours are in agreement with those expected for stars of the appropriate effective temperature. He also indicated that several known shell stars have K - L excesses which can be interpreted as due to infrared emission from the circumstellar shells. The existence of such radiation led Woolf et al. (1970) into further investigations of the excess radiation in the infrared spectra of certain B stars. They observed several bright Be stars at longer infrared wavelengths,  $3.4 \mu\text{m}$ ,  $5 \mu\text{m}$ ,  $8.5 \mu\text{m}$  and  $11.5 \mu\text{m}$ . Their observations showed that Be stars in general have a strong non-stellar component of infrared radiation. One of their main conclusions was that the near infrared continuum of these stars can be interpreted in terms of free-free radiation from an ionized gas around the star. Allen (1973) reported the observations of nearly 250 early-type emission-line stars in the near infrared. He found that two-thirds of these stars exhibit infrared excess radiation which is probably produced by at least two mechanisms; free-free radiation from a shell of ionized gas, and thermal emission from circumstellar dust. Gehrz et al. (1974) observed excess infrared radiation in the  $2.3 - 19.5 \mu\text{m}$  region for 28 of the 33 classical Be stars. They concluded that free-free emission from a hot plasma shell is the most likely source of the infrared excess radiation. They also pointed out that circumstellar-dust emission models for these stars cannot be considered. For the classical Be stars, they derived that "a typical Be star shell, assuming a shell

radius-to-thickness ratio of 5, is characterised by an electron density of  $3.7 \times 10^{11} \text{ cm}^{-3}$ , a radius of  $2.5 \times 10^{12} \text{ cm}$ , and a Thomson optical depth of 0.16".

The star HD45677 is a prototype for the peculiar Be stars. It is an extreme example among the bright early-type shell stars. Merrill (1928) was the first to identify emission lines of Fe II in the optical spectrum of this star. Low et al. (1970) reported the photometric and spectroscopic observations of 6 stars including HD45677. They found that the system HD45677 consists of two major components, one having the spectrum and colours of a B star and the other with colours similar to those of a 600 K blackbody. They suggested two distinct possibilities for the system: (1) the B star may be surrounded by a shell which produces the infrared emission; (2) the presence of an infrared companion which has smaller mass and is still in the early protostar stage of development. Geisel (1970) suggested that the emission lines, especially those of Fe II and [F III] which appear under conditions of low-excitation are good indicators of the presence of circumstellar dust; the excess infrared radiation is linked to mass loss from the star. Swings and Allen (1971) studied the radial velocities of stellar and shell lines and could find no evidence for the presence of a cool companion. They proposed that the infrared excess could be explained by thermal emission from circumstellar dust in which there is a distribution of temperatures. Swings (1973) described a physical model of the system where a dust shell of radius about 30 AU optically thick at  $5 \mu\text{m}$  surrounds the peculiar Be star and its extended atmosphere, ring, and forbidden line regions.

The Wolf-Rayet stars are very hot ( $T$  up to  $10^5 \text{ K}$ ), and bright objects. Their spectra have anomalously strong and broad

emission lines. The extremely broad emission features of ionized He, C, N and O seen in their spectra are interpreted as arising in an expanding atmospheric envelope. WC type Wolf-Rayet stars have emission lines of hydrogen, helium, CIII and CIV. In WN type stars NIII and NIV lines dominate. Allen et al. (1972) made the observations of 40 Northern Wolf-Rayet stars covering both the carbon sequence (WC) and the nitrogen sequence (WN) at 1.2 and 2.2  $\mu\text{m}$ . Their photometry clearly distinguished between WC and WN stars; WC stars appeared significantly redder than WN stars. They explained the 2  $\mu\text{m}$  fluxes observed in WN stars as a combination of free-free and bound-free radiation, or a thin dust shell at temperature of order 1500 K. Furthermore they found that the WC 9 stars have the greatest H - K colour index which can be best explained by thermal radiation from circumstellar dust. In view of the evidence for mass-loss from Wolf-Rayet stars, they assumed that the circumstellar grains condense from material ejected by the star.

V444 Cyg (WN5, O6) and CV Ser (WC8, B0) are binary systems which contain Wolf-Rayet components. Williams et al. (1977) reported the infrared observations of CV Ser at 2.2 and 3.8  $\mu\text{m}$ . Their data showed that the infrared excesses at these wavelengths are eclipsed around secondary minimum and that they originate within the system. They believed that the source of infrared excess is graphite grains situated some 400  $R_{\odot}$  from the WC8 star. Hartmann (1977) observed the infrared eclipse of V444 Cyg at 2.2 and 3.4  $\mu\text{m}$ . Observations of the eclipse of the WN5 component of the V444 Cyg at these wavelengths confirm the idea that free-free emission is the source of the infrared excess observed in this system.

Most of the R Coronae Borealis (R CrB) stars show infrared excesses. In 1969, Stein et al. (1969) reported the infrared

observations of R CrB itself at 3.5, 4.7, 8.5 and 11.5  $\mu\text{m}$ . Their observations showed that a large amount of energy is emitted in the infrared from this object, about 40 per cent of the total luminosity of the star. The infrared data were compared with a 6000 K blackbody spectrum normalised to visual magnitude  $V = 6.4$ , the magnitude at the time of observation. A blackbody curve for 940 K fitted the observed infrared spectrum well. They concluded that the excess infrared radiation of the hydrogen deficient, carbon rich R CrB can be explained in terms of a cloud of circumstellar particles absorbing the visible radiation from the star and reradiating in the infrared. This circumstellar radiation from R CrB has been observed occasionally over the period of 1968 through 1971 and reported by Forrest et al. (1971). Their data indicated that the flux of radiation from the particles surrounding the star is changing. The maximum change occurred at  $\lambda = 3.5 \mu\text{m}$  during the period of 1970 - 1971 when the visual light from the star was quite constant. Forrest et al. (1972) followed R CrB through one minimum, lasting about 3 months and found no increase in infrared flux with decrease in visual flux. This led them to suggest an asymmetric dust cloud model in which an already existing cloud had passed in front of the star. The detailed photometric and spectroscopic observations of RY Sgr, another R CrB type star, by Alexander et al. (1972) were discussed in terms of two possible models: (i) an eclipse of the star by a cloud of particles ejected by the star, and (ii) the ejection of a more or less uniform spherical shell. Feast and Glass (1973) favoured the latter model for the R CrB phenomenon and preferred an explanation in terms of a new release of material at each visual minimum. Humphreys and Ney (1974b) considered that R CrB is a binary system with a cool infrared companion which may be responsible in

some way for this star's behaviour in the visual region. They gave the energy distribution of this peculiar carbon-rich star between 0.5 and  $10\ \mu\text{m}$ . It was shown from this curve that the infrared radiation in R CrB resembles the Cygnid-type infrared stars. The  $3.5\ \mu\text{m}$  light curve suggests that an infrared companion is present in R CrB.

G. Infrared Emission from Binary Stars

A binary system consists of a pair of stars bound together by their mutual gravitational forces. Binaries with a relatively small separation are referred to as close binaries. The systems with small separations can be easily detected by spectroscopic observations, since significant radial velocity changes may be seen in their spectra. If the orbital plane of a binary system is parallel to our line of sight, a periodic change in brightness will obviously be detected by photometric observation.

The astronomical literature has a very large number of photometric and spectroscopic observations of binary stars. A wide variety of models for the types of binary stars of interest to the astronomers has been constructed in order to understand the structure of the systems. Batten (1973) has discussed the effects of circumstellar matter on many of the features of close binary systems. The exchange or loss of mass, occurring in close binaries has been extensively discussed in the literature by many authors (see *Mass Loss from Stars*, Dordrecht, D. Reidel Publ. Comp.). In his review of observational spectroscopic evidence for mass loss in close binaries, Sahade (1969) has discussed the existence of gas streams from one of the components in close binaries and the existence of envelopes that surround close binary systems. He suggested that the

extra lines that appear in the spectrum either in absorption or in emission were the direct observational evidence for the existence of such gas streams.

Piotrowski et al. (1974) assumed that gas streams are responsible for the asymmetries in several eclipsing binary light curves.

The recent literature shows that the study of infrared emission from binary stars provides further evidence for the existence of circumstellar matter and mass loss; thus leading to a deeper understanding of such objects.

A brief discussion will now be given on several stars in which the infrared radiation can be explained by the presence of a cool companion.

Infrared emission between 2 and 22  $\mu\text{m}$  has been observed from several unusual binary stars (Woolf, 1973). These are  $\epsilon$  Aur,  $\zeta$  Aur, W Cep, Z And, UV Aur,  $\nu$  Sgr, KS Per,  $\eta$  Gem and RZ Cnc.

The binary star  $\epsilon$  Aur with a 27.1-year period has an optically observable component, type A8Ia. Huang (1965) proposed a model of  $\epsilon$  Aur in order to explain the behaviour of this star. He suggested that the eclipse of  $\epsilon$  Aur is caused by a solar nebula-like disk composed of solid particles that revolves around the secondary component. The infrared observation of  $\epsilon$  Aur by Woolf (1973) led to a model in which the A star is eclipsed by a partially ionized disk, with an electron density of  $10^{11} \text{ cm}^{-3}$  and a temperature of 7000 K.

The peculiar star  $\nu$  Sgr is a known single-lined spectroscopic binary with a well determined orbit. The secondary component has never been observed spectroscopically. Lines of H $\alpha$ , Ca II, [Ca II], Fe II, and [Fe II] have been observed in emission. All of its

spectral peculiarities arise in the same star, believed to be an A- or F-type supergiant. In order to investigate the nature of the secondary component Lee and Nariai (1967) made the J H K L observations of this system. Their infrared observations together with the U B V R I colours showed that  $\nu$  Sgr is very red at these infrared wavelengths and its spectral energy distribution is similar to that of the T Tauri-type stars. They suggested that  $\nu$  Sgr is an evolved star that has lost its outer hydrogen-rich layers, possibly through tidal interactions with its close component. The spectral energy distribution of  $\nu$  Sgr between 0.6 and 20  $\mu\text{m}$  was given by Woolf (1973). There are three distinct components in the  $\nu$  Sgr curve. At wavelengths shorter than 1.5  $\mu\text{m}$  there is the visually observed star, between 1.5 and 18  $\mu\text{m}$  there is a continuum and at  $\sim 10 \mu\text{m}$  there is a peak. He suggested that the continuum is probably due to graphite for this hydrogen-deficient star. Humphreys and Ney (1974b) discussed the observations of  $\nu$  Sgr and proposed that infrared excess in this system may be produced by a very cool star.

The F-type supergiant HD101584 which has a large and unusual infrared excess has been studied by Humphreys and Ney (1974 a and b). The energy distribution of HD101584 shows that more energy is being radiated by the infrared object in this system and a prominent silicate emission at 10  $\mu\text{m}$  is present. They suggested that the peculiar star HD101584 is a binary system with a very cool M-type companion (2000 - 3000 K) radiating strongly in the infrared. Some of its spectral peculiarities could be due to an atmospheric eclipse, or caused by the ejection of a gaseous shell from the F supergiant.

The star 89 Her is also a candidate for binary systems with

infrared components. This system shows infrared excesses similar to HD101584 which may also be produced by a very cool companion.

Infrared observations between 2 and  $22\ \mu\text{m}$  for  $\zeta$  Aur, W Cep, Z And, UV Aur, HD30353 (KS Per),  $\eta$  Gem and RZ Cnc were discussed by Woolf (1973).

### Cataclysmic Variables

This section is concerned with the objects known as cataclysmic variables. These objects are divided into four classes: classical novae, recurrent novae, dwarf novae and nova-like variables.

Theory predicts that as material ejected from novae during eruption expands and cools, a circumstellar shell of condensed matter will form, giving a large infrared excess.

Hyland and Neugebauer (1970) and Geisel et al. (1970) reported the infrared observations of Nova Ser 1970. Infrared photometry from 1 to  $25\ \mu\text{m}$  of Nova Ser 1970 by Geisel et al. (1970) showed that it has become one of the brightest infrared stars in the sky, reaching  $N = -4.0$  101 days after its eruption.

It is now fairly well established that cataclysmic variables are all close binary stars and that their properties are dominated by mass transfer from a late-type star to a white dwarf. Robinson (1976) gave a list of the cataclysmic variables whose binary nature is well established. The binary nature of cataclysmic variables has also been discussed by Mumford (1967). Several discussions of these variables appeared in the proceedings of IAU Symposium No. 73, The Structure and Evolution of Close Binaries.

### Eclipsing Binary Stars

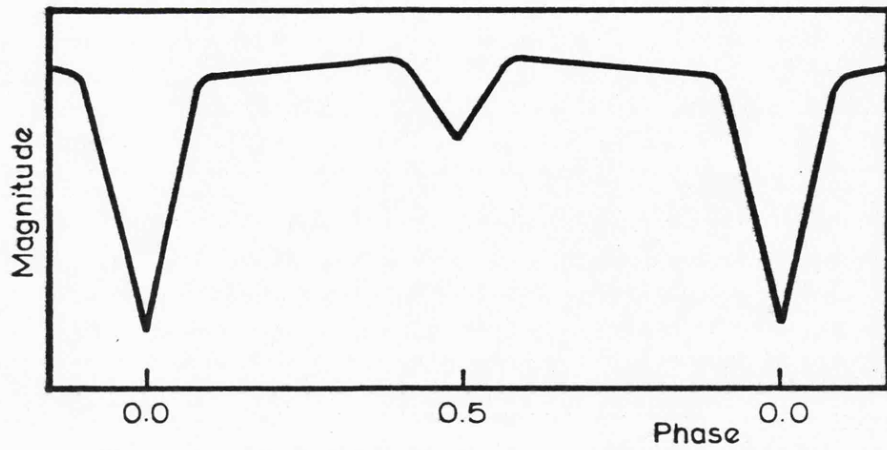
If the inclination,  $i$ , of a binary star orbit is close to

$90^\circ$ , the components will mutually eclipse each other resulting in a periodic reduction in brightness of the binary. When the components are not in eclipse, the total brightness of the system is essentially constant in time. The light curve of such a binary star is obtained by plotting the apparent brightness of the system as a function of time. The light curve shows two minima of different depths corresponding to the two possible eclipses per period. Depending on the inclination of the binary orbit and the sizes of the two stars, total, annular, or partial eclipses occur. The primary minimum is the deeper one which occurs when the hotter star passes behind the cooler component of the system.

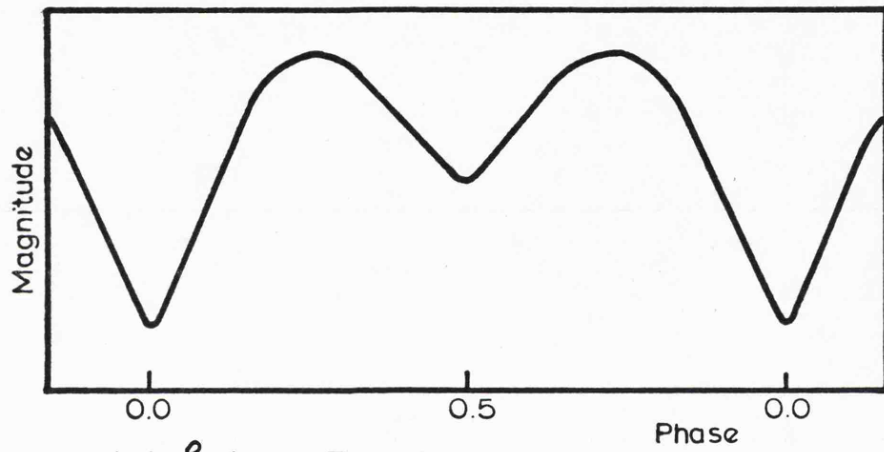
Most eclipsing binaries are also spectroscopic binaries because of their relatively small separations. They can be discovered spectroscopically from the variations in their radial velocities. The light curves and the radial velocity curves of the eclipsing binary systems are used in order to find the parameters needed to complete a description of the binaries. Analysis of photometric observations of eclipsing binaries can be done by using several different techniques which enable us to obtain much better solutions of the light curves. The problems involved are still enormous. Limb darkening of the components, reflection effect and the presence of circumstellar material in close binaries make the analysis more difficult. The observed light curves must be corrected by the process of rectification.

Eclipsing binaries have been divided into three groups, based primarily on observational features. Typical light curves of the three major types of eclipsing binaries are given in Figure 1.1 (a, b and c).

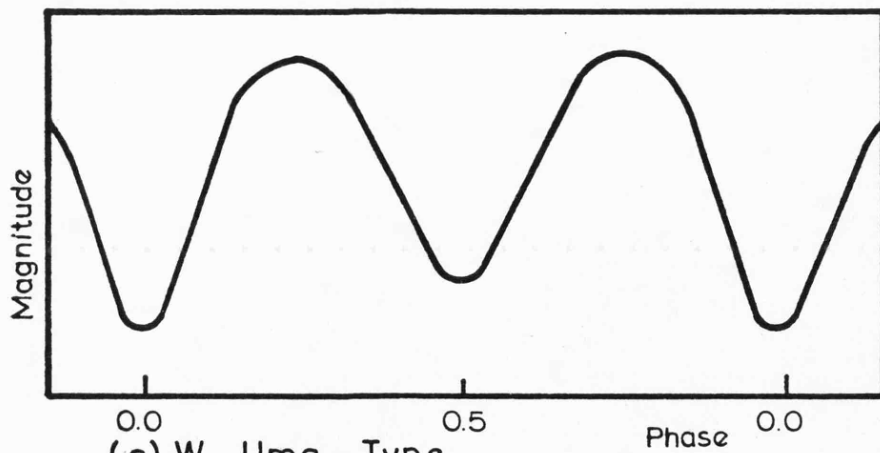
Because of their space orientation with respect to our line



(a) Algol - Type



(b)  $\beta$  Lyr - Type

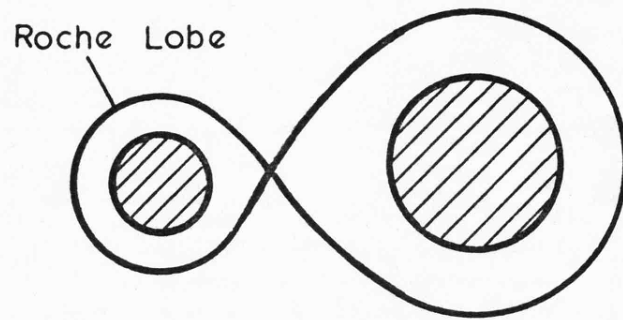


(c) W Uma - Type

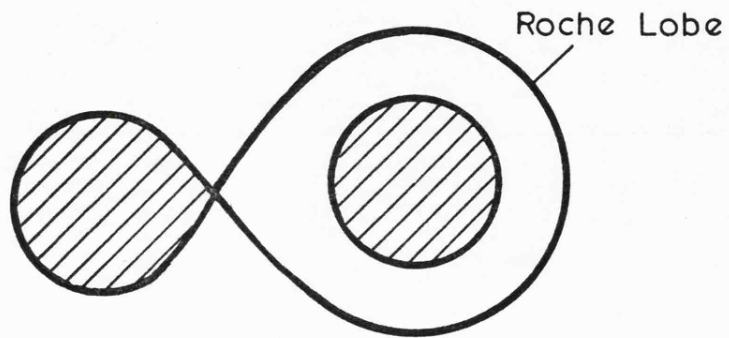
Figure 1.1. Typical light curves of the three major types of eclipsing binary

of sight, close binaries happen to be eclipsing binaries. A classification based on the sizes of the components relative to the system's Roche lobes was proposed by Kopal (1959). Roche lobes are the two volumes enclosed by the energy equipotential common to both stars of the system. The relative dimensions of the Roche limiting surfaces are completely specified by the ratio of masses of the two stars. Kopal's classification divided all binary systems into three groups. These are detached, semi-detached and contact systems. They are illustrated in Figure 1.2 (a, b and c). In detached systems, the volumes of the two components are smaller than their Roche lobes. The primary (more massive) component of a semi-detached system is smaller than its Roche lobe, but the secondary component fills its Roche lobe. In contact systems, the components share a common convective envelope and appear to fill completely their Roche lobes.

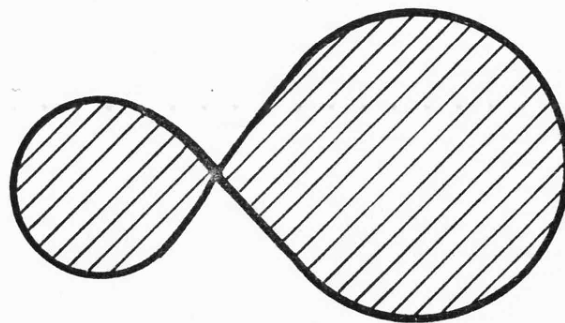
Because of the nature of equipotential surfaces, any material reaching the inner Lagrangian point,  $L_1$ , is free to pass through from one Roche lobe to the other. Kopal (1959) investigated the conditions under which matter can be expelled from rotating stars in expansion and its subsequent motion under the gravitational influence of the two components of close binary systems. Mass transfer obviously introduces material into the volume between and around the component stars. Many binary systems show evidence that streams or clouds are associated with them. It is convenient to refer to this matter between and around the components as circumstellar matter. Batten (1973) defined the circumstellar matter as the matter in the neighbourhood of a binary system that had its origin in one of the components, but is temporarily or permanently no longer under the sole gravitational control of that component. He also summarised the



**(a)** Detached system



**(b)** Semi-detached system



**(c)** Contact system

Figure 1.2 The three classifications of close binary configuration

available evidence for circumstellar matter in three sections: the distortion of velocity curves; spectrophometric evidence, including the existence of emission features; and the distortion of the light curves of eclipsing systems. In each section the evidence is summarised for the three major types of eclipsing binaries; Algol,  $\beta$  Lyr, W UMa-type systems and the cataclysmic variables.

The study of extended atmospheres and circumstellar matter in close binary systems is so complex that all the major problems involved cannot be discussed in great detail here. The best recent discussion is the report of the IAU Symposium No. 51, on "Extended Atmospheres and Circumstellar Matter in Spectroscopic Binary Systems".

A brief discussion will now be given on the three major types of eclipsing binary stars.

(a) Algol-Type Systems

These systems contain a main-sequence primary component of spectral type between about B5 and A5, and a subgiant secondary star, usually of spectral type G or K. In most systems the secondary star fills its Roche lobe. The light curves of these systems can be characterised by almost flat maxima and well-defined minima (see Figure 1.1a). Algol ( $\beta$  Persei) is the prototype of semi-detached systems. This system is now thought to consist of a main-sequence B8 primary star, a K0 subgiant secondary star, and a third component (Hill et al. 1971). Photometric observations of  $\beta$  Per have been made in different wavelength regions of the spectrum. Observations of an effective wavelength of  $1.6 \mu\text{m}$  were reported by Chen and Reuning (1966). Their observed light curve was asymmetrical and showed a deeper secondary minimum than that found in the optical light curves. Jameson et al. (1973) reported a phase-dependent infrared excess at

$5\ \mu\text{m}$  from  $\beta$  Per. They argued that this  $5\ \mu\text{m}$  infrared excess can be explained by optically thin free-free emission from an ionized hydrogen plasma cloud which must lie between the two stars (the primary and the secondary star). Smyth et al. (1975) observed the Algol system at  $2.2\ \mu\text{m}$ . They presented a  $2.2\ \mu\text{m}$  light curve derived from their observations, combined with the observations by Johnson et al. (1966). Their predictions of infrared magnitudes for Algol on the basis of the four models of the system and the theoretical light curve at  $5\ \mu\text{m}$ , constructed from one of the models, showed that there is no firm evidence of general infrared excess at  $5\ \mu\text{m}$ . The light curve at  $2.2\ \mu\text{m}$  also shows no general infrared excess and no phase-dependent excess. Longmore and Jameson (1975) published the infrared observations of  $\beta$  Per for wavelengths of 2.2, 3.6, 4.8 and  $8.6\ \mu\text{m}$ . Their earlier observations at  $5\ \mu\text{m}$  were not included because the filter characteristics were different and a different standard star was used. They also claimed that the very large general infrared excess found previously at  $5\ \mu\text{m}$  was due to an error of a factor  $\pi$  in the determination of the blackbody fluxes of the two stars. The asymmetry of the light curves outside eclipses was evident from these observations. They produced a model based on the B8 primary star, K0 secondary star, and the stream between these two eclipsing stars. This model approximately fits their infrared data and also other observations of the system. Sánchez Magro et al. (1977) reported further observations of  $\beta$  Per at  $4.8\ \mu\text{m}$ . These observations have a greater photometric accuracy than those of Longmore and Jameson (1975) and they claim there is no infrared excess at  $5\ \mu\text{m}$ .

To decide whether the gas stream shows any infrared excess it would be desirable to remeasure the light curve of Algol at 8.6 or even  $11.5\ \mu\text{m}$ .

RZ Sct is a spectacular example of Algol-type binaries. The system consists of a brighter component of spectral type B2II and a fainter component of spectral type AOII-III (estimated from light curves), (see Wilcken et al. 1976). As a matter of fact an example of the apparent variation of spectral class was provided by this system. RZ Sct has been widely investigated spectroscopically and photometrically. Large distortions in the velocity curve are evident. The H $\alpha$  line is observed in emission. The spectral features of the secondary component have not been observed. Both the spectroscopic and photometric data indicate that the gaseous stream exists between the component stars. The system unfortunately has not been observed at infrared wavelengths. Infrared observations of RZ Sct should aid in the construction of a suitable model for this system. Therefore this system was included in our infrared photometric programme.

(b)  $\beta$  Lyr-Type Systems

The prototype of this group of eclipsing binaries is  $\beta$  Lyr, the light curve of which shows a continuous variation even when no eclipse is taking place and presents unusual features. Although it is the best observed system in the sky, the dimensions of the  $\beta$  Lyr are not well determined. Simply, the system consists of a B8.5 primary star with a more massive secondary star surrounded by a plasma disk.

Jameson and Longmore (1976) published five infrared light curves of  $\beta$  Lyr at 1.2, 2.2, 3.6, 4.8 and 8.6  $\mu$ m. These show that at long wavelengths the secondary minimum becomes deeper than the primary minimum. They explained this feature by a plasma cloud around the secondary star which is eclipsed at secondary minimum. It was

assumed that the disk is optically thick across its diameter at all wavelengths and at primary minimum no light is seen from the primary component through the disk around the secondary. They obtained a temperature of 17500 K and a constant electron density of  $1.4 \times 10^{12} \text{ cm}^{-3}$  for the secondary disk and suggested that the secondary star should have an effective temperature greater than the disk temperature and would be of type B4 or earlier. Brown and Huang (1977) analysed light curves of  $\beta$  Lyr at various wavelengths ranging from the far-ultraviolet to the infrared regions of the spectrum in eclipse in order to investigate the nature of the disk around the secondary star. They proposed that the outer regions of the disk are dominated by free electrons and the most likely source of infrared radiation is this electron-scattering envelope.

RT Lac is another  $\beta$  Lyr-type eclipsing binary which is also a double-lined spectroscopic binary with an asymmetric light curve. Milone (1976) obtained the infrared observations of RT Lac in order to provide further evidence for the existence of circumstellar matter in this binary system. He found that this peculiar eclipsing binary, RT Lac, has an apparent infrared excess radiation at J, H, K and L. The peak value was 0.7 mag. at K. The excess has also a phase-dependent component.

(c) W UMa-Type Systems

The W Ursae Majoris-type systems are contact binaries, the light curves of which can be characterised by strongly curved maxima and nearly equal primary and secondary minima (see Figure 1.1c). These systems are also spectroscopic binaries. W UMa systems have been divided by Binnendijk (1970) into A- and W-type systems according to the behaviour of their radial velocity curves. In A-type systems

the radial velocity curve which represents the observations of primary component has the smaller semi-amplitude. Consequently, the primary component is the more massive star which is eclipsed during the primary minimum. In W-type systems again the primary component is the more massive star, but the radial velocity curve of this component shows that the primary minimum is caused by an occultation.

The orbital period of W UMa systems is shorter than one day. The period changes of this type of contact binary are a commonly observed phenomenon. Light variations are continuous throughout the period. The peculiarities of these systems were discussed by Binnendijk (1970) in detail. The common convective envelope model for W UMa systems which gave a qualitative understanding of the light curves was provided by Lucy (1968a, b and 1973). Evolution of such binaries has been discussed by Lucy (1968a), Hazlehurst (1970), Moss and Whelan (1970), Biermann and Thomas (1972 and 1973), Rahunen and Vilhu (1977) and Robertson and Eggleton (1977).

Detailed analyses of the light curves of W UMa systems have been made by several investigators and have shown that it was very difficult to assign any orbital elements to these stars from the light curves alone. In almost all W UMa systems, the effects of limb darkening, reflection, gravity and oblateness are evident in their light curves. A quantitative method of deriving the orbital elements from the light curve which is based on the process of rectification was discussed by Binnendijk (1970). This procedure has, for some years, been felt to be an incomplete description of very close binary systems where distortions, non-spherical surfaces, etc., are important. More recent work has involved the use of "light curve synthesis" involving Roche geometry. Lucy (1973) gave a light

curve synthesis for 44 i Boo, and the main difference was that the photospheres of the stars touch and overflow their inner critical Roche surface.

The spectra of several W-type systems show emission lines of CaII in their spectra. These broad and diffuse emission lines are best seen during the eclipses. In the spectra of both the W- and A-type systems the absorption lines from both components were visible. The intensities of these lines are often variable.

The general features of both the light and spectral changes occurring in W UMa-type systems have been outlined above. In view of these peculiarities it seemed that infrared observations of the W UMa-type systems might be interesting. Therefore the systems of this type were included in this project.

Finally, in this project we have tended to concentrate on binary star systems whose period is less than 12 hours or more than about 10 days. Because such light curves are the easiest to obtain with observing visits to Tenerife of 2 to 3 weeks.

## CHAPTER 2

## INSTRUMENTATION

In this chapter the principal items of the infrared detection system will be considered in general, and descriptions of the photometer designed and used for this project will be given in detail.

A. Infrared Detectors

An infrared detector, which is the heart of the infrared detection system, changes the incident infrared radiation into an electrical signal.

In order to understand the terminology used for the detector performance some of the definitions are given initially.

Responsivity,  $R$ , is the output signal voltage per unit input flux on the detector.

$$R = \frac{V_s}{F} \quad \text{in V/watt} \quad (2.1)$$

where  $V_s$  is the rms value of the output signal voltage and  $F$  watts is the flux of radiation incident upon the detector.

In order to get alternating input and output quantities, a chopper is placed in the beam of the incident radiation; therefore the measurement of such quantities is their root-mean-square (rms) value. The responsivity can also be measured in terms of A/watt.

Responsivity at the chopping frequency  $f$  is given by a simple formula,

$$R_f = \frac{R}{[1 + (2\pi f \tau)^2]^{\frac{1}{2}}} \quad (2.2)$$

where R is the responsivity at zero frequency and  $\tau$  is the time constant of the detector which is defined by the time that it takes for the detector output to reach 63 per cent of its final value after a sudden change in the radiant flux.

Noise-Equivalent-Power of the detector, N.E.P., is defined as the radiant flux that produces an electrical output signal,  $V_s$ , equal to the detector noise voltage, for an electrical bandwidth of  $\Delta f = 1$  Hz.

$$\text{N.E.P.} = \frac{F}{V_s/V_n(\Delta f)^{\frac{1}{2}}} \quad \text{in watts/Hz}^{\frac{1}{2}} \quad (2.3)$$

where  $V_n$  is the noise voltage of the output of the detector. With this formula, it is now possible to compare the output signal of the detector with its output noise for a given incident radiation. According to the formula (2.3) the best detector is the one with the lowest N.E.P.

In 1952, Jones (1953a) suggested the term "detectivity" which is defined as the reciprocal value of the N.E.P. Thus, the Detectivity is

$$D = \frac{1}{\text{N.E.P.}} \quad (2.4)$$

The best detector is the one with the highest detectivity.

It can be easily seen that the quantities defined so far vary from one detector to another. Even for a single detector, the wavelength of the radiation incident on it, the operating temperature, and the chopping frequency all effect its performance,

therefore its detectivity.

The performance of any detector is limited by the presence of noise in its output. The properties of noise have been studied by many authors. In the following paragraphs, a brief summary of noise and its sources will be presented. A much more detailed study of detector noise is provided by Jones (1953b), Smith et al. (1957), and Hudson (1969).

Electrical noise is simply unwanted spontaneous fluctuations in an electrical system. When viewed on an oscilloscope, noise voltages show random fluctuations about an average voltage with some peaks and dips which are independent of time.

Let the fluctuating voltage be denoted by  $V(t)$ , and let  $\bar{V}$  be its mean value. Then, mathematically, the mean-square voltage fluctuation is

$$\bar{V}^2 = \overline{(V(t) - \bar{V})^2} \quad (2.5)$$

or

$$\bar{V}^2 = \frac{1}{\tau} \int_t^{t+\tau} (V(t) - \bar{V})^2 dt \quad (2.6)$$

with the average taken over a time interval  $\tau$ . Since noise fluctuations are both positive and negative, the mean-square noise voltage is first determined. Then, the noise power is defined by  $P = \bar{V}^2/R$  where  $R$  is the circuit resistance involved. Alternatively the spectral distribution of the noise is considered and the noise spectral density,  $G(f)$ , in a given bandwidth,  $\Delta f$ , is evaluated.

There are many sources which produce noise. The types of noise given next are the most common ones found in an infrared

system.

Johnson or Thermal Noise. The random motion of free electrons in any conducting material results in collisions with the atoms of the substance. This explains the resistance of the conductor, and the random motion of electrons generates voltage fluctuations across the terminals of the conducting material, known as Johnson noise. This type of noise was discovered experimentally by Johnson (1928), and investigated theoretically by Nyquist (1928). From the experimental results the Johnson noise voltage is

$$\overline{V_n^2} = 4 k T R \Delta f \quad (2.7)$$

where  $k$  is Boltzmann's constant,  $T$  the temperature of the conductor in K,  $R$  its resistance, and  $\Delta f$  the electrical bandwidth of the system. Thus, for a given temperature, the noise voltage depends on the resistance of the conducting material.

1/f Noise. It is found that the power spectrum of the noise increases at very low frequencies, that is, the noise power is inversely proportional to frequency. This type of noise is thought to be caused by surface and lattice defects. It is also sometimes called current noise since it depends approximately on the square of the current through the detector.

Generation-Recombination Noise. In a semiconductor charges are carried by electrons and holes. The generation and recombination of these mobile carriers produce random fluctuations resulting in variations in the number of the available carriers. Hence these variations at intermediate frequencies are the source of generation

and recombination noise. The charge carriers are generated by incident photons and lattice vibrations. Clearly the detector should be cooled to eliminate the lattice vibrations of excited carriers.

Photon Noise. The source of this type of noise is the fluctuations in the incident radiation. Derivation of photon noise and its expression is given by Jones (1953b) in detail and will be discussed in the physical characteristics of photon detectors. For an ideal detector photon noise is the same as generation-recombination noise since there are no thermally excited carriers.

Temperature Noise. In thermal detectors, fluctuations in the temperature of the detector is the source of temperature noise. The variations in the rate at which heat is transferred cause these temperature fluctuations.

When detecting an output signal of a detector together with its output noise it is conventional to speak of the signal-to-noise ratio. In the presence of noise measured with an electrical bandwidth of  $\Delta f$  Hz, together with the assumption that the noise voltage per unit bandwidth is independent of frequency, Jones (1953b) suggested the term "specific detectivity,  $D^*$ ". It has been shown from experimental studies that the detectivity varies inversely with the square root of the detector area. Therefore the Specific Detectivity is given by

$$D^* = \frac{\sqrt{A}}{\text{N.E.P.}} = \frac{V_s/V_n(\Delta f)^{\frac{1}{2}}}{F} \sqrt{A} \quad \text{in cm(Hz)}^{\frac{1}{2}} \text{ watt}^{-1} \quad (2.8)$$

Thus the specific detectivity can be defined as the signal-to-noise ratio when one watt radiant flux is incident on unit sensitive area,  $A$ , of a detector and the noise is measured with an electrical bandwidth of  $\Delta f = 1$  Hz.

To state the initial measurement conditions,  $D^*$  is followed by two or sometimes three parameters in parentheses. Thus the specific detectivity for the PbS cell used in our measurements is written

$$D^* (500 \text{ K}, 90) \quad \text{or}$$

$$D^* (\text{peak}, 90)$$

where the parameters indicate that the specific detectivity of the PbS cell is measured with a 500 K source at a chopping frequency of 90 Hz, and "peak" means the wavelength of maximum detectivity.

Infrared detectors can be classified as thermal detectors (also called bolometers) and photon detectors. In thermal detectors the incident radiation increases the detector temperature and this alters some property of the detector usually its resistance. In the other group of detectors, which can be further divided into photoelectric, photovoltaic, and photoconductive detectors, the photons incident on such detectors directly affect the electrons of the detector, and therefore the response of the detector depends on the number of photons incident on it. Photoelectric detectors can be used at visible wavelengths but not at infrared wavelengths.

(a) Thermal Detectors

The temperature coefficient of resistance of a bolometer, which is the fractional change in resistance of the bolometer material per degree change in temperature, should have a very high value so that very small amounts of incident radiation can be detected.

The excess temperature of a thermal detector, when the radiation is incident on it is given by

$$|\Delta T| = \frac{\epsilon W_0}{g(1 + \omega^2 \tau^2)^{\frac{1}{2}}} \quad (2.9)$$

where  $W_0$  is the incident radiation power,  $\epsilon$  the detector absorption efficiency,  $g$  the thermal conductance,  $\omega$  the angular chopping frequency, and  $\tau$  the time constant of the detector.

This equation is the result of a fairly simple treatment by Longmore (1975). This result can now be applied to a bolometer which has resistance  $R_B$ , operating current  $i$ , and temperature coefficient of resistance  $\alpha$ . The signal voltage  $\Delta V$  is given by

$$\Delta V = i \Delta R_B .$$

From the definition

$$\alpha = \frac{1}{R_B} \frac{dR_B}{dT} ,$$

hence

$$\Delta V = i \alpha R_B \Delta T . \quad (2.10)$$

$i$  can be found from the heating effect of the current at equilibrium temperature  $T$ ,

$$i^2 R_B = g(T - T_s) \quad (2.11)$$

where  $T$  and  $T_s$  are temperatures of the detector and its surroundings respectively. From equations (2.9), (2.10) and (2.11), the responsivity of the bolometer is given by

$$\frac{\Delta V}{W_0} = \alpha \epsilon \left[ \frac{R_B (T - T_s)}{g(1 + \omega^2 \tau^2)} \right]^{\frac{1}{2}} \quad (2.12)$$

With this formula, the physical concepts of bolometer operation are illustrated.

A number of bolometer materials have been used in the

past. Among them, silicon (Bachman et al., 1970), germanium (Zwerdling et al., 1968), and thallium selenide (Nayar, 1974) can be given as bolometer materials. Nayar (1974) built a far infrared bolometer which operates at 1.6 K and has a N.E.P. of  $8.3 \times 10^{-15}$  watts/Hz<sup>1/2</sup> using the semiconducting thallium selenide cooled to liquid helium temperature. His measured responsivity of the bolometer was  $6 \times 10^5$  V/watt compared with the calculated responsivity of Tl Se bolometer of  $7 \times 10^5$  V/watt. The best general purpose helium cooled bolometer is the Gallium doped Ge bolometer due to Low (1961).

(b) Photon Detectors

Because of the direct interaction between the incident photons and the electrons of the detector, the incident photon transfers its energy to an electron of the detector material. If this electron has enough energy, then it escapes from the surface of the material. This is called the photoelectric effect. In a semiconductor photons may cause electrons to rise from the valence to the conduction band producing charge carriers. The photon produces either an electron-hole pair containing both positive and negative carrier or only a single sign carrier depending respectively on whether intrinsic or extrinsic semiconductor material is used. Biasing the detector causes changes in the number of charge carriers, which in turn varies the current passing through the detector. This is called the photoconductive effect. The electron-hole pairs produced by the incident photons in the vicinity of a p-n junction are separated by the electric field across the junction producing a photovoltage. This is called the photovoltaic effect. The above mentioned photoeffects form the basis for the photon

detectors.

To understand these effects and their application to photon detectors a brief discussion of the band theory of solids will be given.

In the simple Bohr model of an atom the nucleus is surrounded by a cloud of electrons revolving in orbits of various shapes. Of these orbital electrons, all but one are bound tightly to the nucleus in discrete energy levels with discrete orbital diameters. The outermost electrons in the orbits of atoms are called valence electrons. When a large number of such atoms are brought together, as they are in a solid, the discrete energy levels will build up nearly continuous bands so that it is impossible to distinguish which valence electron belongs to which atom. Consequently such electrons are free to move. These continuous bands, separated from one another by energy gaps are called the allowed bands. The regions where there are no electron energy levels are called the forbidden bands. Therefore the allowed energies are gathered in bands, with the bands separated by energy gaps. Bands built by valence electrons are called valence bands. Generally speaking, since a valence band is completely filled, the nearly empty band is called a conducting band.

The band arrangements of an electrical conductor, an insulator, and a semiconductor are illustrated in Figure 2.1 (a, b, and c) respectively.

The detectors which have been used with the photometer for this project are photoconductor and photovoltaic type of photon detectors. Therefore these types of detectors will be discussed in detail.

Photoconductive detectors may be grouped into two types:

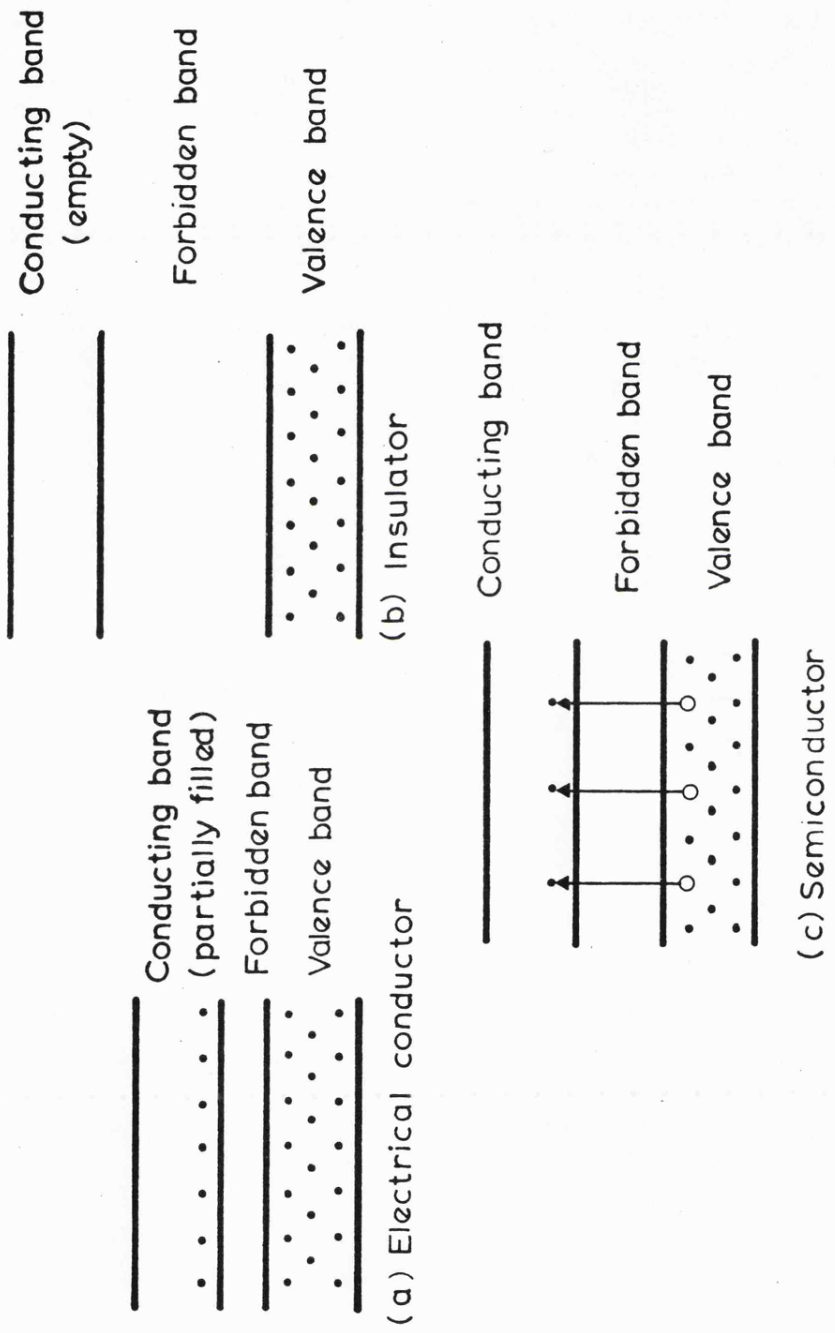


Figure 2.1 Energy bands of conductor, insulator and semiconductor.

intrinsic detectors and extrinsic detectors. In an intrinsic semiconductor, the energy gap between the full valence band and the empty conducting band is small, that is, only a fraction of an electron volt wide. Therefore a small increase in temperature causes some of the valence electrons to jump to the conducting band leaving positively charged holes in the valence band. Hence, an electron-hole pair of charge carriers is produced resulting in variations in conductivity. To produce the electron-hole pairs, the incident photons should provide sufficient energy. Since the energy of the photon depends on the wavelength of the incident radiation, there is a wavelength limit beyond which the energy is insufficient to produce such pairs. The limit wavelength which is called the cut-off wavelength is given by,

$$\lambda_c = \frac{1.24}{E_f} \quad (2.13)$$

where  $E_f$  is the forbidden energy gap expressed in electron-volts.

Intrinsic detectors are not suitable for wavelengths beyond 7 - 8  $\mu$ m.

On the other hand extrinsic semiconductors, which can be made by a doping process, a wide range of cut-off wavelengths is arranged by some convenient dopant material. A detailed discussion on extrinsic detectors is given by Levinstein (1965).

A photovoltaic detector is one which can be distinguished by a p-n junction. When the electron-hole pairs are separated by the incident radiation at the p-n junction, the detector generates a current in the external circuit.

### Physical characteristics of photon detectors

When a photoconductive detector is placed in a circuit which consists of a bias battery and a load resistor, then the signal voltage  $V_s$  from the detector can be expressed in terms of the physical parameters of the whole system.

The signal voltage is given by the expression

$$V_s = \frac{E R_L R_C}{(R_L + R_C)^2} \frac{\Delta n}{n} \quad (2.14)$$

where  $R_C$  and  $R_L$  are detector and load resistance respectively,  $E$  the emf of the bias battery, and  $\Delta n$  the change in the number of charge carriers,  $n$ , produced by incident radiation.

Since  $Q$  is the incident photon flux and  $A$  the detector area, the change in the number of carriers is given by

$$\Delta n = \eta Q A \tau \quad (2.15)$$

where  $\eta$  is the quantum efficiency and  $\tau$  the time constant of the detector material.

From equations (2.2), (2.14), and (2.15) the signal voltage is written as

$$V_s = \frac{E R_L R_C}{(R_L + R_C)^2} \frac{\eta Q A \tau}{n} \frac{1}{(1 + 4 \pi^2 f^2 \tau^2)^{\frac{1}{2}}} \quad (2.16)$$

where  $f$  is the chopping frequency.

Since one is interested not only in signal voltage but also in the signal-to-noise ratio generated by a detector for an incident radiation flux, noise voltage due to random fluctuations in the number of the charge carriers is given by the expression

$$V_n = \frac{2 E R_L R_C}{(R_L + R_C)^2} \left( \frac{\tau}{\langle \Delta n^2 \rangle} \right)^{\frac{1}{2}} \left( \frac{\Delta f}{1 + 4 \pi^2 f^2 \tau^2} \right)^{\frac{1}{2}} \quad (2.17)$$

where  $\Delta f$  is the electrical bandwidth and  $\langle \Delta n^2 \rangle$  is the variance in the number of charge carriers. The number of carriers is determined by either lattice vibrations or background radiation; therefore in the first case, generation-recombination noise results; in the second, photon noise. In the case of G-R noise,  $\langle \Delta n^2 \rangle = n$  and for photon noise the variance is

$$\langle \Delta n^2 \rangle = \sum n_{\lambda} \left( 1 + \frac{1}{\exp(hc/\lambda kT) - 1} \right)$$

where  $h$  is Planck's constant,  $k$  Boltzmann's constant, and  $T$  the temperature (K).

In order to find the theoretical specific detectivity  $D^*$ , equations (2.8), (2.16), and (2.17) are used. Thus, it is written as

$$D^* = \frac{1}{2} \eta \left( \frac{A\tau}{n} \right)^{\frac{1}{2}} \frac{Q}{H} \quad (2.18)$$

where  $H$  is the radiant flux incident per unit area on a detector and the  $\langle \Delta n^2 \rangle$  has been replaced by  $n$  in equation (2.17).

If the detector is operated under such a condition that the noise is generated by only background radiation at a sufficiently low temperature, then

$$n = \eta Q_B A \tau \quad (2.19)$$

and (2.18) becomes

$$D^* = \frac{1}{2} \left( \frac{\eta}{Q_B} \right)^{\frac{1}{2}} \frac{Q}{H} \quad (2.20)$$

where  $Q_B$  is the background photon flux.

At a particular wavelength

$$H = \frac{hc}{\lambda} Q .$$

Thus for a background limited detector, the theoretical limit of  $D^*$  is given by

$$D^* = \frac{\lambda}{2hc} \left( \frac{\eta}{Q_B} \right)^{\frac{1}{2}} \quad (2.21)$$

For photovoltaic detectors, the limit is increased by the factor of  $\sqrt{2}$  (Hudson 1969, page 349).

It may be concluded that an improvement in the detectivity,  $D^*$ , of either intrinsic or extrinsic detectors can be made by reducing the background radiation. This can be done by cooling the detector and its surroundings, and also using a cooled filter which selects the wavelength range. The limits mentioned above for intrinsic and extrinsic infrared detectors were studied in detail by Blouke et al. (1973) and Bratt et al. (1961).

A detailed description of the detectors used with the photometer for this project now follows in the next paragraphs. Two types of detectors have been used with the photometer: Lead Sulphide, PbS and Indium Antimonide, InSb.

#### Lead Sulphide Infrared Detectors

The properties of PbS detectors have been widely investigated. The electrical and photoconductive properties of PbS detectors have been studied in detail under various operating conditions by Humphrey (1965). The forbidden energy gap of this material measured at 25°C is in the range between 0.30 eV and 0.40 eV. These energies correspond to cut-off wavelengths of 4.1  $\mu\text{m}$  and 3.1  $\mu\text{m}$ , respectively. PbS is widely used at room temperature in the visible and near infrared regions. The response of the detector can be increased by cooling to temperatures considerably below room temperature. According to the Santa Barbara Research Centre (SBRC)

information, their components of PbS detectors have spectral response of  $1\ \mu\text{m}$  to  $3.5\ \mu\text{m}$  at 295 K ambient temperature,  $1\ \mu\text{m}$  to  $4\ \mu\text{m}$  at 193 K intermediate temperature, and  $1\ \mu\text{m}$  to  $4.5\ \mu\text{m}$  at 77 K, low temperature. Cooling the detector also increases the cut-off wavelength. At 77 K low temperature, the cut-off wavelength is  $4.0\ \mu\text{m}$ . Therefore further cooling results in a decrease in the response of the detector unless a cooled filter is used to reduce the background radiation.

The various types of noise can be found in PbS detectors. At short wavelengths, e.g.  $2\ \mu\text{m}$ , where the detector is not background limited its ultimate detectivity is limited by  $1/f$  noise.

The PbS detector which was tested in the laboratory and used with the photometer is manufactured by SBRC. Manufacturers specifications are given below:

Operating temperature	193 K
Element sizes	1 mm x 1 mm
Field of view	$180^\circ$
Bias voltage	100 V
Impedance	1.9 M-ohm
$D^*$ (500 K, 90)	$8.6 \times 10^9\ \text{cm}(\text{Hz})^{\frac{1}{2}}\ \text{watt}^{-1}$
$D^*$ (peak, 90)	$4.1 \times 10^{11}\ \text{cm}(\text{Hz})^{\frac{1}{2}}\ \text{watt}^{-1}$

For laboratory testing and stellar measurements, in the cryostat the PbS detector is used with cooled interference filters and an F2 Fabry lens. The blackbody calibration source which will be described later in this chapter was used to measure its N.E.P. in the laboratory. The resulting N.E.P. of the PbS detector cooled to 77 K at  $2\ \mu\text{m}$  with the chopping frequency of 12.5 Hz was  $3.0 \times 10^{-14}$  watts/Hz $^{\frac{1}{2}}$ .

### Indium Antimonide Infrared Detectors

The properties of InSb detectors were described by Avery et al. (1957) and Goodwin (1957). Investigations of the semiconducting properties of InSb showed that the forbidden energy gap of this material, measured at room temperature as 0.18 eV is adequate for a potential infrared detector.

Photoconductive and photoelectromagnetic detectors operating at room temperature, and photoconductive and photovoltaic detectors operating at low temperatures, making use of InSb material are available in the near infrared region. The manufacture of InSb photoconductive detectors and their design theory are discussed by Morten and King (1965). The arrangement for an infrared photocell based on the photoelectromagnetic effect in InSb is given by Hilsum and Ross (1957). The photoelectromagnetic detectors show response to  $7 \mu\text{m}$  at room temperature. Since their detectivity is relatively low compared to that of photoconductive and photovoltaic types, they are rarely used.

A material of very high purity is required for a photoconductive InSb type detector. An impurity atom then replaces either indium or antimony producing an Impurity-Activated InSb detector discussed by Levinstein (1965).

Photoconductive InSb detectors operating at room temperature are made from a single crystal prepared by a special technique (see Morten and King, 1965). Photovoltaic InSb detectors are prepared by producing a p-n junction at the surface of a single crystal (see Bratt et al. 1961).

InSb detectors may be operated from room temperature to 77 K, with an increase in detectivity by some factor and also a reduction in the cut-off wavelength to  $5.5 \mu\text{m}$  as a result of cooling.

The InSb detector used with the photometer in this project is a photovoltaic type of photon-detector manufactured by Barnes

Engineering Ltd. According to the manufacturer's specifications its operating temperature is 77 K, element sizes 1 mm x 1 mm, and the resistance at 77 K, 25 M  $\Omega$ .

Johnson noise limited operation of photovoltaic InSb detectors is given in detail by Hall et al. (1975). Briefly, photovoltaic detectors produce a signal voltage when sufficient photons of energy are absorbed at the p-n junction. This absorbed energy generates an electron-hole pair at the junction. This pair is then separated by the electric field across the junction producing a potential difference. When no radiation is incident on the detector, it has the electrical characteristics of a normal diode. The most common description of the electrical characteristics of such a component is the current-voltage characteristic of the device. The current-voltage characteristic curve of a photovoltaic detector in the presence of the incident radiation is displaced downward along the current axis in comparison with the normal diode curve. Thus the possible operating points can be selected by the use of such a detector. The signal produced can be detected by measuring either the variation in current with a constant voltage or the change in voltage.

The detector may be represented by an equivalent circuit shown in Figure 2.2, where  $R_D$  and  $C_D$  indicate the resistance and the capacitance of the detector respectively. A detailed circuit diagram of the preamplifier for the operation of InSb will be given later in this chapter with the electronics of the detection system.

#### Sources of noise in InSb detectors.

Noise produced in InSb may be due to various sources. Since InSb detectors, when operated at 77 K, are sensitive to radiation

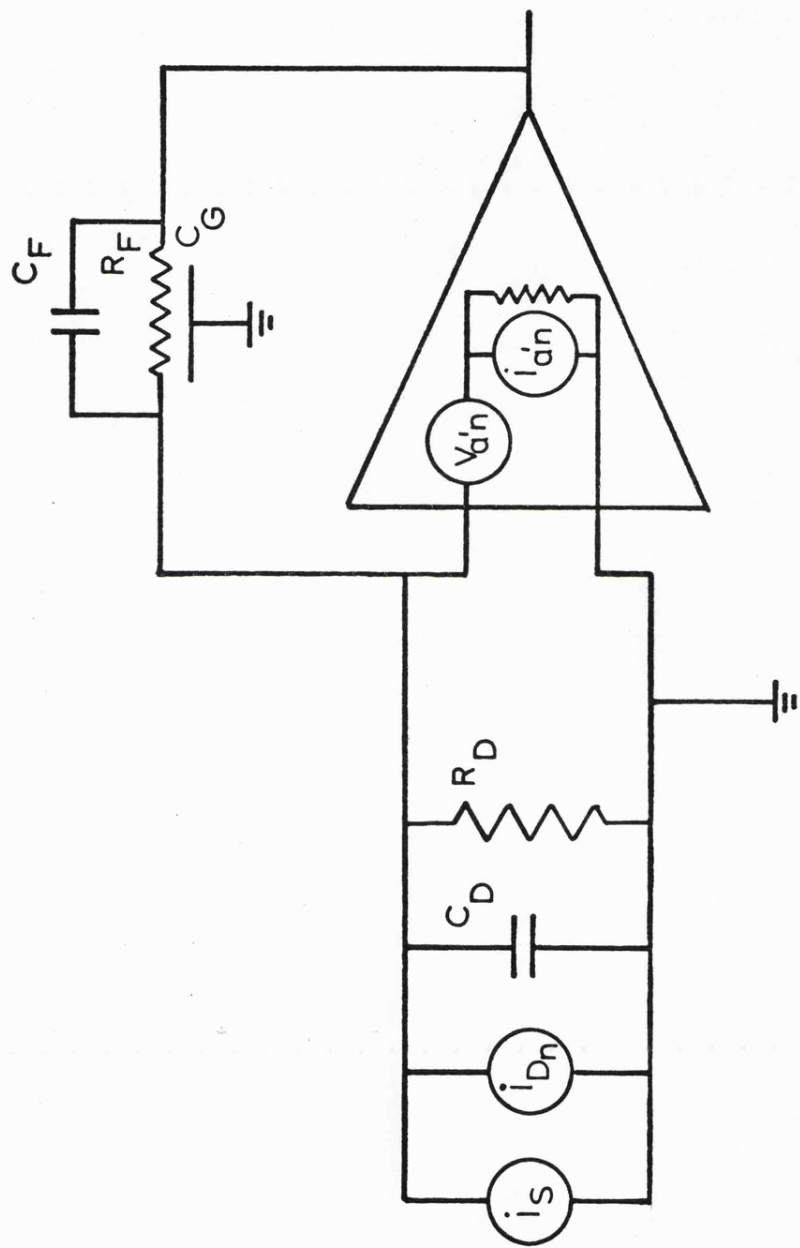


Figure 2.2 Diode equivalent circuit by Hall et al. (1975)

out to  $5.5 \mu\text{m}$ , at  $3.6 \mu\text{m}$  and  $5 \mu\text{m}$  photon noise produced by background radiation is the dominant source of noise. Therefore, the formula (2.17) for the photon noise applies.

The operating circuit of InSb uses the detector in such a way that no current passes through the detector. Thus there can be no  $1/f$  noise which depends approximately on the square of the current through the detector.

At  $2 \mu\text{m}$  and shorter wavelengths the detector sensitivity is limited by Johnson noise which is given by formula (2.7) as

$$\overline{V_n}^2 = 4 k T R_D \Delta f \quad (2.7)$$

where  $R_D$  is the resistance of the detector,  $T$  operating temperature,  $\Delta f$  the electrical bandwidth, and  $k$  Boltzmann's constant.

The noise equivalent power, N.E.P., of InSb.

The performance of InSb detector may be described by its signal-to-noise ratio for an incident radiation. Therefore the signal current generated by the radiation of  $F(\lambda)$  watts/ $\mu\text{m}$  must be found.

Each photon of wavelength  $\lambda$  incident on the detector has a quantum energy of  $hc/\lambda$  and liberates an amount of charge  $e$  with a spectral quantum efficiency of  $\eta(\lambda)$ . Thus the total amount of radiation will generate a total signal current in a filter bandwidth  $d\lambda$ ,

$$I_s = \int_0^{\infty} F(\lambda) \frac{\lambda}{hc} e \eta(\lambda) d\lambda \quad (2.22)$$

where  $h$  is Planck's constant and  $c$  is the velocity of light.

The quantum efficiency is independent of wavelength in the  $1 - 6.2 \mu\text{m}$  range. Then the signal current for a given monochromatic

incident power, P in watts, is

$$I_s = \lambda \eta P \frac{e}{hc} \quad (2.23)$$

where e, h, and c are in SI units and  $\lambda$  in microns.

Therefore by substituting the appropriate values in equation (2.23) we have

$$I_s = \frac{V_s}{R_D} = \frac{\lambda \eta P}{1.24} \quad (2.24)$$

Since the detector is operated at 77 K, the Johnson noise voltage given above can be reduced to

$$V_n = 65.2 \times 10^{-12} \left( \Delta f R_D \frac{T}{77} \right)^{\frac{1}{2}} \quad (2.25)$$

Thus the detector N.E.P., the radiant power for which the signal voltage is equal to the noise voltage for an electrical bandwidth of 1 Hz is

$$\text{N.E.P.} = \frac{8.1 \times 10^{-11}}{\lambda \eta R_D^{\frac{1}{2}}} \left( \frac{T}{77} \right)^{\frac{1}{2}} \quad (2.26)$$

It can be easily seen that for operation at 77 K, the N.E.P. improves as  $R_D^{\frac{1}{2}}$ . From the above the theoretical N.E.P. at 77 K can be calculated.

If  $\eta = 0.6$  and  $R_D = 25 \text{ M}\Omega$ , then at  $2.2 \mu\text{m}$  wavelength, the N.E.P. is  $1.2 \times 10^{-14} \text{ watts/Hz}^{\frac{1}{2}}$ .

On the other hand the resistance of the detector may be increased by cooling to 63 K. Further improvements in the resistance can be made by J flashing. We measure  $R_D' = 100 \text{ M}\Omega$  at this temperature. Then the N.E.P. at  $2.2 \mu\text{m}$  is found to be  $5.6 \times 10^{-15} \text{ watts/Hz}^{\frac{1}{2}}$ .

The theoretical N.E.P. of the detector depends entirely on the operating temperature, detector resistance, and the quantum

efficiency.

Laboratory and telescope performance of InSb.

A simple device which can be mounted on the opposite side of the photometer from the eyepiece, replacing the chopper, was used as the blackbody calibration source for laboratory testing of the detectors. It consists of a rotating modulator and a  $45^\circ$  coated mirror fixed on the base of the blackbody source. This  $45^\circ$  mirror reflects the chopped source signal on to the detector built in the cryostat. To control the flux incident on the detector a variable aperture is placed between the source and the rotating modulator. The amount of flux seen by the detector is the difference in flux between the aperture area at room temperature and at the source temperature. Since the room temperature is negligible the flux seen from the aperture is that at the source temperature only. The test was carried out by using a soldering iron with a concave tip as the blackbody source. The aperture size used was known, and the distance between the aperture and the detector was measured. From these parameters and the temperature of the soldering iron the amount of flux seen by the detector was calculated. For measurements of the InSb detector results were as below:

Blackbody source temperature	=	643 K
Aperture size	=	0.1 cm
Detector area	=	0.01 cm <sup>2</sup>
Detector distance	=	32.4 cm
Filter bandwidth	=	0.40 $\mu$ m
Filter effective wavelength	=	2.2 $\mu$ m

Thus, the flux seen by the detector was found to be  $2.2 \times 10^{-10}$  watts.

Output signal and noise of the InSb detector can be both measured

on a PSD. Then from equation (2.3), the N.E.P. of the detector, at 77 K, was  $2.1 \times 10^{-14}$  watts/Hz $^{\frac{1}{2}}$ . At an operating temperature of 63 K for the InSb detector the N.E.P. was found to be  $9.4 \times 10^{-15}$  watts/Hz $^{\frac{1}{2}}$ .

The signal-to-noise ratio of the InSb detector, and thus its effective N.E.P., may be calculated from observed stellar measurements. For this reason a calibration star and sky background were alternately observed using a single beam device. The signal measured,  $S$ , was the difference between average readings of  $t$  seconds integration time with the star and the background. The noise  $N$ , may be taken as the standard deviation of the background readings. Thus the signal-to-noise ratio  $S/N$ , in  $t$  seconds, was found. The  $S/N$  ratio is then reduced to a 1 Hz bandwidth.

The flux  $F(\lambda)$ , from the calibration star observed, can be calculated from its known magnitude at  $\lambda$  microns and the absolute calibration in watts per  $\text{cm}^2$  micron. Hence the flux seen by the detector in watts is

$$f = F_{\lambda} A_T d\lambda \quad (2.27)$$

where  $A_T$  is the area of the telescope and  $d\lambda$  the bandwidth of the filter used. This flux corresponds to a signal-to-noise ratio reduced to a 1 Hz bandwidth. Thus, the N.E.P. of the detector can be calculated from the known signal-to-noise ratio.  $\alpha$  Vir (BS.5056) was observed as a calibration star. Its K magnitude is given by Johnson et al. (1966) as 1.68 mag. The mean signal measured was 31000 counts per 4 seconds with the coherent filter in. The standard deviation of the background readings with the coherent filter in was 7 counts per 4 seconds (rms). Thus, the  $S/N$  ratio reduced to 1 Hz bandwidth was found to be 1300. On the other hand, the flux on the detector

calculated was  $5 \times 10^{-11}$  watts. Consequently, the N.E.P. of the detector was found to be  $4 \times 10^{-14}$  watts/Hz $^{\frac{1}{2}}$ .

More recently we have installed an InSb detector bought from the SBRC. This has a maximum resistance of 5000 M $\Omega$  when flashed and cooled to 63 $^{\circ}$ K. The N.E.P. is considerably better compared with the Barnes detector, decreasing as would be expected by the square root of the resistance.

#### B. The Photometer

An infrared photometer which is specially designed for attachment to the telescope consists of optical components, the chopping equipment, and the cryostat contained in a framework of light-weight material such as aluminium.

The photometer designed and built in Leicester is of the conventional form and was used at the Cabezón Observatory in Tenerife. It is attached to the 60" British IR telescope behind the primary mirror by a ring of bolts. The radiation beam which is collected immediately from the secondary mirror, enters the photometer and is folded through 180 $^{\circ}$  by two 45 $^{\circ}$  mirrors. The first 45 $^{\circ}$  mirror, which reflects the infrared radiation beam but transmits visible radiation to an eyepiece, was made as a beam splitter. A gold coated glass was used for this purpose. The transmitted visible beam goes to a standard 45 $^{\circ}$  plane mirror and is reflected to the guiding eyepiece mounted on the side of the photometer frame. The second 45 $^{\circ}$  mirror is the sky chopper which will be described later in this chapter. The reflected infrared beam from the chopper passes to the outer window of the cryostat placed above the chopper and then to the detector built inside the cryostat.

The position of the guiding eyepiece is adjustable using

setting screws. It has an angular field of view of 4.4 arcmin. in a 60" telescope. The illuminated graticule placed in front of the eyepiece has two parallel horizontal lines and a vertical line. The single vertical line is in the centre of the field of view and the distance between two horizontal lines is chosen to correspond with the location of the two beams reflected by the chopper.

In designing an infrared photometer, one should keep as an important criterion the achievement of the maximum possible source signal incident on the detector. Misalignment in the photometer can result in loss of signal from the source. An initial alignment of the photometer before mounting on the telescope can be done with a simple device consisting of a framework holding a concave mirror at one end and a pin-hole light source at the other. First, it is mounted inside the photometer above the beam splitter, then with the help of a ground-glass plate marked with a cross and placed at the position that the detector would take, the pin-hole can be easily focused on the cross by moving the device up or down in the photometer. This alignment device is mounted parallel to the incident radiation beam. The chopper and the gold mirror are set at  $45^{\circ}$ . The necessary adjustment of the eyepiece is then made with setting screws, for focusing the pin-hole image on one of the graticule crosses.

When the ground-glass plate is replaced by the detector, a final alignment can be made by maximising the signal from the pin-hole light if necessary. The ground-glass plate is also used to focus the telescope on a star when the photometer is attached to the telescope.

A cryostat room is built to hold the cryostat above the sky chopper. Below the cryostat room are mounted the room

temperature filter wheel and the polarimeter. The filter wheel is a rotating disk with eight apertures to hold filters. The disk locks into position by means of a clip, therefore different wavelength filters can be used at any desired time. The polarimeter can be screwed to the base of the cryostat room when the photometer is used for polarimetric measurements.

The photometer viewed from side and top sections is shown in Figure 2.3 (a and b). The whole framework of the photometer is made of duralumin, weighs approximately 20 kg, and measures 28".5 high and 8" wide.

#### C. The Cryostat

In order to cool the detector to the required temperature, low temperature coolants, which must be kept in cryostats, are used. In a cryostat, the container for the coolant is isolated from external heat by a vacuum.

The operating temperature of the detector can be chosen by the availability of low temperature coolants. The most commonly used coolants are liquid nitrogen and liquid helium. Liquid nitrogen under a pressure of 760 mm Hg boils at 77.3 K. The boiling temperature of liquid helium under standard atmospheric pressure is 4.2 K.

The cryostat which has been used with the photometer is a nitrogen cooled cryostat. The nitrogen container is cylindrical, constructed of brass. It is welded on the end of a thin stainless steel neck. The detector was mounted on the base of the container such that it was in good thermal contact with the coolant. This container is enclosed in an aluminium casing, the top and base of which are sealed with O rings. There is a small hole in this base

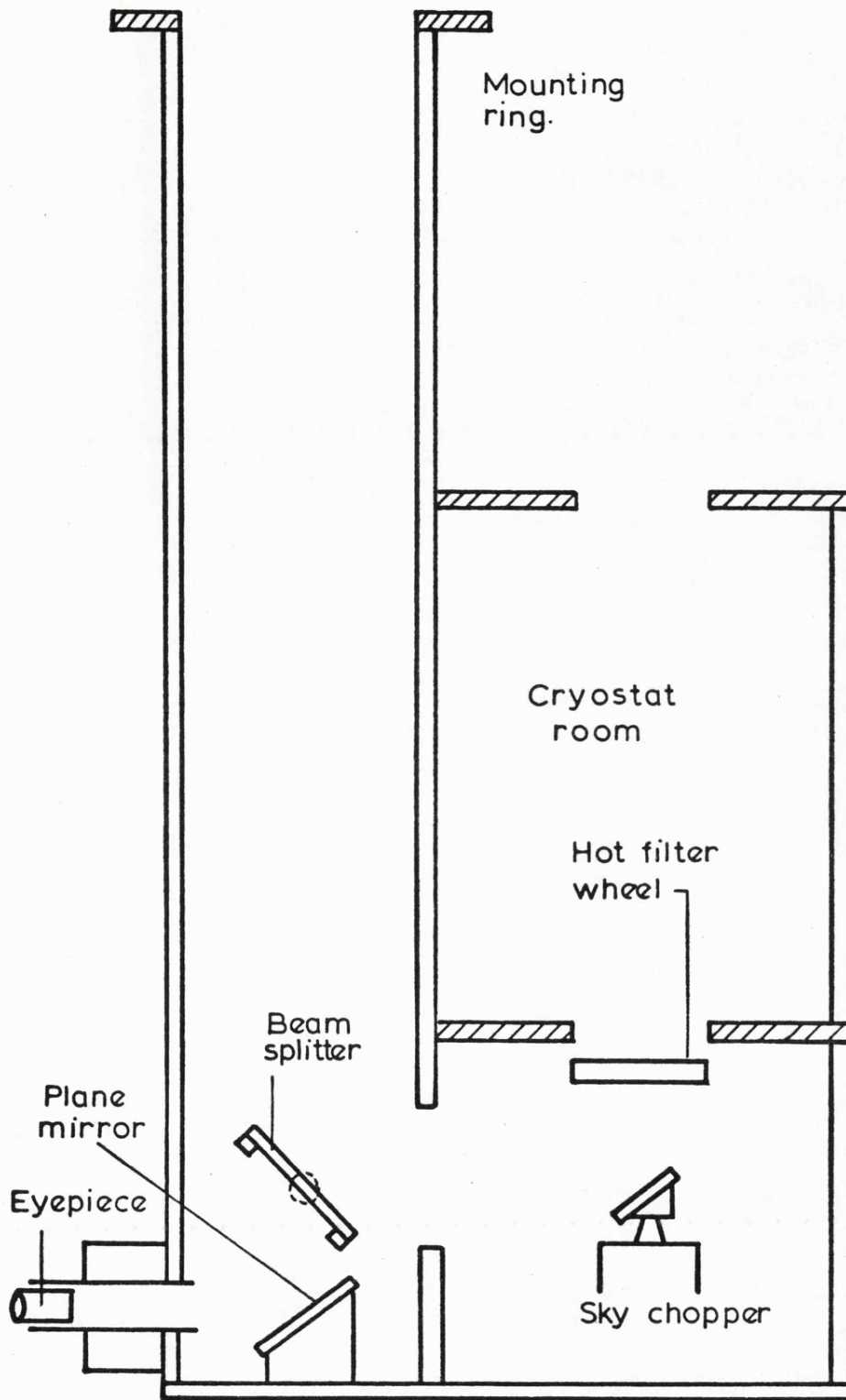


Figure 2.3a The photometer ( side section )

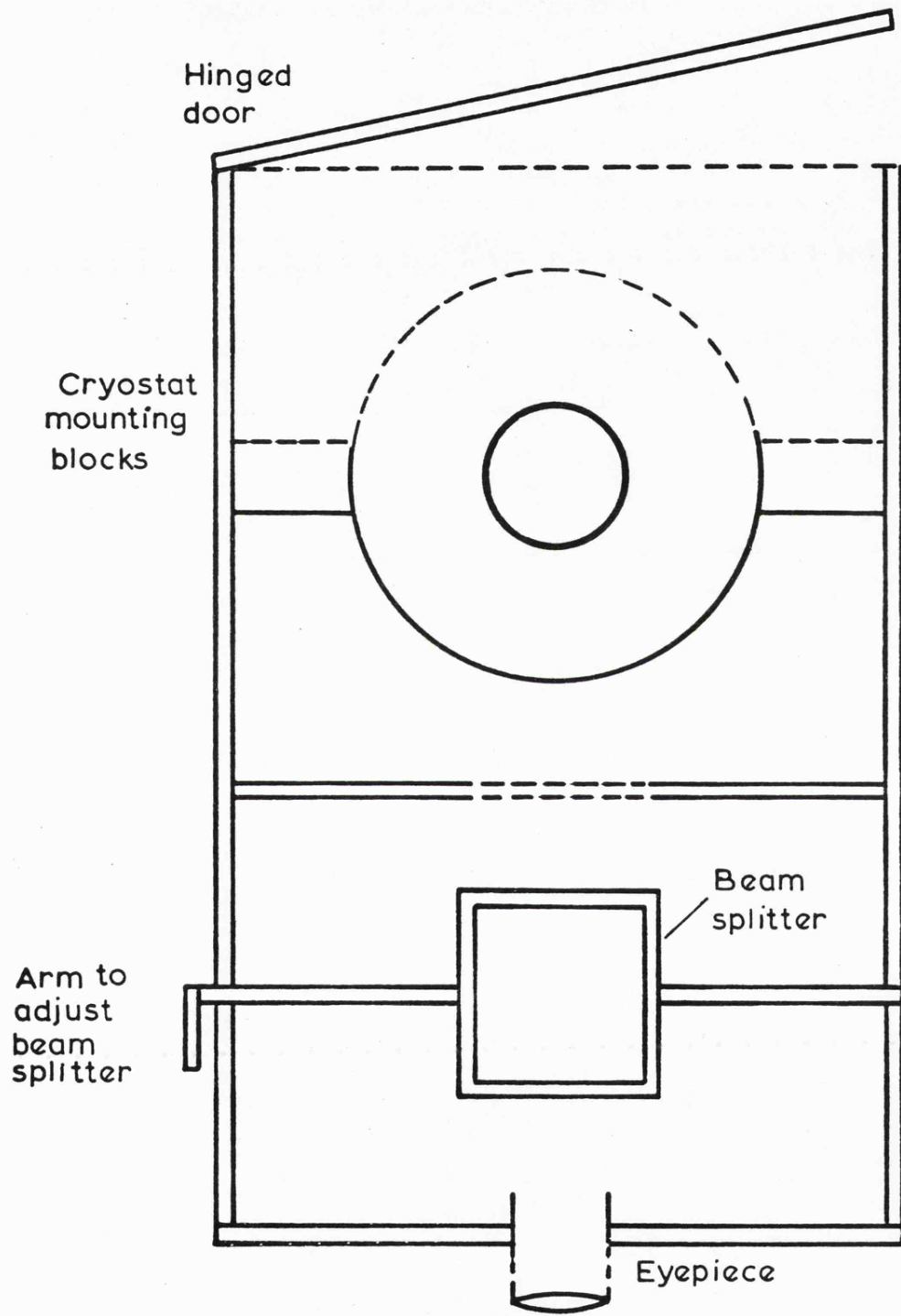


Figure 2.3b The photometer (top section)

provided for mounting a window. The window material used was  $\text{CaF}_2$ .

The detector bias and signal leads were taken through the top of the cryostat to the preamplifier and bias voltage source. The preamplifier was mounted on the side of the cryostat.

The entire volume outside the nitrogen container is evacuated to about  $10^{-5}$  torr. A few grams of activated charcoal are stuck with araldite to the nitrogen container. These act as a getter to maintain a very good vacuum when the system is cooled.

Below the Fabry lens are mounted the cold interference filters and the focal plane aperture stops (ranging from  $\frac{1}{2}$  to 5 mm). These are both mounted in, or contained in, wheels which may be rotated from outside the cryostat by means of rods and gear wheels.

The cryostat viewed from side and top sections is illustrated in Figure 2.4 (a and b).

#### D. Choppers

There are three most important reasons for using an optical modulator or a chopper in the path of the incident radiation with an infrared photometer. A chopper is included:

- (i) To provide an alternating input and output signal to and from the detector.
- (ii) To decrease certain types of noise (i.e.  $1/f$  noise).
- (iii) To produce background cancellation.

The amount of infrared radiant flux from most of the stellar sources incident on the detector is very small. Therefore the signal from the detector must go through a process of amplification. Thus it is very much easier to amplify an alternating signal than a direct signal.

If  $1/f$  noise is a serious problem the signal-to-noise ratio

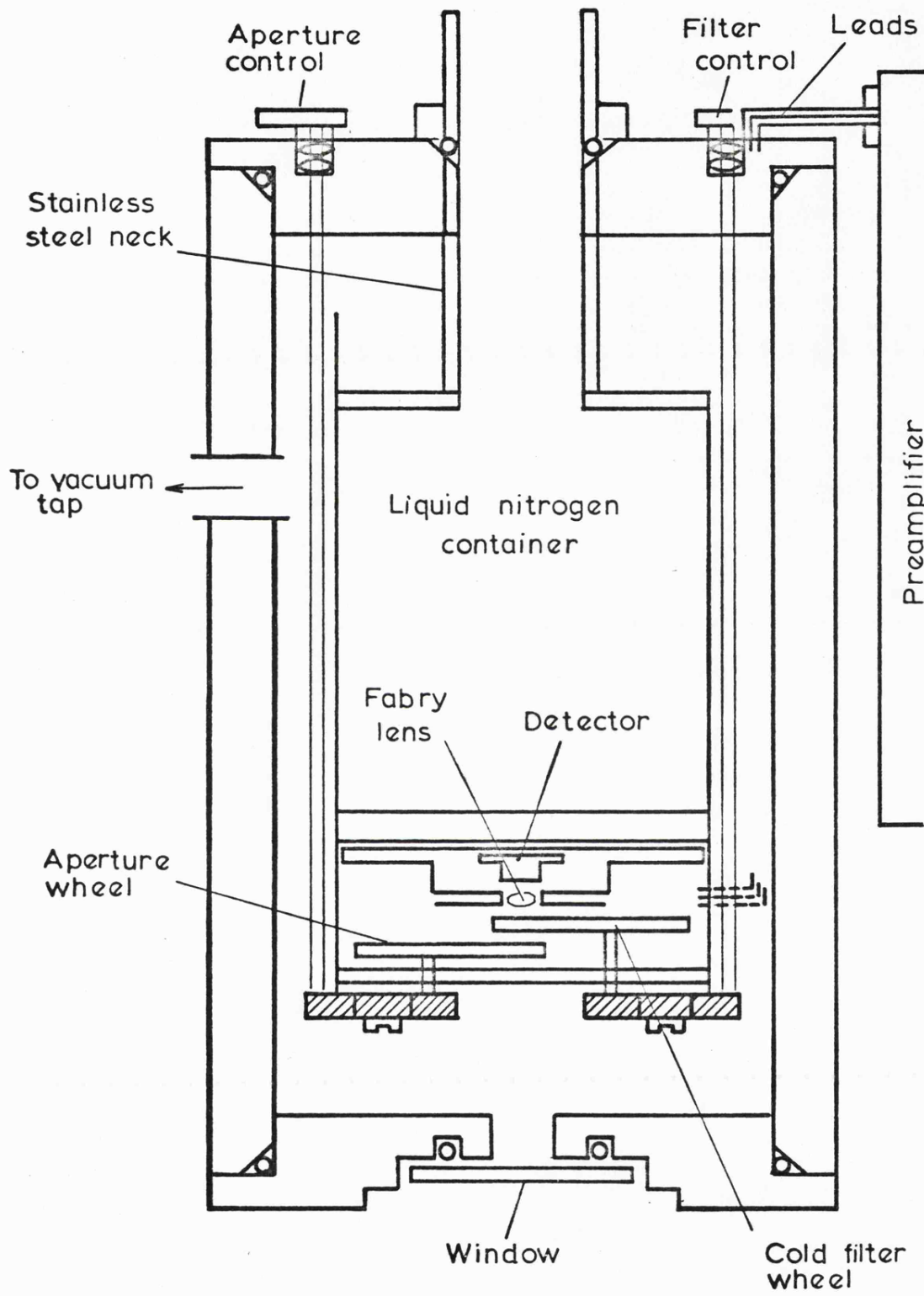


Figure 2.4 a The liquid nitrogen cryostat  
(side section)

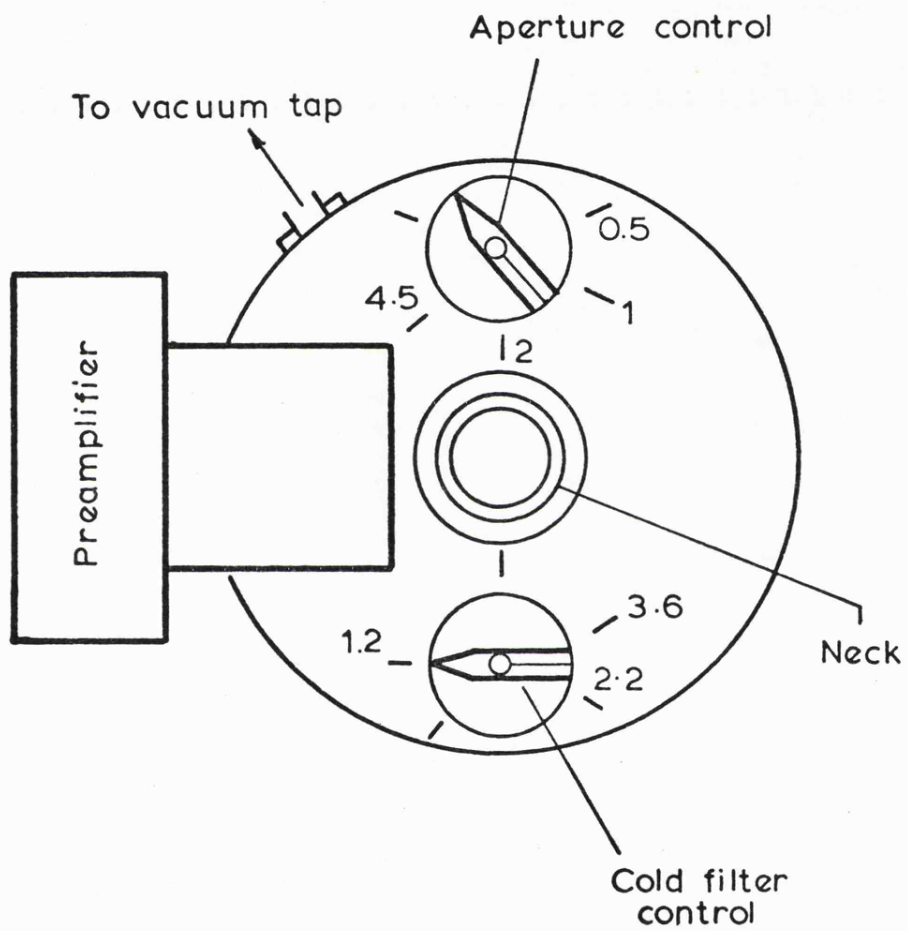


Figure 2.4b The liquid nitrogen cryostat  
(top section)

may be improved by using fast chopping frequencies.

At long wavelengths, for example at  $10 \mu\text{m}$ , all the photometer components, telescope mirrors and surroundings, and the sky, will emit strongly. This background radiation can be greater than the signal by many orders of magnitude. Thus the use of a chopping mechanism will eventually suppress unwanted signals from the background. If the detector sees only the sky plus star and the telescope mirrors, then subtracting the sky background will produce sky cancellation. This can be done by first imaging the sky plus star on the detector, then just a neighbouring area of sky.

Three different techniques are used to discriminate against unwanted background radiations.

(i) To nod the primary mirror of the telescope at 10 Hz or greater frequencies.

(ii) To nod the secondary mirror at frequencies up to 20 Hz.

(iii) To use a focal-plane chopping mechanism.

Nodding the telescope mirrors at the required frequencies is not practical when one considers the size of the flux collectors. But by nodding the primary mirror the detector always sees the same parts of the telescope mirrors. This is advantageous for producing a sky cancellation. Nodding the secondary mirror of the telescope has the disadvantage that the detector sees a different part of the primary mirror in each beam.

The 60" telescope used for this project has no nodding facilities. Therefore, the third technique which is called focal-plane chopping was used with the photometer. Further discussion on the focal-plane chopping methods and the choppers used with our photometer will be given next.

At short infrared wavelengths for measuring large signals, such as those from the calibration source in the laboratory, one method makes use of a rotating disk of equally spaced open and opaque segments. When the disk rotates the detector sees source and disk material alternately. The disk is called a rotating chopper. However, at longer wavelengths, the method has two disadvantages; first the emission from the disk material itself becomes an unwanted signal; and second, sky background radiation becomes important compared to the source radiation.

The second method uses a rotating split-level mirror in the form of a disk set at  $45^\circ$ . The top and side sections of the rotating split-level chopper are shown in Figure 2.5 (a and b). When the disk rotates the detector sees the upper and lower levels of the mirror alternately. The size of the throw of the beam will then depend on the thickness of the upper level of the disk. A sufficiently high frequency chop can be obtained with the rotating mirror. The chopped signal from the detector is a series of square waves at the chopping frequency, equal to the number of segments of the disk multiplied by the rotational frequency of the mirror itself. However, the disadvantage of this method is that the reflections from the edge of the upper mirror produce a large offset. Resulting distortions in the square wave can be seen as the peaks at the corners. At  $2.2 \mu\text{m}$  and shorter wavelengths this method is employed perfectly. But at longer wavelengths the effect of the edge reflections increases with wavelength.

In order to get rid of the effect of edge reflections, a third method is introduced. A single mirror vibrating from one position to another is placed in the position of the second  $45^\circ$  mirror of the photometer, mounted on the end of a solenoid vibrator

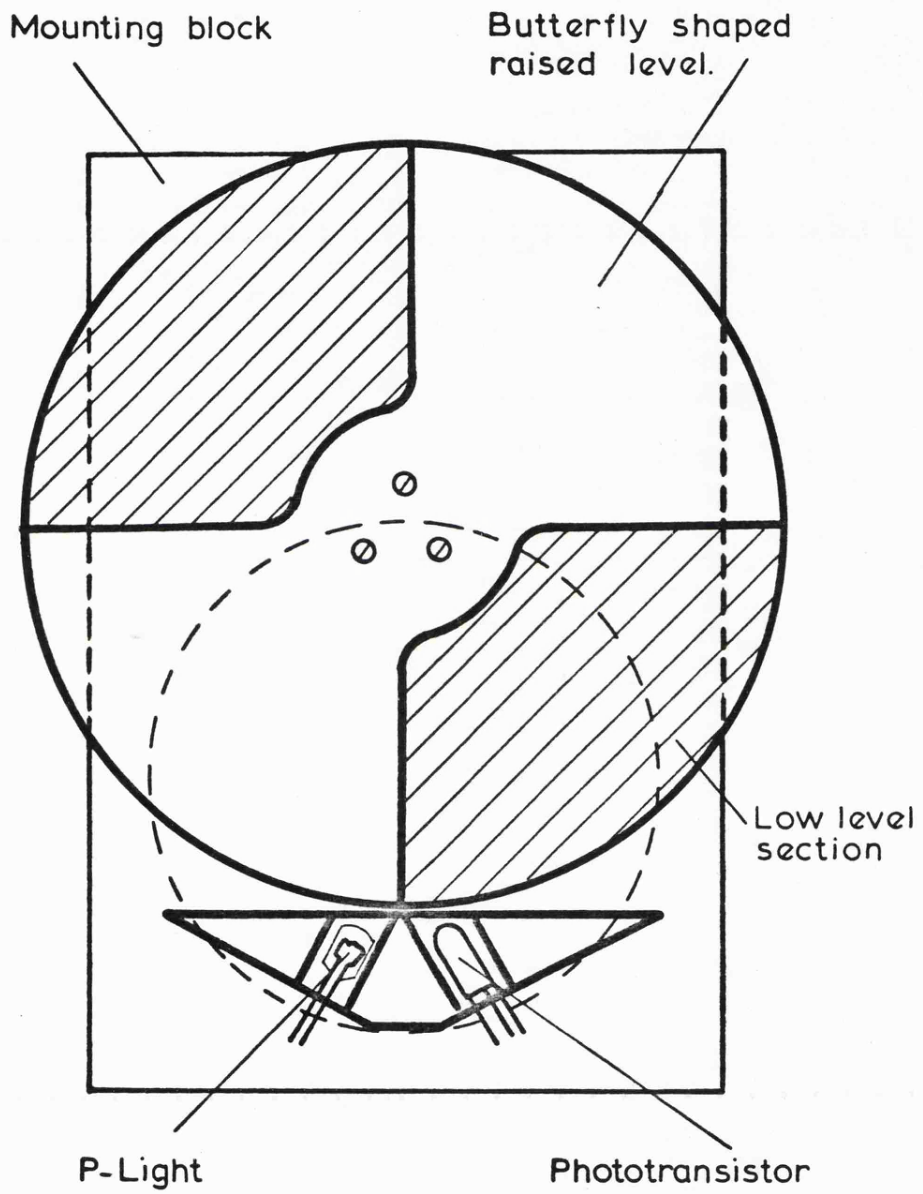


Figure 2.5a Rotating split-level chopper-top section

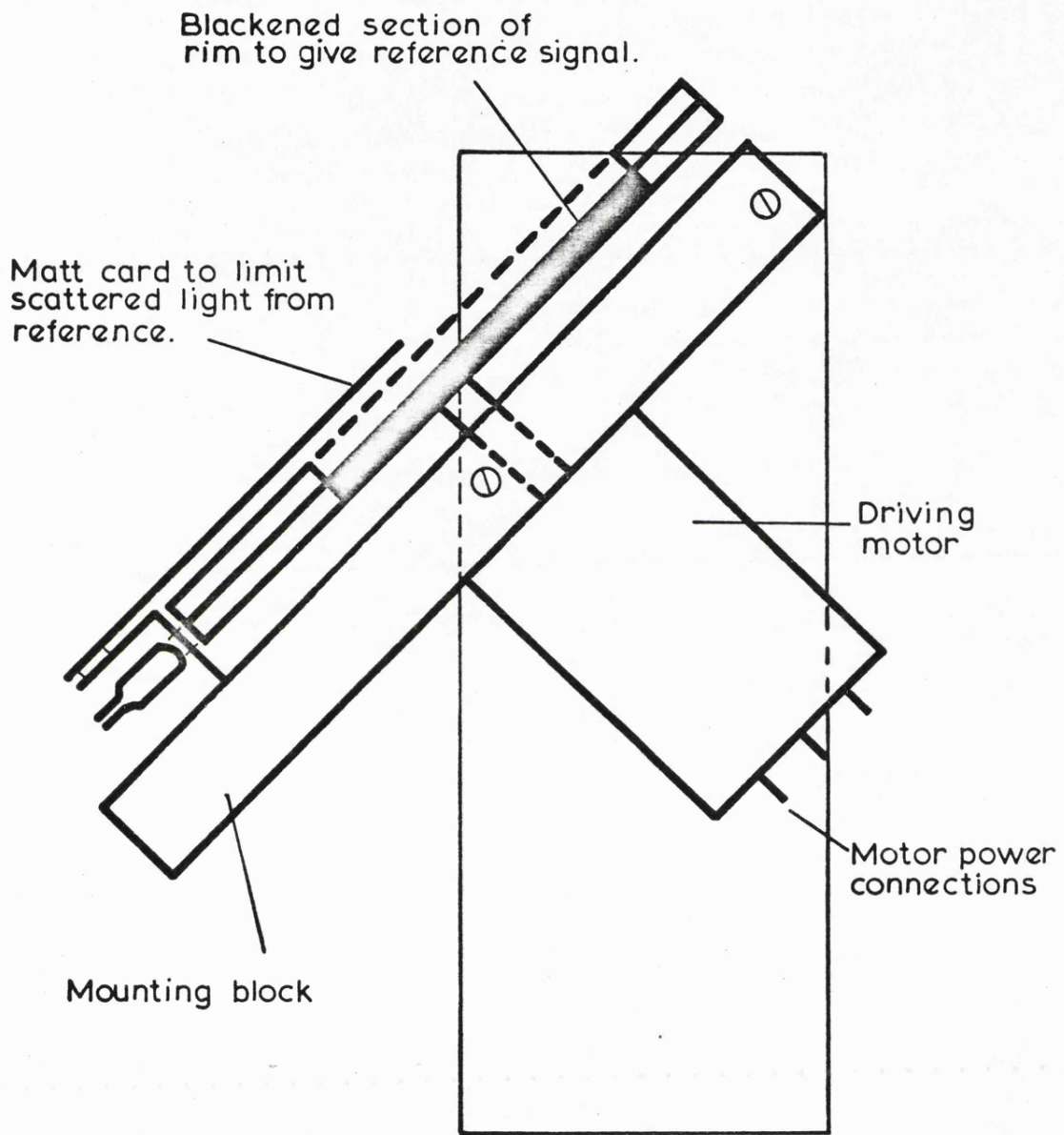


Figure 2.5b Rotating split-level chopper - side section

manufactured by Ling Dynamics Ltd. If the mirror and its mount have a low mass it is possible to get a good square motion up to frequencies of 20 Hz by simply applying a square wave voltage to the solenoid.

Greater amplitudes and higher frequencies can be obtained by using a servo system. However this tends to shorten the operating life of the solenoid. Thus for simplicity and reliability we use the unservoed method.

It is important that the movement of the mirror should be parallel to the optic axis of the detector, since the detector then sees the minimum movement across the primary mirror of the telescope. Larger chop amplitudes for smaller physical motion can be obtained by moving the chopper mirror as an optical lever, but this makes the detector see very large movements across the primary mirror. Figure 2.6 shows the vibrating chopper.

All three methods have been used with our photometer to produce the square wave of the chopped signal.

#### E. Filters, Windows and Lenses

In infrared photometry, the purpose of the optical components is to collect radiation of the required wavelength and deliver it to the detector built inside the cryostat. A window which transmits all the required wavelengths is mounted at the bottom of this cryostat. A single required wavelength can be selected by using bandpass filters placed either inside or outside the cryostat. There are many window materials that transmit infrared radiation. A detailed discussion on such materials and their physical properties has been given by Hudson (1969). He makes a list of 16 preferred optical materials for the infrared. The

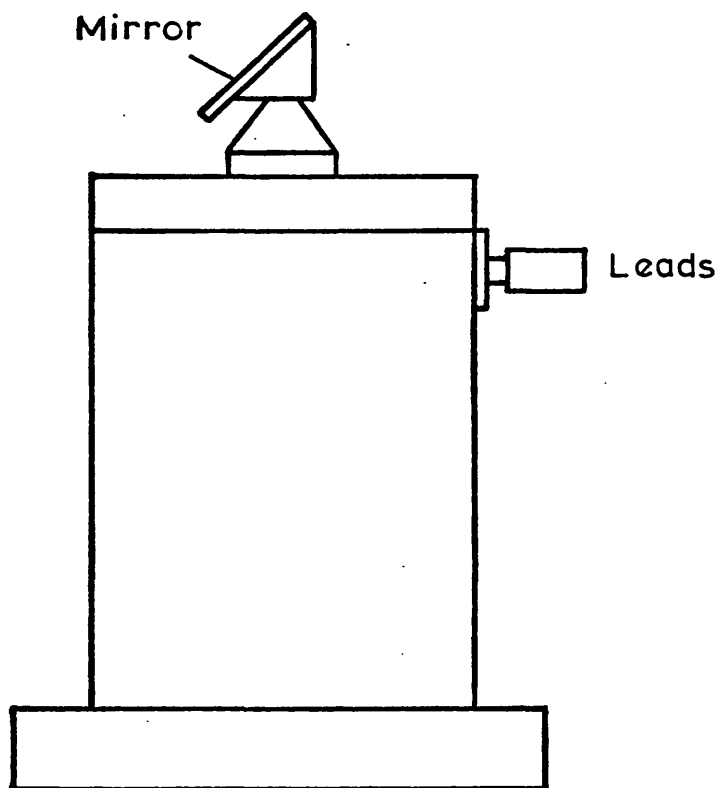


Figure 2.6 The vibrating chopper

spectral range given in the list is described as the wavelength interval over which a material of 2 mm thick has 10 per cent or more transmission. The transmittances of optical materials can be increased by antireflection coating. Some of the incident radiant flux is reflected from the surface of materials. To eliminate the reflection at a given wavelength an antireflection coating can be used. Hudson (1969) and Cox et al. (1961) have listed some of the useful materials for coatings.

The transmission curves for some IRTRAN materials, each of which represent a well known material (shown in parentheses), are shown in Figure 2.7. The wavelength range has been extended to the visible part of the spectrum to show the transmittance of each material at its short-cutoff-wavelength.

The window material of our cryostat is made of  $\text{CaF}_2$  which has a transmittance of greater than 80% (Figure 2.7) over a wide range of wavelengths compared to the other IRTRAN materials.

There are mainly two types of filters. The absorption filter transmits the required wavelength but absorbs unwanted ones. The reflection or interference filter reflects unwanted wavelengths but transmits the required one. Today interference filters are widely used in near infrared photometry. The spectral transmission curve of any filter describes its characteristics. The spectral bandwidth of the filter is defined as the wavelength interval transmitted by the filter in terms of the centre wavelength  $\lambda_0$ . Interference filters can be manufactured to give bandwidths  $\Delta\lambda/\lambda_0$  of 0.02 with over 80% transmission for the region from 1 to 13  $\mu\text{m}$ . Temperature and angle of incidence are important test conditions of spectral performance of any filter always given along with its spectral transmission curve. Baker and Yen (1967) have discussed the

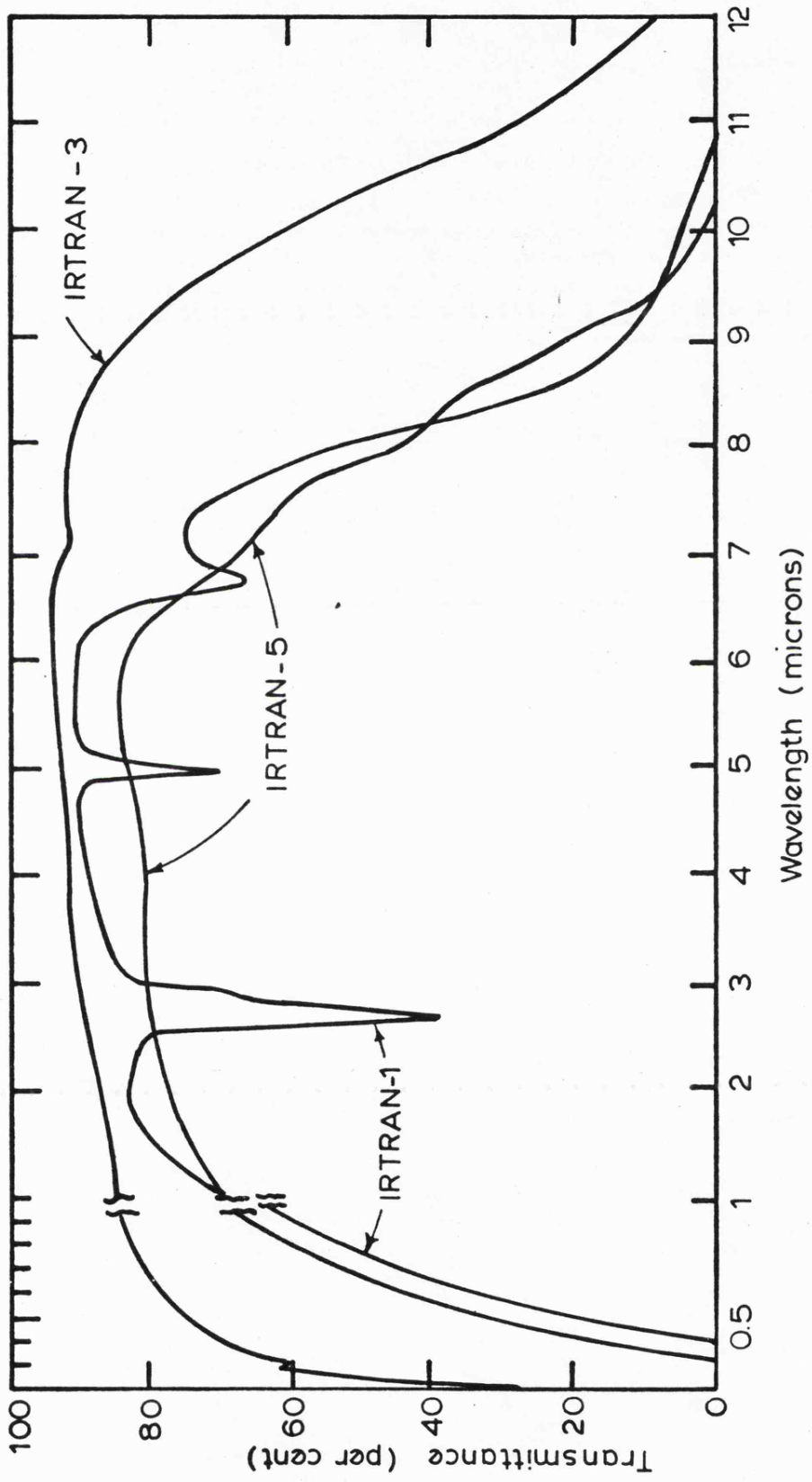


**Figure 2.7** Transmission curves of common optical materials.  
IRTRAN - 3 (Ca F<sub>2</sub>), sample thickness 2 mm

effects of the variation of these two conditions on infrared filter characteristics. They found that the filters shift towards shorter wavelengths if the angle of incidence is increased or the temperature decreased. The angle of incidence is measured from a normal to the filter surface. For cone angles less than  $15^{\circ}$ , the angle effect is insignificant. The peak transmission also decreases with an increase in cone angle for focused radiation.

Interference filters are made by the vacuum-deposition of single- or multi-layers of material on a convenient optical material. Most manufacturers of filters use computer programs for the designing equations of any interference filter. The theory of interference filters has been summarised by Jamieson et al. (1963).

Of the two previously mentioned filter wheels the first, mounted below the cryostat room, holds up to eight filters at room temperature, and the second which was held in the cryostat, can be used with four cooled filters. One of the eight apertures in the hot filter wheel is left empty. When the cold filters are in use, this empty aperture is locked into position. The arrangement of the filters employed in the two filter wheels is given in Table 2.1. Filter bandwidths are shown in brackets.

Three of the four filters shown in Table 2.1 have been used for our stellar measurements. These are 1.2, 2.2, and  $3.6 \mu\text{m}$  filters of which transmission curves are shown in Figure 2.8.

The OW1 glass used in the fourth cold filter position cuts off all wavelengths longer than  $2.5 \mu\text{m}$ . Therefore it can be satisfactorily used in combination with a hot  $1.2 \mu\text{m}$  filter.

One of the factors which influences the accuracy of stellar photometry is a systematic error caused by the movement of the star image over the detector cell due to guiding errors and seeing.

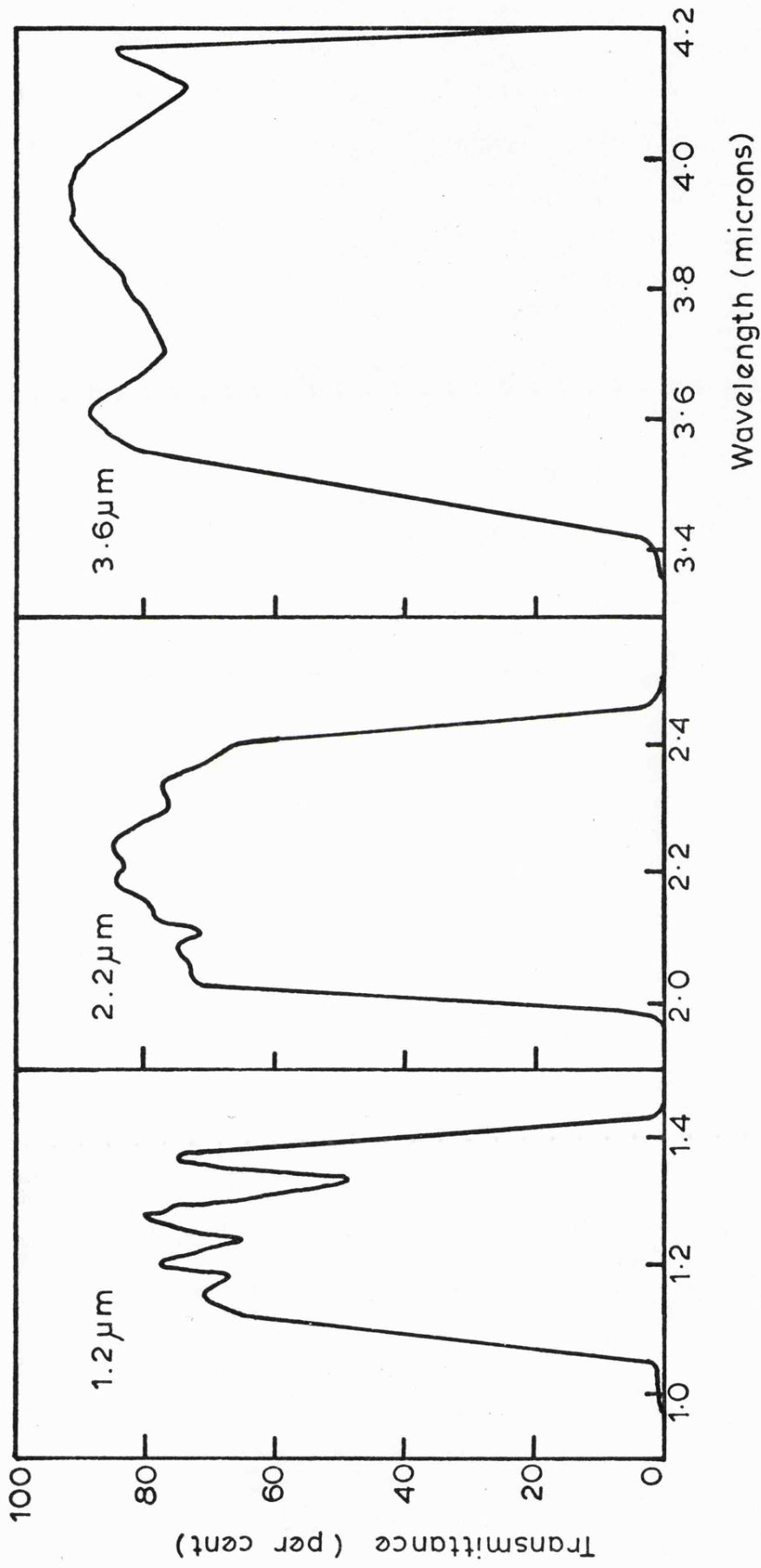


Figure 2.8 Transmission curves of the filters

Table 2.1

Filter arrangement in the two filter wheels

Filter position		Hot Filter wheel	Cold Filter wheel
Hot	Cold	Wavelength ( $\mu\text{m}$ )	Wavelength ( $\mu\text{m}$ )
1	1	Empty	2.2 (0.49)
1	2	Empty	3.6 (0.49)
1	3	Empty	4.8 (0.7)
2	4	1.2 (0.12)	OW1 Glass

This might be caused by the photometer design in which the star image is focused directly onto the detector. The response of the detector is probably not uniform over its whole area. Thus, as the star image moves across the cell, the signal from the detector will change. This problem also occurs in visual photometry. The response of a photomultiplier varies over its photocathode area. The usual solution is to use a Fabry lens which defocuses the star image onto the cell. With the Fabry lens system the image of the primary mirror is formed on the detector, so that the star light is defocused over the detector area. The Fabry lens can be placed between the detector and a stop. The stop with a known aperture is at the actual position of the star image. Thus the star image can move across the aperture without affecting the distribution of light on the detector, and consequently the noise introduced by seeing, guiding errors, and movement of the image across the detector area is eliminated. The only problem of using Fabry lens system in infrared photometry seems to be that because infrared detectors are very small ( $\sim 1 \text{ mm} \times 1 \text{ mm}$ ) the Fabry lens needs to have a very small  $f$  number (usually  $< 3$ ). Germanium, silicon, KRS5, and Irtran 2 (Zn S) are commonly used materials suitable for infrared lenses.

The Fabry lens used in our photometer is made of  $\text{CaF}_2$  of which a transmission curve has previously been shown in Figure 2.7. Figure 2.9 illustrates the Fabry lens system alone.

#### F. Electronics

This section is concerned with the electronic devices of the infrared system which are employed to achieve the final display of the signal for an observer. A radiant flux of the source

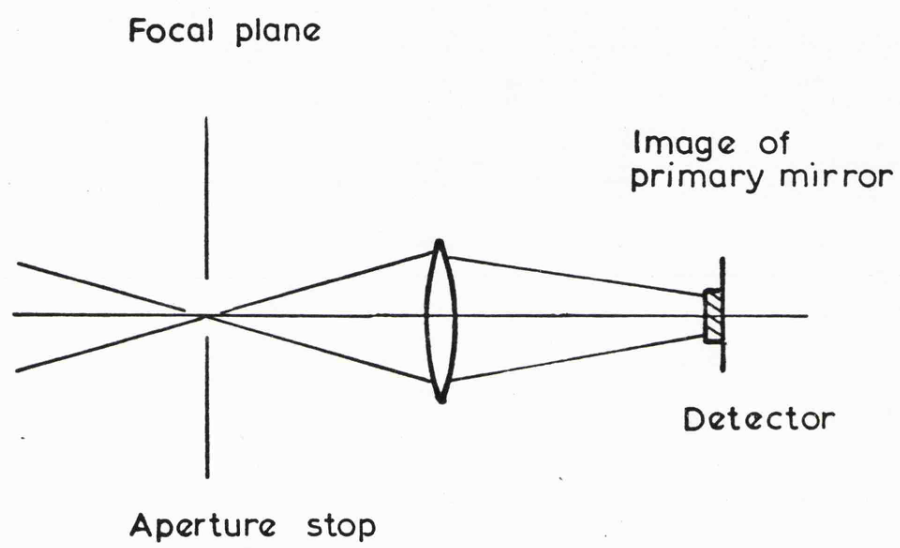


Figure 2.9 Fabry lens system

collected by the optical components of the detection system is converted to an electrical signal in the detector. Then the signal and the noise introduced in the detector are amplified in a preamplifier. The arrangement of this first amplifying stage, where the value of the signal-to-noise ratio is of great importance, should be such that the noise introduced is small compared to the detector noise.

Subsequent electronic operations are used to increase the signal-to-noise ratio by reducing the electrical bandwidth. Finally, the output is displayed in numbers.

A block diagram, Figure 2.10, shows the arrangement of the signal processing system. The operation of the system components will be described briefly in the following section.

(a) Preamplifier

The preamplifier is mounted on the side of the cryostat to avoid pick-up in long cables. It is built from a circuit by Hall et al. (1975) used with the InSb detector. The circuit diagram of the preamplifier is given in Figure 2.11. The function of the circuit is described in detail by Hall et al. (1975). Briefly the circuit aims to amplify the AC voltage from the detector while not allowing any DC current to pass through the detector. Thus there can be no  $1/f$  noise.

(b) Reference Signal Generator

For the rotating chopper a simple phototransistor-based device which consists of a 12 v L.E.S. bulb and the phototransistor mounted on a base against the edge of the chopper wheel was used to produce the reference signal. The phototransistor sees the light

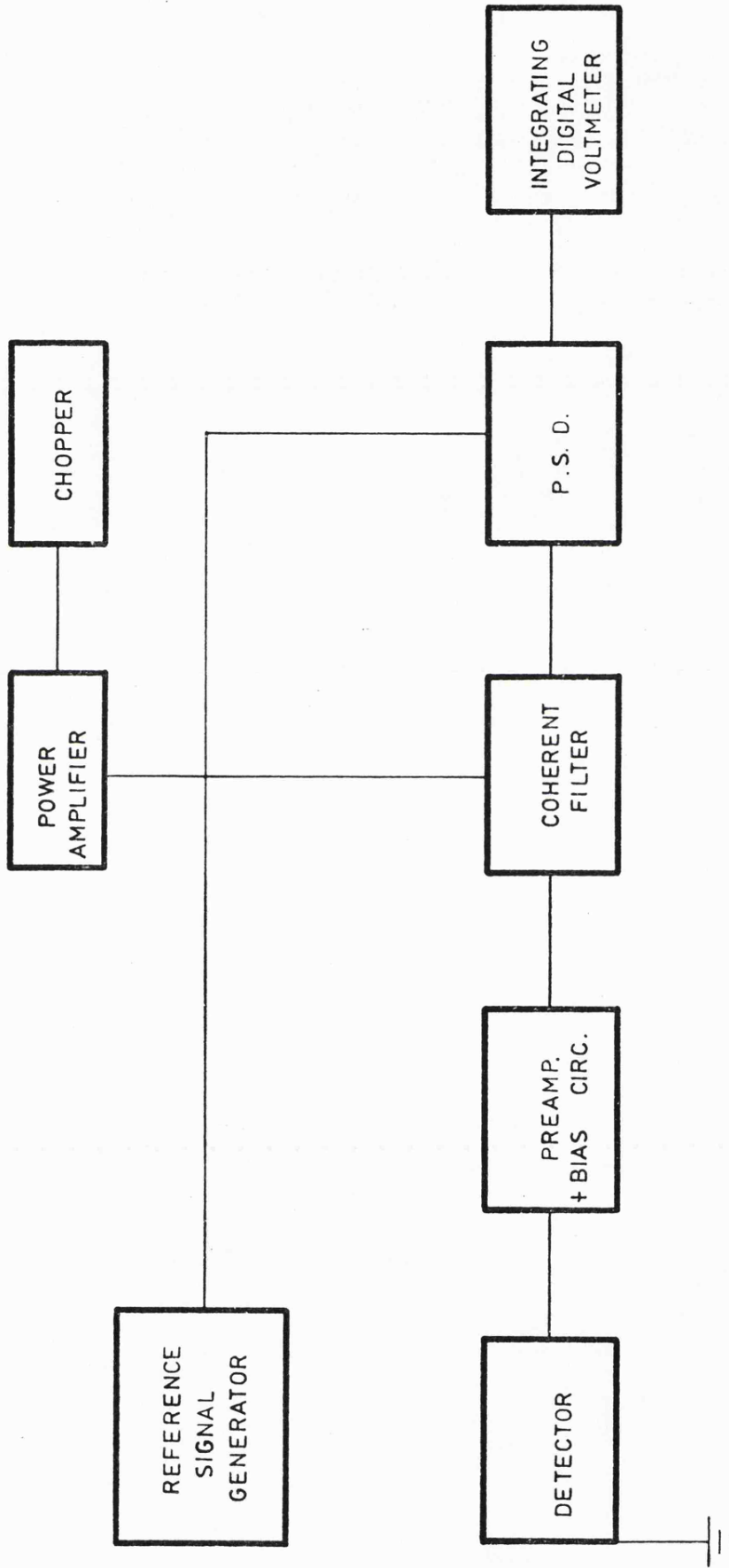


Figure 2.10 Block diagram of the signal processing system.

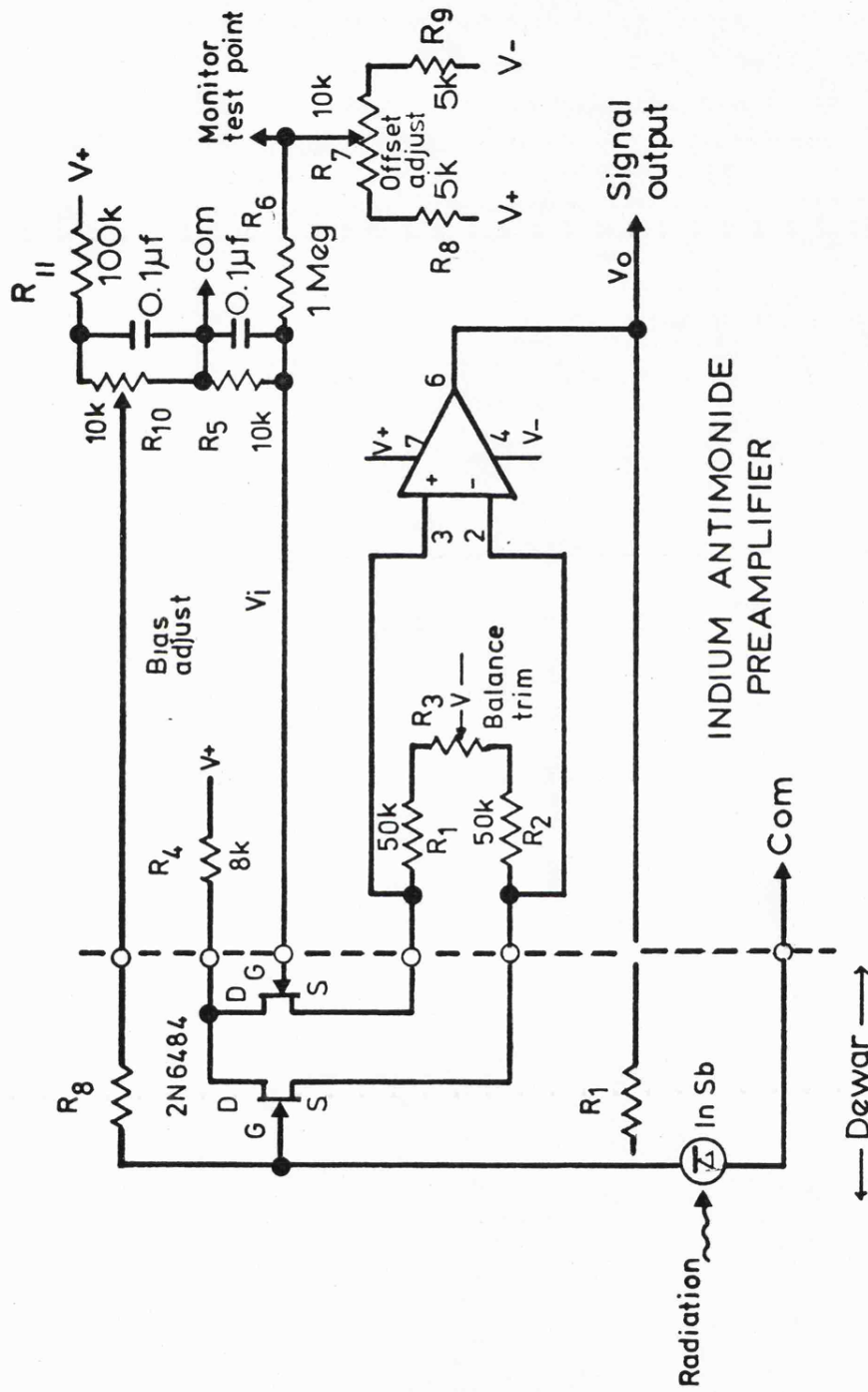


Figure 2.11 Detailed circuit diagram for In Sb preamplifier  
by Hall et al.(1975)

which is reflected from the wheel edge. The sections of the edge exactly corresponding to the upper segments of the disk mirror are painted black. Therefore, when the wheel rotates, the phototransistor sees the polished metal and the black sections of the edge alternately.

For the vibrating chopper the reference signal is taken directly from the squarewave generator via a phase shifter. The frequency used is  $12\frac{1}{2}$  Hz and is obtained by dividing down the mains frequency. This avoids beating with any AC pick-up.

(c) Coherent Filter

A coherent filter is used to limit the frequency bandwidth offered to the phase sensitive detector to 3 Hz. It also amplifies the signal by a factor of 100. This allows greater sensitivity without overloading the phase sensitive detector. This filter cannot be a simple tuned circuit since any drift in the chopping frequency would seriously change the gain. Thus the coherent filter requires a reference signal and acts as a 3 Hz bandwidth filter always centred on the reference frequency.

The coherent filter model used is a Brookdeal Type 467.

(d) Phase Sensitive Detector, P.S.D.

The output of the coherent filter is connected to a phase sensitive detector which gives a direct voltage output. The amplitude of the voltage output is proportional to the amplitude of the alternating input voltage at the same phase and frequency as the reference signal.

The output is smoothed by an RC circuit whose time constant  $\tau$  may be varied from  $10^{-3}$  sec to 30 sec.  $\tau$  is then effectively the

observation time. The disadvantage of setting the observation time by this method is that a time of approximately  $3\tau$  is required for the RC circuit to charge up before any observation can be made. To avoid this  $\tau$  is usually set at 300 ms and an integrating digital voltmeter is used to average signals over a period of, say, 10 seconds.

A Brookdeal model 411 P.S.D. was used for this purpose. Time constants from 1 ms to 10 s are available on this model.

(e) Integrating Digital Voltmeter, I.D.V.M.

The final output signal can be observed with a digital number display. For most of the stellar infrared sources, integration times of longer than 10 seconds are required to obtain a reasonable signal-to-noise ratio. The I.D.V.M. averages the output from P.S.D. for any desired time, usually 10 seconds in each channel.

The output from the I.D.V.M. may either be written down directly in a notebook, recorded on magnetic tape, or directed to the computer to be processed in real time.

The I.D.V.M. can count up and down, thus subtracting the signal of channel 2 from channel 1, to give a direct measure of the source signal. For normal photometry 10 sec up and down readings are repeated until a suitable signal-to-noise ratio is obtained. The noise is, of course, simply given by the r.m.s. deviation of the signals.

## CHAPTER 3

## OBSERVING TECHNIQUES

Since the discussion of the infrared photometer has been completed in the previous chapter, the aim in discussing observing techniques in this chapter is to present information concerning the methods for observing infrared radiation from the selected eclipsing binary systems.

A. Observing Program

It was necessary to make detailed observing programs before any observing session at the Cabezón Observatory from which the systems to be observed could easily be selected. To obtain sufficient observations of the stars and to provide complete light curves of the selected binary systems within a limited observing session, the time allocation for each system in one night's work must be carefully prepared. Since the phases of the light curve for any eclipsing binary system can be computed from the known light elements of the system, the preliminary time arrangement is made to combine observations over several periods to form a complete light curve. An eclipsing binary system with a short period of a few hours is a good candidate for observing in a single night.

Right Ascension ( $\alpha$ ) and Declination ( $\delta$ ) of the systems can be taken from any variable star catalogue as can their light elements. Then the observer must have finder charts that guide him to the regions of the sky required.

The General Catalogue of Variable Stars, GCVS, by Sternberg State Astronomical Institute of the Moscow State University and the Smithsonian Astrophysical Observatory, SAO, Star atlas of Reference

Stars have been primarily used for the above purposes. The expected phases of the light curve for every selected binary system were calculated by a computer program before every observing session.

B. Selecting Standard Stars

The choice of standard stars for use in magnitude calibration of binary systems from photometric observations is of paramount importance. When selecting standard stars for infrared photometry of binary systems, an observer should consider at least three essential points carefully:

(i) The standard star should be close to the binary system; this is not always possible however.

(ii) The infrared magnitudes of the standard star at required wavelengths should be known accurately.

(iii) The magnitudes of the standard star at infrared wavelengths should be reasonably bright.

If the standard star selected is sufficiently close to the binary system the airmass correction will be negligible.

During recent years there have been a number of multicolour photometric observations, including infrared wavelengths (near infrared). With more improvements being made to the photometric instruments, resulting in increased sensitivity of the detectors, more accurate infrared magnitudes of the stars have been found. The extensive multicolour photometry program of Johnson et al. (1966) is extremely useful for the photometric data, especially at near infrared wavelengths. The other major source of K magnitudes for bright stars is the California Institute of Technology Two-micron Sky Survey.

The adopted magnitudes of certain common standard stars

with their numbers in the Bright Star Catalogue are given in Table 3.1.

### C. Observing

To make observations a set of readings was taken on both the standard star and the binary system. The standard star was observed less frequently to permit continuous observations on the binary star.

Due to observing conditions, 10 - 40 second integration times were chosen in each channel. An integrating digital voltmeter (IDVM) was set to count up and down for 10 - 40 sec. The IDVM is operated manually as the beam switches from one channel to the other. To observe a star, it is first placed in channel A. The star signal measured in channel B is in antiphase with the reference signal. Thus the resultant reading of the star is (Reading A) - (Reading B). The number of readings in each set was usually 9.

For each set of readings the local time was recorded in the middle reading of each set. The local time as recorded during the observations was converted to Greenwich Standard Time, or Universal Time (UT).

### D. Data Reduction and Errors

The mean readings are proportional to the brightnesses of the two stars being compared.

In order to reduce the ratio of the brightnesses to the magnitudes, the well known formula;

$$m_{EB}(\lambda) - m_S(\lambda) = -2.5 \log_{10} \left[ \frac{A_{EB}(\lambda)}{A_S(\lambda)} \right] \quad (3.1)$$

is used where  $m_{EB}(\lambda)$  and  $m_S(\lambda)$  are the magnitudes of the eclipsing

Table 3.1

## Adopted Magnitudes of Standard Stars

Star	B.S.	1.2 $\mu\text{m}$ (J)	2.2 $\mu\text{m}$ (K)	3.6 $\mu\text{m}$ (L)
$\epsilon$ And	163	2.84	2.21	
$\alpha$ Aql	7557	0.39	0.26	0.21
$\alpha$ Ari	617	0.10	-0.64	-0.74
$\alpha$ Boo	5340	-2.18	-3.00	-3.14
$\beta$ Boo	5602	1.93	1.34	
$\alpha$ Cep	8162	2.11	1.96	1.85
$\alpha$ Cyg	7924	1.00	0.89	0.78
$\alpha$ CMa	2491	-1.34	-1.31	-1.29
$\alpha$ CMi	2943	-0.40	-0.64	-0.67
$\beta$ Gem	2990	-0.49	-1.09	-1.17
$\alpha$ Her	6406	-2.26	-3.51	-3.72
$\alpha$ Leo	3982	1.55	1.62	1.60
$\alpha$ Lyr	7001	0.02	0.02	-0.02
$\alpha$ Ori	2061	-3.00	-4.00	-4.30
$\alpha$ Tau	1457	-1.84	-2.81	-3.00

binary and the standard star respectively at wavelength  $\lambda$ , and  $A_{EB}(\lambda)$  and  $A_S(\lambda)$  are the mean readings of the eclipsing binary and the standard star respectively.

The error of each observation was taken as the standard deviation of the mean of the readings for each set. The reliability of a set of readings with a certain standard deviation was estimated.

The observed dates and times are first converted into Julian days and decimals of a day. Then heliocentric corrections are applied to the times of observations using appropriate tables by Landolt and Blondeau (1972).

The phases for the observed binary systems were calculated according to the ephemeris given in either GCVS or a recent publication on the binary. Because of the period change in some binary systems the most recent and reliable ephemeris was used.

The light curves were constructed by plotting the magnitudes of the stars observed against their calculated phases.

#### E. Atmospheric Corrections

One of the most serious limitations in ground-based infrared photometry results from the attenuation of radiant flux through the Earth's atmosphere. Water vapour, carbon dioxide and ozone are the major sources of infrared absorption. Fortunately nitrogen, oxygen and argon produce no absorption in the infrared. In order to maximise transmission of infrared radiation it is necessary to build ground-based observatories at high altitudes. On the other hand, infrared observers make use of high altitude vehicles, such as balloons, aircraft, rockets and satellites to make observations at wavelengths which would be impossible at ground level.

However a number of "infrared windows" exist where the

absorption in the infrared is greatly reduced, thus making ground-based observations possible. These windows do not necessarily permit total radiant flux to be detected. The atmospheric windows and the absorbing molecules are shown in Figure 3.1. These narrow transmission bands, or windows, are centred near  $1.2 \text{ m}\mu$  (J),  $1.65 \text{ m}\mu$  (H),  $2.2 \text{ m}\mu$  (K),  $3.6 \text{ m}\mu$  (L),  $4.8 \text{ m}\mu$  (M),  $10 \text{ m}\mu$  (N) - short to long wavebands corresponding to the letters given in brackets. Ground-based observations at longer wavelengths may be done under the good atmospheric conditions. These bands are at wavelengths around  $18 - 22 \mu\text{m}$ ,  $27 \mu\text{m}$ ,  $34 \mu\text{m}$ ,  $50 - 300 \mu\text{m}$ , and  $350 \mu\text{m}$ .

#### Atmospheric Extinction

Extinction in the Earth's atmosphere is a combination of two processes: absorption and scattering. These two processes weaken the radiation of different wavelengths passing through the atmosphere. The sources of infrared absorption in the atmosphere have already been discussed. The atmospheric particles and molecules are responsible for the scattering.

It is very important in infrared astronomy to make the necessary corrections to the observations of stars to account for this extinction.

The apparent magnitude  $m(\lambda)$  at a certain wavelength is a function of airmass  $M(z)$  at zenith distance  $z$ ,

$$m(\lambda) = m_0(\lambda) + \Delta m_0(\lambda) M(z) \quad (3.2)$$

where  $m_0(\lambda)$  is the magnitude which would be observed outside the Earth's atmosphere and  $\Delta m_0(\lambda)$  is the loss of magnitude at the zenith and equals  $-2.5 D(0)$  where  $D(0)$  represents the optical density of the atmosphere for one airmass ( $z = 0$ ).

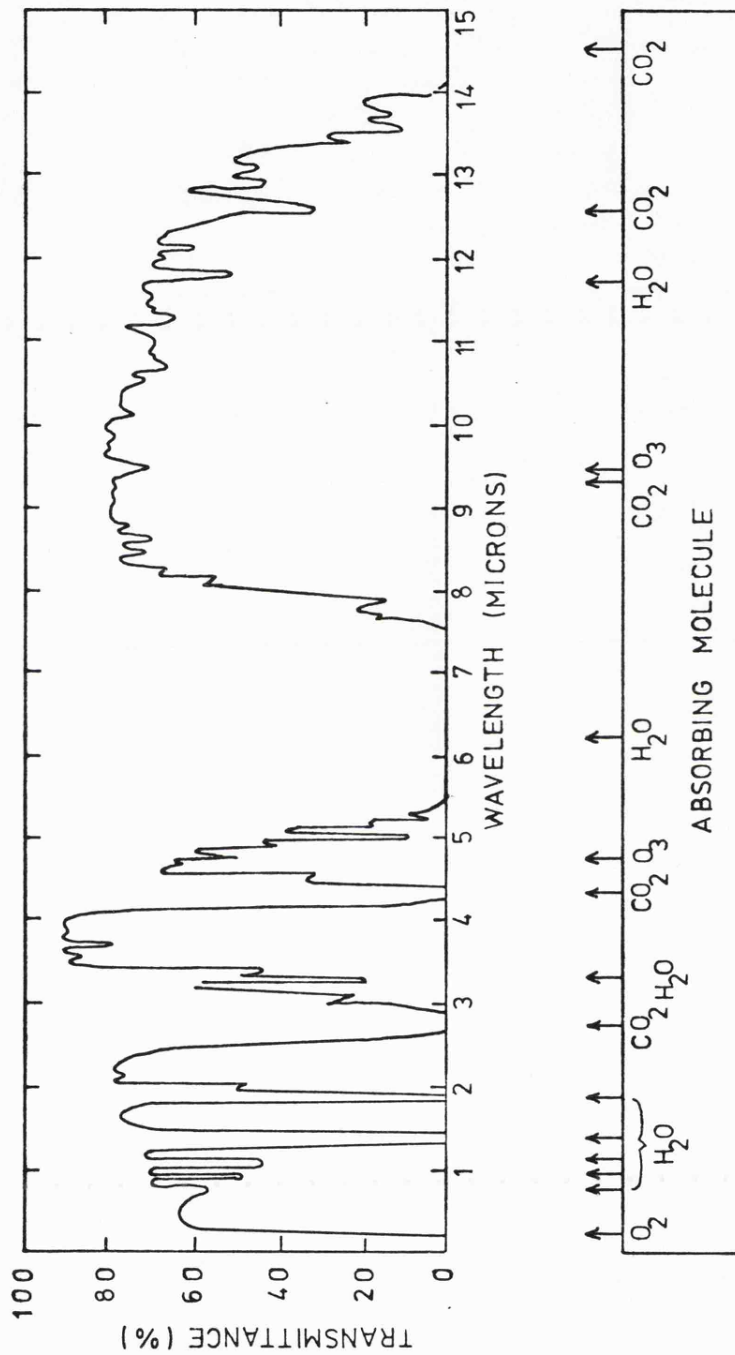


Figure 3.1 ATMOSPHERIC TRANSMITTANCE

The airmass can be expressed by a simple form when the atmosphere is reduced to a plane-parallel structure. This is the case when the zenith distance of a star is less than  $60^\circ$ . Then,

$$M(z) = \sec z . \quad (3.3)$$

More complicated formulae apply when  $z > 60^\circ$ , but this cannot be relied on since water vapour and  $\text{CO}_2$  are not evenly distributed with height in the atmosphere.

In practice a graph of  $\log_{10}$  (mean standard readings) is plotted against  $\sec z$ . Any deviations from a straight line can then be seen and also changes of the atmospheric extinction with time. Stellar magnitudes can now be obtained directly by using standard readings extrapolated to the appropriate airmass.

An example of the extinction curves observed for  $\beta$  Boo and  $\alpha$  Cyg is given in Figure 3.2.

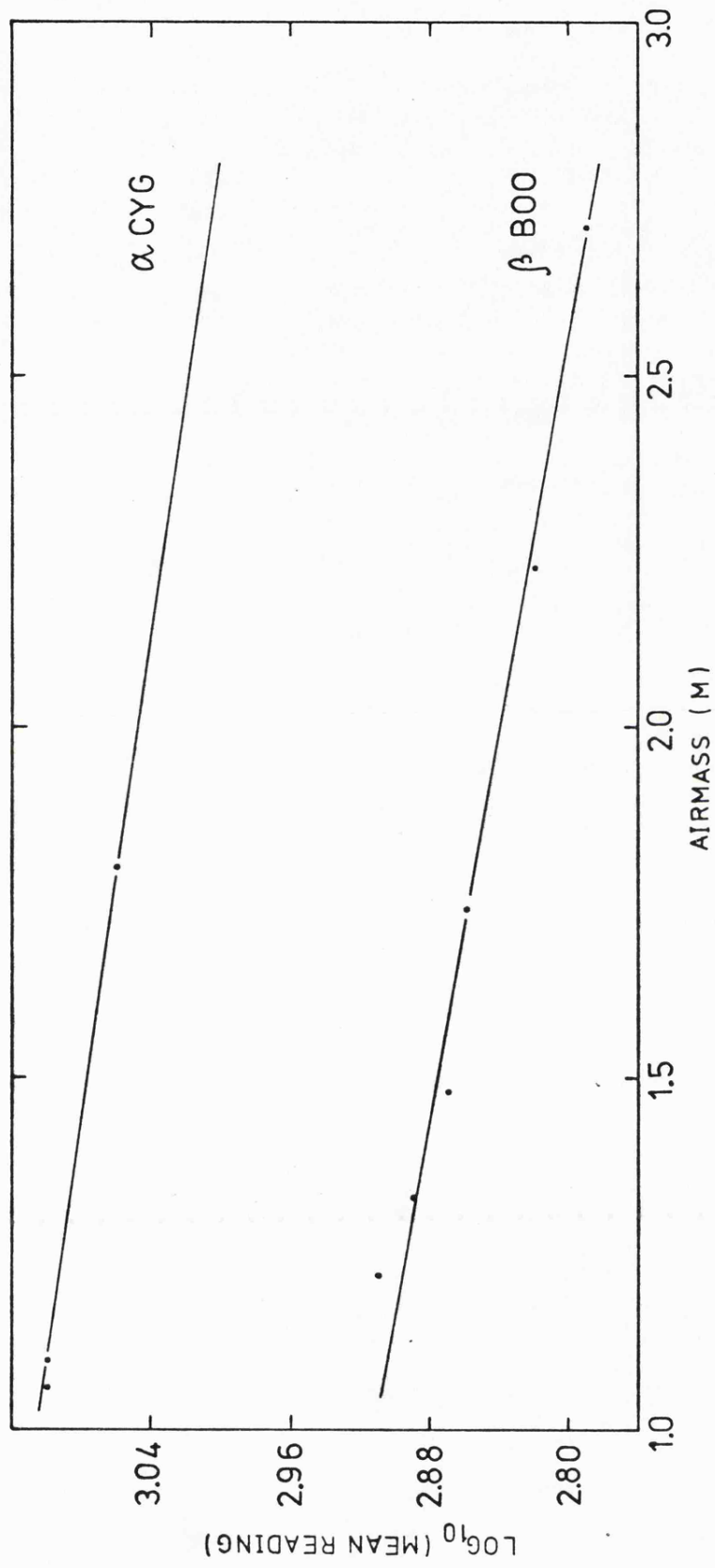


Figure 3.2 ATMOSPHERIC EXTINCTION CURVES OBTAINED ON 1976 SEPTEMBER 6-7.

## CHAPTER 4

## OBSERVATIONS AND DISCUSSION OF W URSAE MAJORIS-TYPE STARS

The background to the observations of W UMa-type eclipsing binary stars given here was outlined in the introduction. In this chapter the infrared light curves of the three observed eclipsing binary stars are given. Their significant characteristics are then discussed since successful analysis of the curves depends upon well defined features known to be real.

The stars observed were AB And, 44 i Boo, and SW Lac, the optical light curves of which can be characterised by strongly curved maxima and nearly equal primary and secondary minima.

AB ANDROMEDAE

BD + 36<sup>o</sup> 5017;  $\alpha = 23^{\text{h}}06^{\text{m}}46^{\text{s}}$ ;  $\delta = +36^{\circ} 21'.1$  (1900)

The eclipsing binary AB And was discovered by Guthnick and Prager (1927). This system has been observed photoelectrically in the B and V wavelength regions by several investigators, whose main aim was to examine the peculiarities in the light curve and to derive the orbital elements of the system. Many determinations of the times of conjunction from the observed minima were made in order to investigate the variability of the period of AB And. Binnendijk (1959) has listed earlier times of minima and indicated that the light elements given by other investigators do not successfully predict recent times of minima. Landolt (1969) also showed that the period of this system is continuously increasing.

Struve et al. (1950) reported the results of radial velocity measurements of occasional spectrograms obtained at the McDonald Observatory. Their programme of eclipsing binaries included a few

W Uma-type binaries together with the system AB And. They described the spectrum of AB And as spectral type G5.

Binnendijk (1959) presented a total of 391 yellow and 390 blue photoelectric observations of the system. It was found from these measurements that the light in the maxima shows a reflection effect ( $\cos \theta$  term), which has an opposite sign to that predicted by the theory, and also that the B - V colour shows a reddening during both minima. Therefore, he did not attempt to determine the orbital elements of the system. The normal light curves of AB And obtained by Binnendijk (1959) are given in Figure 4.1. This figure also shows the colour-index curve of the system.

During the past decade several investigators have presented further observations of this system from which new determinations of ephemeris and orbital elements have been made [ see Kalchaev and Trutse (1968), Landolt (1969), and Rigterink (1973) ]. Kalchaev and Trutse (1968) determined the orbital elements of the system. The differential light curve ( $\Delta V$  against phase) and the differential (B - V) and (U - B) colour-index curves for the system were given by Landolt (1969). Asymmetries in his light curve were evident. From the differential colour-index curves he calculated (B - V) = +0.90 and (U - B) = +0.59 for the eclipsing star. After referring to a UBV colour diagram, he suggested that the eclipsing star is probably an unreddened K2 main sequence star. Rigterink (1973) reported the new photoelectric observations of AB And in the B and V wavelength regions. These observations indicated that primary minimum is 0.03 mag. brighter than when the system was observed by Landolt (1969) and Binnendijk (1959). He analysed the light curve using both the classical method of rectification outlined by Binendijk (1970) and the method of light curve synthesis developed by Wilson and Devinney (1971). His

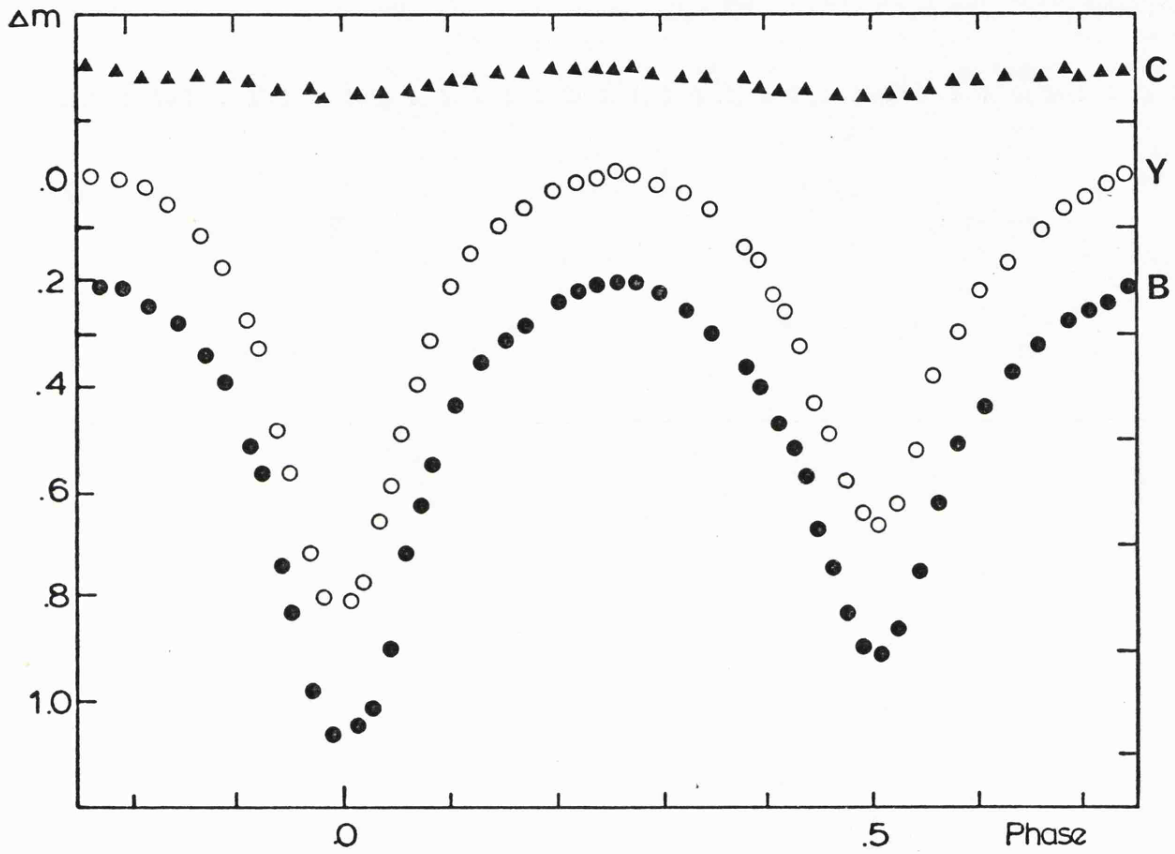


Figure 41 Blue and yellow light curves of AB And by  
Binnendijk (1959)

Y = Yellow, B = Blue, C = B - V.

resultant orbital elements determined by the method of Wilson and Devinney are given in Table 4.1. This solution indicated that the greater component of the system completely fills the Roche lobe while the smaller component almost does. The mass ratio of the system was found to be 0.69, and the temperature of the components 5370 K.

An analysis by Berthier (1975) of the light curve of AB And produced a slightly different model for the system. He discussed a certain number of differences between his method and the methods used by Rigterink (1973), and showed that it is possible to obtain a better agreement between theory and observations by the choice of the parameters involved in the solution. He found from his analysis that AB And is a contact system with a rather thin convective envelope, and that the secondary component is slightly hotter than the primary.

Table 4.1

Orbital elements of AB And determined by method of  
Wilson and Devinney [ Based on results by Rigterink (1973) ]

$r_s$ (pole)	= 0.312	$r_g$ (pole)	= 0.388
$r_s$ (point)	= 0.382	$r_g$ (point)	= 0.516
$r_s$ (side)	= 0.324	$r_g$ (side)	= 0.409
$r_s$ (back)	= 0.350	$r_g$ (back)	= 0.439
$i = 80^{\circ}.83$			

$L_s$ (V)	= 0.412	$L_g$ (V)	= 0.588
$L_s$ (B)	= 0.407	$L_g$ (B)	= 0.593

(s and g indicate the smaller and the greater components respectively)

44 i BOOTIS

$$\Sigma 1909 = \text{A.D.S.9494}; \quad \alpha = 15^{\text{h}}00^{\text{m}}27^{\text{s}}; \quad \delta = +48^{\circ}02'.6 \text{ (1900)}$$

The system of 44 i Boo is a well known visual binary discovered by W. Herschel in 1781. The orbital elements of the visual binary were given by Strand (1937). These are:

$$\begin{aligned} P &= 219.5 \text{ years} & a &= 3''.609 \\ i &= \pm 83^{\circ}.46 & e &= 0.42 \\ \omega &= 27^{\circ}.71 \end{aligned}$$

The variability of the fainter component was found photographically by Schilt (1926). It has a spectrum resembling that of W UMa. His measurements showed that the magnitude difference between the components of the visual pair, at the maximum light of the fainter component, was 0.76 mag. in photographic light.

Thus, 44 i Boo is a triple system consisting of a brighter component, hereafter referred to as star 1, and stars 2 and 3 which form the W UMa-type eclipsing binary. There is a general agreement that the combined spectrum of stars 2 and 3 is G2V. The eclipsing system is also a spectroscopic binary, the radial velocity curves of which were observed by Popper (1943). Binnendijk (1967) also published the radial velocity curves of 44 i Boo measured on spectrograms which were obtained by Harper during the years 1922-1939 at the Dominion Astrophysical Observatory. These curves are given in Figure 4.2. The solid curve in this figure represents the observations of the primary component of the eclipsing binary. This curve has the smaller semi-amplitude and consequently the primary component is the more massive star. It can also be seen that the primary component is in front during the primary minimum. Therefore, the eclipsing binary can be classified as a W-type system.

Good sets of photometric observations on 44 i Boo have been

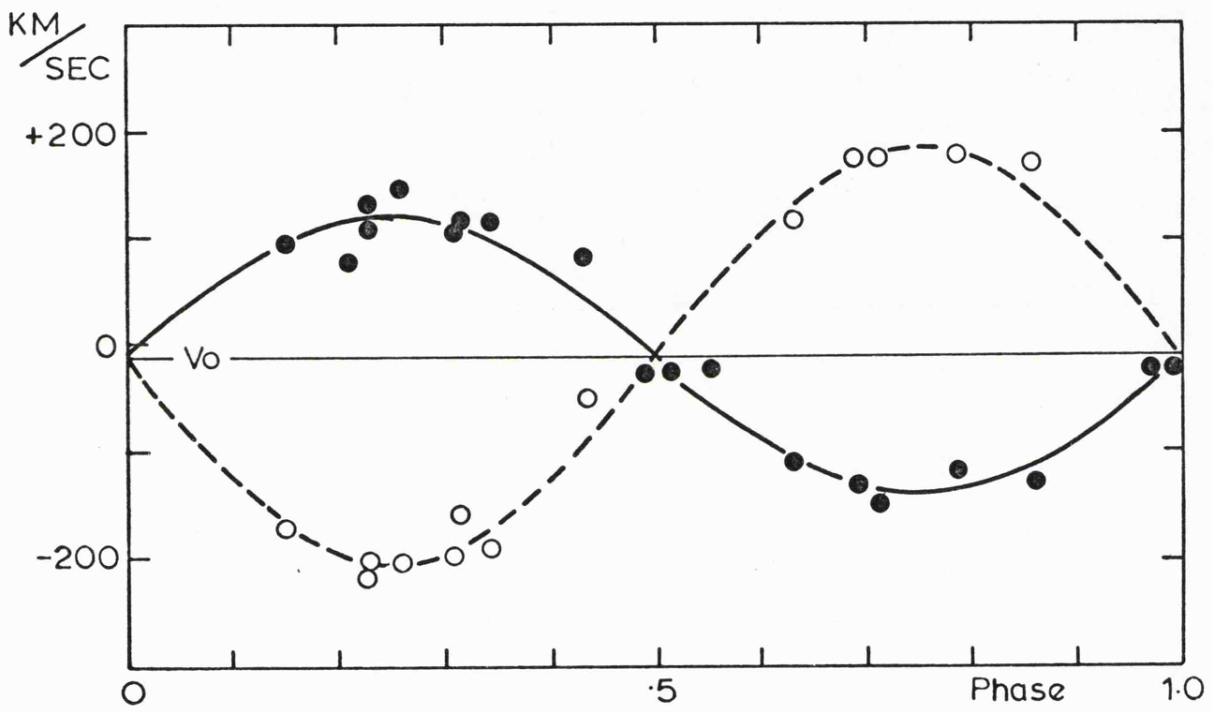


Figure 4.2 Velocity curves of 44 i Boo (eclipsing binary only)  
by Binnendijk (1967)

completed by Eggen (1948), Binnendijk (1955), and Kurpinska and van't Veer (1970). Binnendijk (1955) included all previously published observations to show the changes in the light curves. Most recent authors measured the combined light of the system because the separation of the visual pair had become too small. Eggen (1948) discussed the photoelectric observations of the combined light of this triple system obtained by Stebbins and Huffer in 1930 (unpublished) and by himself in 1947. He derived the approximate photometric elements from the 1930 light curve. A peculiar distortion of the light curve at the maximum was confirmed by the 1947 observations.

The photoelectric yellow observations of the combined light of the system made by Binnendijk (1955) are given in Figure 4.3. The magnitude differences for these individual observations were corrected for the zero-point shifts in such a way that this difference is zero at the maximum of the light curve. He discussed the changes in the period and light curve. The fluctuations of the zero point of the magnitudes from night to night were evident in this light curve. He determined the orbital elements of the system from the normal light curve which was freed from the light of star 1. These elements are given in Table 4.2(a), where the symbols have the usual meanings. The combination of spectroscopic and photometric data yielded the absolute elements of the components which are given in Table 4.2(b).

Eight-colour photometric observations of 44 i Boo in the range  $0.35 - 0.60 \mu\text{m}$  have been reported by Kurpinska and van't Veer (1970). These observations showed that in the range  $0.40 - 0.35 \mu\text{m}$  both minima are redder than the maximum; and in the range of  $0.60 - 0.40 \mu\text{m}$  the maximum shows reddening.

The period change of the system has been discussed in a number of papers. From photoelectric observations of this system during

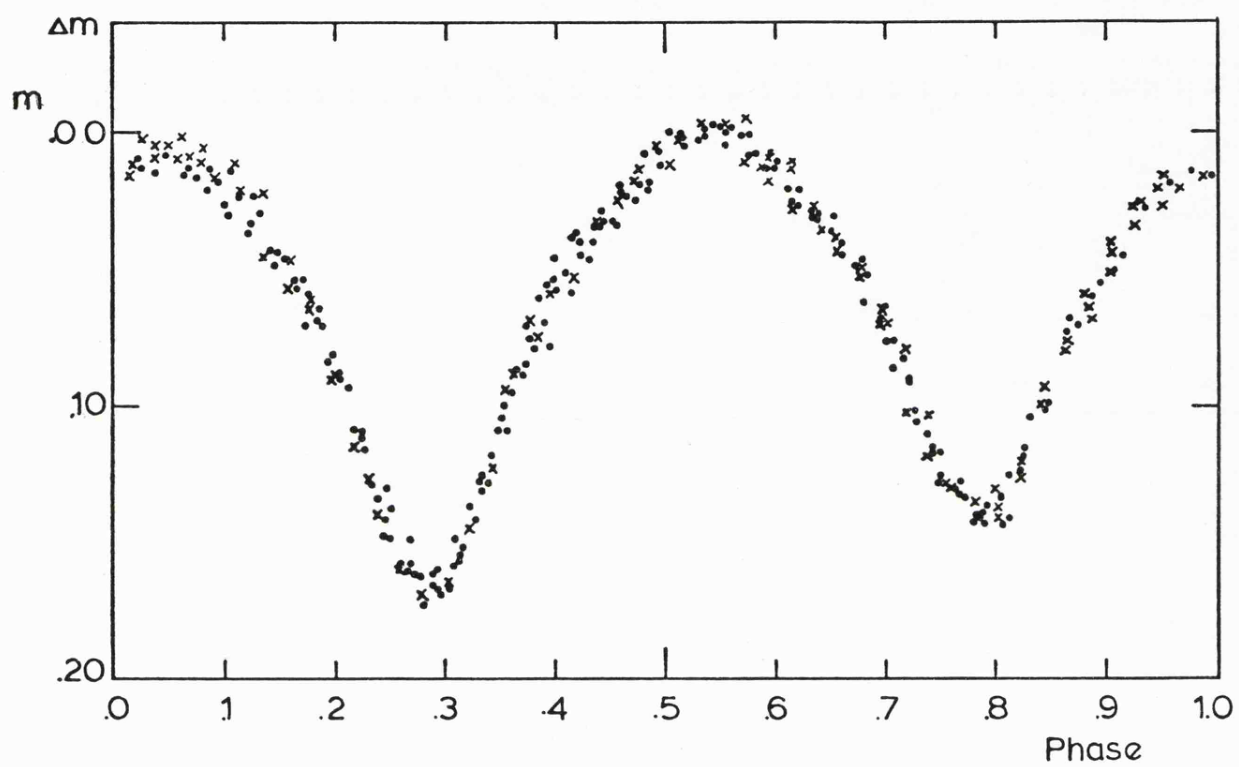


Figure 4.3 V light curve of 44 i Boo by Binnendijk (1955)

Table 4.2(a)

Orbital elements of 44 i Boo determined by Russell's method

[ Based on results by Binnendijk (1955) ]

$$\begin{array}{ll}
 a_g = 0.46 & a_s = 0.32 \\
 b_g = 0.41 & b_s = 0.28 \\
 k = 0.70 & i = 68^{\circ}.1 \\
 L_g = 0.62 & L_s = 0.38
 \end{array}$$

(g and s indicate the stars 2 and 3 respectively)

Table 4.2(b)

Absolute elements of 44 i Boo

[ Based on results by Binnendijk (1955) ]

$$\begin{array}{ll}
 a_2 = 0.46 \times 10^6 \text{ km} & a_3 = 0.92 \times 10^6 \text{ km} \\
 a_g = 0.63 \times 10^6 \text{ km} & a_s = 0.44 \times 10^6 \text{ km} \\
 b_g = 0.56 \times 10^6 \text{ km} & b_s = 0.39 \times 10^6 \text{ km} \\
 m_g = 0.96 m_{\odot} + .03 m_{\odot} & m_s = 0.48 m_{\odot} + .02 m_{\odot}
 \end{array}$$

(g and s indicate the stars 2 and 3 respectively;  $a_2$  and  $a_3$  refer to the radii of the circular absolute orbits in the true plane;  $m_{\odot} = 2 \times 10^{33} \text{ gr}$  )

the years 1969-1971 Bergeat et al. (1972) made a number of determinations of the times of minima. Their analysis of the data combined with that published by other observers has shown that the period of the system varies. Pohl (1967) found that the period did not change between 1958 and 1967. However, after that date the period has increased. According to a statistical analysis made by van't Veer (1972) the change must have taken place over a time interval of probably less than 200 days.

#### SW LACERTAE

$$\text{BD} + 37^{\circ} 4717; \alpha = 22^{\text{h}} 49^{\text{m}} 04^{\text{s}}; \delta = +37^{\circ} 24'.4 \text{ (1900)}$$

The eclipsing binary SW Lac, a W UMa-type system, was discovered by Miss Ashall in 1918 on plates taken at Harvard Observatory. Light curves of this system were obtained from photoelectric observations made by Brownlee (1957), Hinderer (1960), Broglia (1962), Chou (1963), and Bookmyer (1965).

The spectrum of each component star was determined by Wyse (1934) as G3p and G3p. Struve (1949) observed the radial velocity curves of SW Lac. He then derived the spectroscopic orbital elements from his plates obtained at the McDonald Observatory. He assumed a circular orbit since the accuracy of the data did not justify computing an elliptical orbit. It can be seen from the radial velocity curves that the larger, more massive component of the system is the eclipsing star at the primary minimum. This component is also the cooler; thus, the primary eclipse is an occultation.

Brownlee (1957) presented the light curves in three colours (U, B, V). It was shown that, while the system was well-behaved in the 1953 observations, variations of light curve can be seen in his 1954 curves. The variation at maxima was as much as 0.2 mag. in B and

V. The primary and secondary minima were nearly the same depth in 1954, however, in the 1953 curves they had differed by 0.12 mag. He pointed out that it was impossible to make a precise photometric orbital solution due to the cycle to cycle variation of the light curve. However, a sample solution was given by him.

Optical light curves of the system in B and V obtained by Chou (1963) indicated eccentricity of its orbit and a large amount of intrinsic variability of the components. The displacement of the secondary minimum from the 0.5 phase was visible in these curves. It was also found that the depths of both minima vary with time.

The study of this system was extended by Bookmyer (1965). Five well-defined light curves were constructed from her observations in B and V. She discussed the variations among these curves and five other photoelectric light curves obtained by other investigators between 1953 and 1962. This limited data indicated that the amplitude of the curves has been decreasing with time. This was due primarily to a decrease in the heights of the maxima. She also noted that in every curve, maximum light at phase 0.75 is approximately equal to or higher than that at phase 0.25. She analysed the observations defining Curve IV for an orbital solution. The intensity differences between this curve and the other curves obtained by her were removed by representing the differences by a progressing cosine curve over the full cycle of light variation. Consequently, she treated the normal points defining all five curves as one set of data. This set of data was then used to determine the orbital elements of the system. These elements together with the absolute elements of the system are given in Table 4.3 (a and b).

The light curves of SW Lac obtained by Bookmyer (1965) in 1961 are given in Figure 4.4.

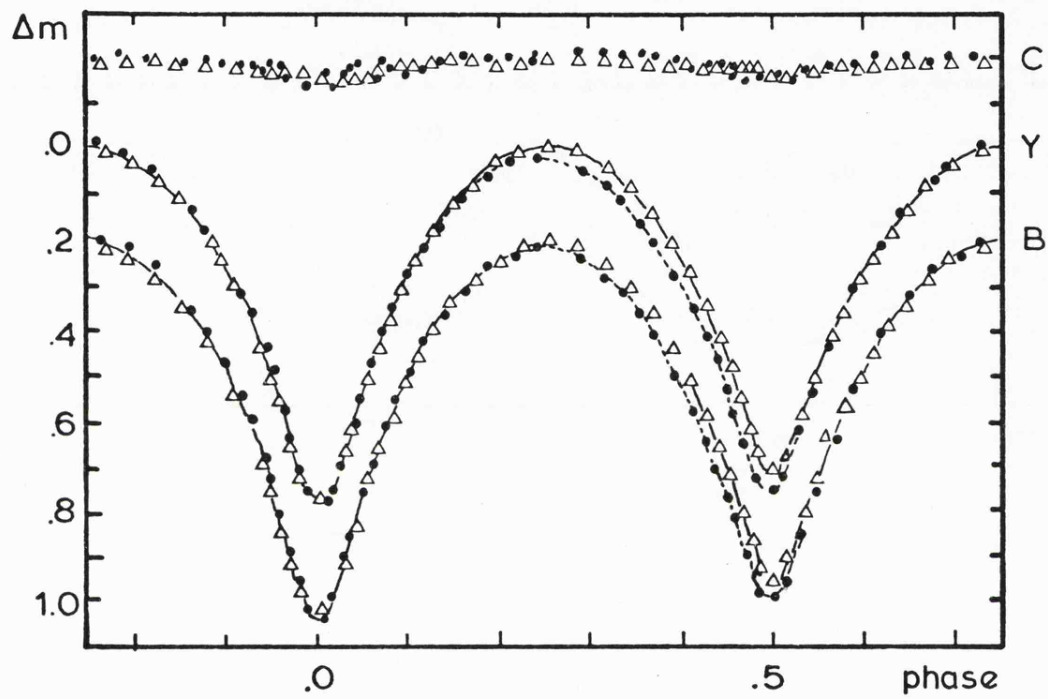


Figure 4.4 Blue and yellow light curves of SW Lac  
by Bookmyer (1965)

Y = yellow, B = blue, C = B - V.

Table 4.3(a)

## Orbital elements of SW Lac

[ Based on results by Bookmyer (1965) ]

$a_g = 0.41$	$a_s = 0.33$
$b_g = 0.35$	$b_s = 0.28$
$k = 0.80$	$i = 75^{\circ}.6$
$L_g = 0.570 (V)$	$L_s = 0.430 (V)$
$L_g = 0.566 (B)$	$L_s = 0.434 (B)$

Table 4.3(b)

## Absolute elements of SW Lac

[ Based on results by Bookmyer (1965) ]

$a_1 = 0.85 \times 10^6 \text{ km}$	$a_2 = 0.96 \times 10^6 \text{ km}$
$a_g = 1.06 r_{\odot}$	$a_s = 0.85 r_{\odot}$
$b_g = 0.90 r_{\odot}$	$b_s = 0.72 r_{\odot}$
$m_g = 1.22 m_{\odot}$	$m_s = 1.07 m_{\odot}$

$$(r_{\odot} = 0.696 \times 10^6 \text{ km}; m_{\odot} = 2 \times 10^{33} \text{ gr})$$

The period variations of SW Lac have been the object of a number of analyses. van't Veer (1972) provided the O - C curve for all the photoelectrically determined minima since 1953. This plot shows that the changes have occurred in the period of SW Lac. Bookmyer (1965) indicated that there is a displacement of secondary minimum from phase 0.5, however, the amount of this displacement varies.

### Infrared Observations

All the observations were made with the 1.5 m Infrared Flux Collector at the Cabezón Observatory in Tenerife. The photometer with an InSb detector operating at 63 K was used. A detailed description of the photometer has been given in Chapter 2, and Chapter 3 describes the procedure for the observations of the eclipsing binary stars selected for this project.

### AB And

A total of 91 infrared observations of AB And at 1.2 and 2.2  $\mu\text{m}$  was made on the nights of 1977 September 27 and 29. Each observation is the average of a number (usually 6) of consecutive 10 second integrations in each channel. The error of each observation is taken as the standard deviation of the mean of the readings. This error was found to be  $\leq \pm 0.03$  magnitudes. However, most of the observations had errors of  $\pm 0.01$  magnitudes.

$\epsilon$  And was used as the standard star throughout the observations; its J and K magnitudes are given by Johnson et al. (1966) as 2.84 and 2.21 respectively. Corrections were made for atmospheric extinction as described in Chapter 3. The heliocentric correction,  $dt = +0.005$ , was applied to all observation times. The phases of the observations were computed according to the ephemeris given by

Rigtering (1973),

$$J.D.Hel.Min.I = 2440128.79453 + 0.33189305 E .$$

The primary minimum of the  $1.2 \mu m$  light curve of AB And is at phase 0.970, whereas the corresponding minimum of the  $2.2 \mu m$  light curve occurs at phase 0.967. Therefore, corrections were applied to the phases in order to place the primary minimum at phase 0.0.

Since the number of observations was small compared with that used for good optical light curves, the usual procedure of forming normal points from individual observations at approximately the same phase, was not followed in constructing the light curves of the system. Fortunately there was at least one observation for each phase interval of 0.025, except at times when standard star observations were being made.

The observations of AB And are tabulated in Tables 4.4 and 4.5; Figures 4.5 and 4.6 show the light curves of AB And at  $1.2$  and  $2.2 \mu m$  respectively.

#### 44 i Boo

Infrared observations of the combined light of the triple system 44 i Boo at  $2.2 \mu m$  were made on the nights of 1976 June 20, 21, 23 and September 6 and 7. A total of 95 measurements was made on these five nights. Each set of observations consisted of 9 consecutive 10 second integrations in each channel. The error of each observation was found to be always  $\leq \pm 0.01$  magnitudes.

$\beta$  Boo was used as the standard star throughout the observations; its K magnitude is given by Johnson et al. (1966) as 1.34. All observations were corrected for atmospheric extinction, and heliocentric

corrections were applied to all observation times. The ephemeris used was that of Pohl (1967),

$$\text{J.D.Hel.Min.I} = 2438513.4160 + 0.26781430 \text{ E.}$$

The primary minimum occurs at phase 0.071, however this is corrected to 0.0 phase in the observed light curve of the system given in Figure 4.7. This light curve does not describe the eclipsing binary system since it is necessary to subtract the light of star 1. The total visual magnitude (stars 1, 2, and 3) is given as 4.86 by both Eggen (1948) and Binnendijk (1955), whereas the BS catalogue quotes 4.76. The visual magnitudes and B - V colours of the components of the visual pair at maximum light of the fainter component are given by Eggen (1967):

$$\begin{array}{llll} \text{star 1} & V_1 & = & 5.25 & B_1 - V_1 & = & +0.60 \\ \text{star 2,3} & V_{2,3} & = & 5.85 & B_{2,3} - V_{2,3} & = & +0.85, \end{array}$$

and these data do give 4.76 for the total light. Kuiper (1929) gives the visual magnitude difference between star 1 and stars 2 and 3 as 0.63 which agrees with Eggen (1967). Binnendijk (1955) used Schilt's value of 0.76 mag. for the difference between the components of the visual pair in order to find the magnitudes of the mean light curve freed from the light of star 1. He assumed that this magnitude difference can be used for all effective wavelengths since the components are equal spectral types. However, this assumption can only be true if the colour indices of the total system are appropriate for the spectral types of the components. The observed spectral types of many close binaries do not correspond to their colours, being nearly always earlier than expected. Inspection of Table 5 of Binnendijk (1970) shows that most of the W Uma-type binaries have B - V colours appreciably redder than

their spectral type would imply.

The spectral type of star 1 is generally supposed to be G2V. This spectral type corresponds to B - V and V - K values of +0.63 and +1.44 respectively (Johnson, 1966a). It can be seen that the B - V colour of star 1 given by Eggen (1967) corresponds to that of a G2V star.

Since  $(V - K)_{G2V} = +1.44$  and  $V_1$  is 5.25, it follows that the K magnitude of star 1 is 3.81. From the observed light curve, the K magnitude at maximum light,  $K_{Tot\ max}$ , and the K magnitude at primary minimum,  $K_{Tot\ min}$ , for the total light of the system are such that

$K_{Tot\ min} - K_{Tot\ max} = 0.217$ . Hence the ratio of intensities at K for

maximum and primary minimum  $I_{Tot\ min} / I_{Tot\ max} = 0.819$ . Similarly

the ratio of intensities at K for star 1 and that of total system at maximum light  $I_1 / I_{Tot\ max} = 0.484$ .

For an arbitrary phase, p, of the observed light curve,

$$I_1 + I_{2,3\ p} = I_{Tot\ p} \quad (4.1)$$

where  $I_{2,3\ p}$  is the intensity at K for the phase p of the light curve

and  $I_{Tot\ p}$  is the total intensity at K for the phase p. From the

equation (4.1) it follows that

$$\frac{I_1}{I_{Tot\ max}} + \frac{I_{2,3\ min}}{I_{Tot\ max}} = \frac{I_{Tot\ min}}{I_{Tot\ max}} \quad (4.2)$$

and

$$\frac{I_1}{I_{Tot\ max}} + \frac{I_{2,3\ max}}{I_{Tot\ max}} = 1 \quad (4.3)$$

Therefore on using the obtained values of  $I_1/I_{\text{Tot max}}$  and

$I_{\text{Tot min}}/I_{\text{Tot max}}$ , the ratio of intensities at K for the primary minimum

and maximum of the light curve of the eclipsing system,

$I_{2,3 \text{ min}}/I_{2,3 \text{ max}}$ , is found to be 0.649; hence the K magnitudes at

minimum and maximum for the eclipsing system are such that

$$\Delta K_{0.0} = K_{2,3 \text{ min}} - K_{2,3 \text{ max}} = 0.469 \text{ where } \Delta K_{0.0} \text{ is the depth of the}$$

primary minimum for the eclipsing system.

The calculations can be repeated for every observed point of the light curve to obtain  $\Delta K_p = K_{2,3 p} - K_{2,3 \text{ max}}$ , where  $\Delta K_p$  and

$K_{2,3 p}$  denote the magnitude difference and the K magnitude of the

eclipsing system at phase p of the light curve. The values of  $\Delta K_p$  for all phases will now describe the light curve of the eclipsing system at  $2.2 \mu\text{m}$ .

Table 4.6 gives the heliocentric Julian Dates, the corrected phases, the  $2.2 \mu\text{m}$  magnitudes of the total system, and the values of  $\Delta K_p$  for the eclipsing system. In Figure 4.8 the values of  $\Delta K_p$  are plotted against the corrected phases. This curve now represents the eclipsing binary only at  $2.2 \mu\text{m}$ .

#### SW Lac

The infrared observations of SW Lac at  $1.2$  and  $2.2 \mu\text{m}$  were made on the night of 1977 September 24. Observations on this single night covered one period only at both wavelengths. Each observation is the average of 6 consecutive 10 second integrations in each channel. The errors of all observations were found to be  $\leq \pm 0.03$  magnitudes. However, most of the observations had errors of  $\pm 0^{\text{m}}.01$ . The standard

star used was  $\epsilon$  And. All observations were corrected for atmospheric extinction and the heliocentric correction,  $dt = + 0.004$ , was applied to all observation times. The ephemeris used was that of Purgathofer and Prochazka (1967),

$$\text{J.D.Hel.Min.I} = 2434271.37023 + 0.32072277 \text{ E.}$$

The primary minimum of the  $1.2\mu\text{m}$  light curve is at phase 0.968, whereas the corresponding minimum of the  $2.2\mu\text{m}$  light curve occurs at phase 0.961. Therefore, corrections were made to place the primary minimum at phase 0.0.

The observations of SW Lac are tabulated in Tables 4.7 and 4.8; Figures 4.9 and 4.10 show the light curves of SW Lac at  $1.2$  and  $2.2\mu\text{m}$  respectively.

Table 4.4Infrared Observations of AB And at 1.2  $\mu$  m

JD2440000+	Corr. Phase [Phase+0.030]	1.2 $\mu$ m	JD2440000+	Corr. Phase [Phase+0.030]	1.2 $\mu$ m
3414.440	0.742	8.15	3414.711	0.558	8.60
3414.447	0.763	8.15	3416.339	0.463	8.60
3414.452	0.778	8.14	3416.347	0.487	8.73
3414.458	0.796	8.16	3416.354	0.508	8.79
3414.475	0.847	8.23	3416.371	0.560	8.58
3414.481	0.865	8.26	3416.388	0.611	8.30
3414.488	0.886	8.29	3416.402	0.653	8.25
3414.495	0.907	8.35	3416.407	0.668	8.23
3414.511	0.956	8.59	3416.413	0.686	8.20
3414.518	0.977	8.74	3416.424	0.719	8.12
3414.524	0.995	8.83	3416.430	0.737	8.10
3414.604	0.236	8.11	3416.443	0.777	8.13
3414.611	0.257	8.10	3416.448	0.792	8.14
3414.629	0.311	8.14	3416.524	0.021	8.75
3414.634	0.326	8.15	3416.530	0.039	8.63 +
3414.647	0.365	8.19 *	3416.537	0.060	8.49
3414.654	0.386	8.21 *	3416.554	0.111	8.28 +
3414.666	0.423	8.34	3416.560	0.129	8.20
3414.672	0.441	8.44	3416.565	0.144	8.17
3414.679	0.462	8.57	3416.581	0.192	8.10
3414.686	0.483	8.69	3416.588	0.214	8.07
3414.699	0.522	8.78	3416.594	0.232	8.04
3414.704	0.537	8.69			

+ : indicates error of  $\pm 0^m.02$  ,

\* : indicates error of  $\pm 0^m.03$  ,

Observations without any symbol have errors of  $\pm 0^m.01$ .

Table 4.5Infrared Observations of AB And at 2.2  $\mu$ m

JD2440000+	Corr. Phase [Phase+0.033]	2.2 $\mu$ m	JD2440000+	Corr. Phase [Phase+0.033]	2.2 $\mu$ m
3414.443	0.754	7.58	3414.707	0.549	8.03
3414.449	0.772	7.58	3416.337	0.460	7.94
3414.455	0.790	7.58	3416.343	0.478	8.08
3414.461	0.808	7.61	3416.349	0.496	8.18
3414.478	0.859	7.68	3416.357	0.521	8.16
3414.484	0.877	7.71	3416.372	0.566	7.90 *
3414.490	0.895	7.75	3416.386	0.608	7.75
3414.497	0.916	7.82	3416.399	0.647	7.69
3414.514	0.968	8.08	3416.404	0.662	7.67
3414.522	0.992	8.19	3416.410	0.680	7.63
3414.528	1.010	8.20	3416.422	0.716	7.56
3414.601	0.230	7.54	3416.428	0.734	7.53
3414.608	0.251	7.54	3416.439	0.768	7.54
3414.623	0.296	7.54	3416.446	0.789	7.54
3414.632	0.323	7.56	3416.527	0.033	8.11
3414.638	0.341	7.57	3416.533	0.051	8.02
3414.650	0.377	7.63	3416.551	0.105	7.75
3414.664	0.419	7.72	3416.557	0.123	7.69
3414.670	0.438	7.81	3416.563	0.141	7.64
3414.677	0.459	7.90	3416.579	0.189	7.53
3414.683	0.477	8.04	3416.585	0.208	7.52
3414.696	0.516	8.17	3416.590	0.223	7.53
3414.702	0.534	8.15	3416.597	0.244	7.49 +

+ : indicates error of  $\pm 0^m.02$  ,

\* : indicates error of  $\pm 0^m.03$  ,

Observations without any symbol have errors of  $\pm 0^m.01$ .

Table 4.6Infrared Observations of 44 i Boo at 2.2  $\mu\text{m}$ 

JD2440000+	Corr. Phase [ Phase-0.071 ]	2.2 $\mu\text{m}$	$\Delta$ Kp
2950.435	0.450	3.192	0.360
2950.439	0.465	3.197	0.371
2950.441	0.472	3.212	0.407
2950.443	0.480	3.217	0.418
2950.448	0.498	3.224	0.435
2950.451	0.510	3.214	0.411
2950.454	0.521	3.246	0.489
2950.457	0.532	3.230	0.450
2950.478	0.610	3.130	0.222
2950.481	0.622	3.112	0.184
2950.483	0.629	3.118	0.196
2950.486	0.640	3.108	0.175
2950.489	0.651	3.102	0.163
2950.491	0.659	3.080	0.117
2950.504	0.707	3.075	0.107
2950.506	0.715	3.076	0.109
2950.509	0.726	3.067	0.010
2950.511	0.734	3.055	0.067
2950.515	0.749	3.057	0.071
2950.518	0.760	3.072	0.101
2950.529	0.801	3.081	0.119
2950.535	0.823	3.082	0.121
2950.539	0.838	3.097	0.152
2950.541	0.846	3.100	0.159
2950.544	0.857	3.112	0.184
2950.559	0.913	3.150	0.266
2950.562	0.924	3.187	0.348
2950.565	0.935	3.179	0.330
2950.568	0.946	3.219	0.423
2950.573	0.965	3.217	0.418
2950.588	0.021	3.232	0.454
2950.592	0.036	3.224	0.435

Table 4.6 cont...

Table 4.6 cont.

JD2440000+	Corr. Phase [Phase-0.071]	2.2 $\mu$ m	$\Delta$ Kp
2950.595	0.047	3.187	0.348
2950.598	0.058	3.168	0.305
2950.601	0.070	3.174	0.320
2950.616	0.126	3.077	0.111
2950.623	0.152	3.068	0.093
2950.626	0.163	3.058	0.073
2950.633	0.189	3.052	0.061
2951.412	0.098	3.126	0.213
2951.418	0.120	3.112	0.184
2951.423	0.139	3.090	0.138
2951.426	0.150	3.076	0.109
2951.428	0.158	3.064	0.085
2951.431	0.169	3.067	0.091
2951.445	0.221	3.056	0.069
2951.448	0.232	3.064	0.085
2951.450	0.240	3.046	0.049
2953.414	0.573	3.141	0.246
2953.422	0.603	3.117	0.194
2953.462	0.752	3.051	0.059
2953.468	0.775	3.072	0.101
2953.484	0.835	3.096	0.150
2953.489	0.853	3.108	0.175
2953.498	0.887	3.128	0.218
2953.529	0.003	3.238	0.469
2953.536	0.029	3.225	0.438
2953.548	0.074	3.184	0.342
2953.557	0.107	3.162	0.292
3028.335	0.323	3.066	0.089
3028.339	0.338	3.066	0.089
3028.350	0.379	3.098	0.154
3028.353	0.390	3.117	0.194
3028.358	0.409	3.138	0.239

Table 4.6 cont...

Table 4.6 cont.

JD2440000+	Corr. Phase [Phase-0.071]	2.2 $\mu$ m	$\Delta$ Kp
3028.362	0.424	3.153	0.272
3028.373	0.465	3.200	0.378
3028.378	0.484	3.224	0.435
3028.383	0.502	3.224	0.435
3028.388	0.521	3.231	0.452
3028.398	0.558	3.169	0.308
3028.403	0.577	3.147	0.259
3028.407	0.592	3.135	0.233
3028.428	0.670	3.064	0.085
3028.432	0.685	3.069	0.095
3028.437	0.704	3.079	0.115
3028.448	0.745	3.069	0.095
3028.452	0.760	3.083	0.123
3029.328	0.031	3.196	0.369
3029.334	0.053	3.135	0.233
3029.339	0.072	3.128	0.218
3029.344	0.091	3.094	0.146
3029.353	0.124	3.082	0.121
3029.358	0.143	3.075	0.107
3029.363	0.162	3.053	0.063
3029.369	0.184	3.053	0.063
3029.379	0.221	3.021	0.000
3029.386	0.247	3.027	0.012
3029.392	0.270	3.035	0.027
3029.396	0.285	3.035	0.027
3029.408	0.330	3.056	0.069
3029.414	0.352	3.080	0.117
3029.419	0.371	3.104	0.167
3029.424	0.389	3.115	0.190
3029.443	0.460	3.210	0.402
3029.450	0.486	3.234	0.459

Table 4.7Infrared Observations of SW Lac at 1.2  $\mu\text{m}$ 

JD2440000+	Corr. Phase [Phase+0.032]	1.2 $\mu\text{m}$	JD2440000+	Corr. Phase [Phase+0.032]	1.2 $\mu\text{m}$
3411.404	0.270	7.33	3411.576	0.806	7.35
3411.411	0.292	7.34	3411.584	0.831	7.48 +
3411.418	0.314	7.36	3411.592	0.856	7.51 +
3411.438	0.376	7.45	3411.599	0.878	7.58
3411.445	0.398	7.50	3411.617	0.934	7.77
3411.452	0.420	7.57	3411.624	0.956	7.89
3411.458	0.438	7.65	3411.630	0.975	7.97
3411.464	0.457	7.76	3411.634	0.987	8.08
3411.485	0.523	7.93	3411.642	0.012	8.04 +
3411.490	0.538	7.83	3411.648	0.031	7.93
3411.497	0.560	7.74	3411.653	0.046	7.81
3411.504	0.582	7.64	3411.666	0.087	7.60
3411.521	0.635	7.47	3411.671	0.103	7.54
3411.528	0.657	7.42	3411.674	0.112	7.50
3411.535	0.679	7.35	3411.678	0.124	7.44
3411.542	0.700	7.33	3411.697	0.184	7.37
3411.547	0.716	7.32	3411.704	0.205	7.37 *
3411.570	0.788	7.33			

+ : indicates error of  $\pm 0^{\text{m}}.02$  ,

\* : indicates error of  $\pm 0^{\text{m}}.03$  ,

Observations without any symbol have errors of  $\pm 0^{\text{m}}.01$ .

Table 4.8Infrared Observations of SW Lac at 2.2  $\mu\text{m}$ 

JD2440000+	Corr. Phase [Phase+0.039]	2.2 $\mu\text{m}$	JD2440000+	Corr. Phase [Phase+0.039]	2.2 $\mu\text{m}$
3411.401	0.268	6.78	3411.567	0.785	6.74
3411.407	0.286	6.78	3411.573	0.804	6.78
3411.414	0.308	6.79	3411.579	0.823	6.79
3411.435	0.374	6.86	3411.588	0.851	6.91 +
3411.442	0.396	6.92	3411.596	0.876	6.94 *
3411.448	0.414	6.97	3411.614	0.932	7.17 +
3411.455	0.436	7.05	3411.621	0.954	7.25 +
3411.461	0.455	7.14	3411.626	0.969	7.35
3411.479	0.511	7.39	3411.632	0.988	7.39
3411.487	0.536	7.31	3411.637	0.004	7.43
3411.494	0.558	7.20	3411.645	0.028	7.30
3411.481	0.580	7.09	3411.651	0.047	7.21
3411.518	0.633	6.92	3411.664	0.088	7.05
3411.523	0.648	6.90	3411.668	0.100	7.00
3411.532	0.676	6.80	3411.672	0.113	6.94
3411.538	0.695	6.78	3411.676	0.125	6.90
3411.544	0.714	6.76	3411.680	0.138	6.84

+ : indicates error of  $\pm 0^{\text{m}}.02$  ,

\* : indicates error of  $\pm 0^{\text{m}}.03$  ,

Observations without any symbol have errors of  $\pm 0^{\text{m}}.01$ .

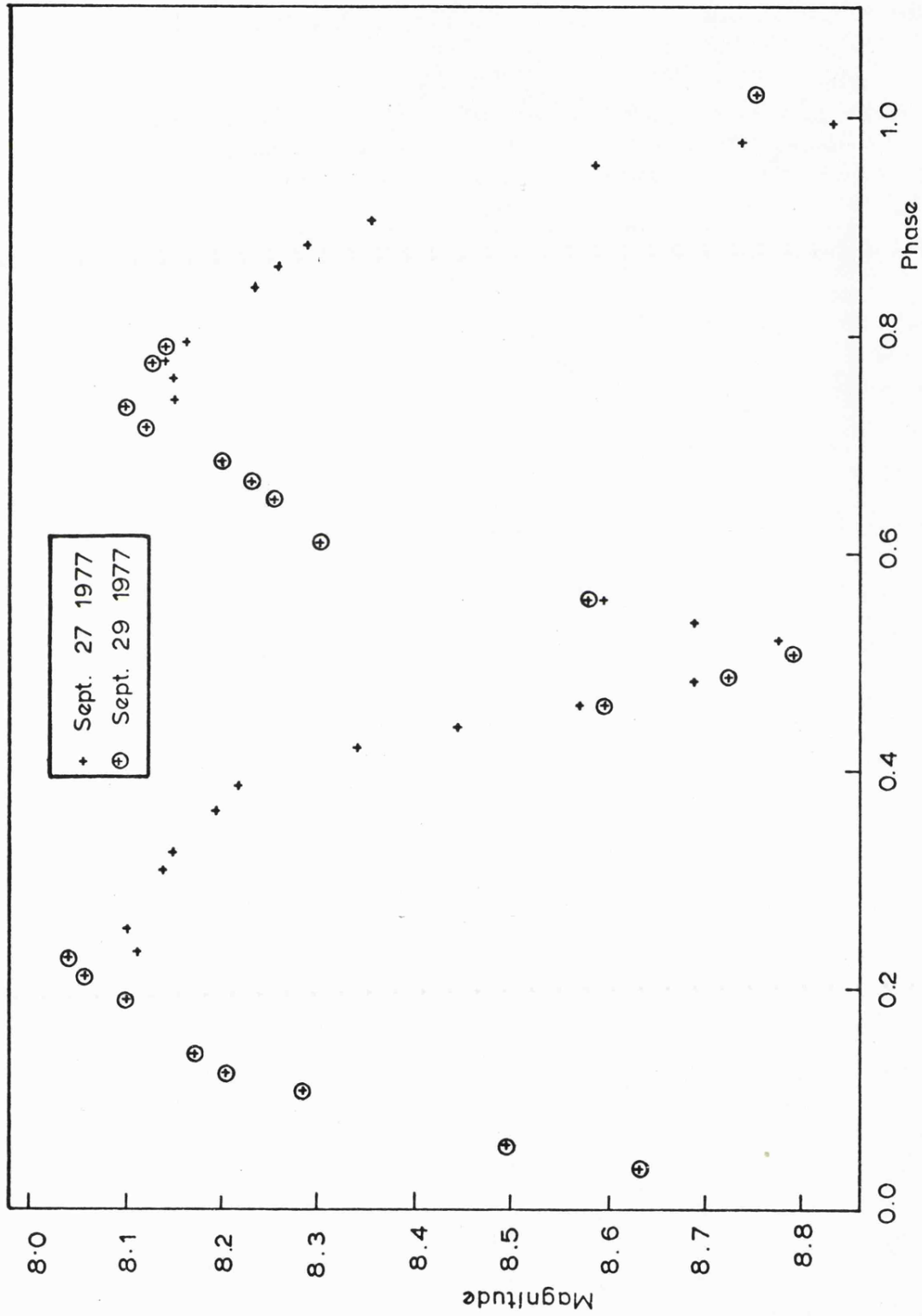


Figure 4.5 1.2  $\mu$ m light curve of AB And

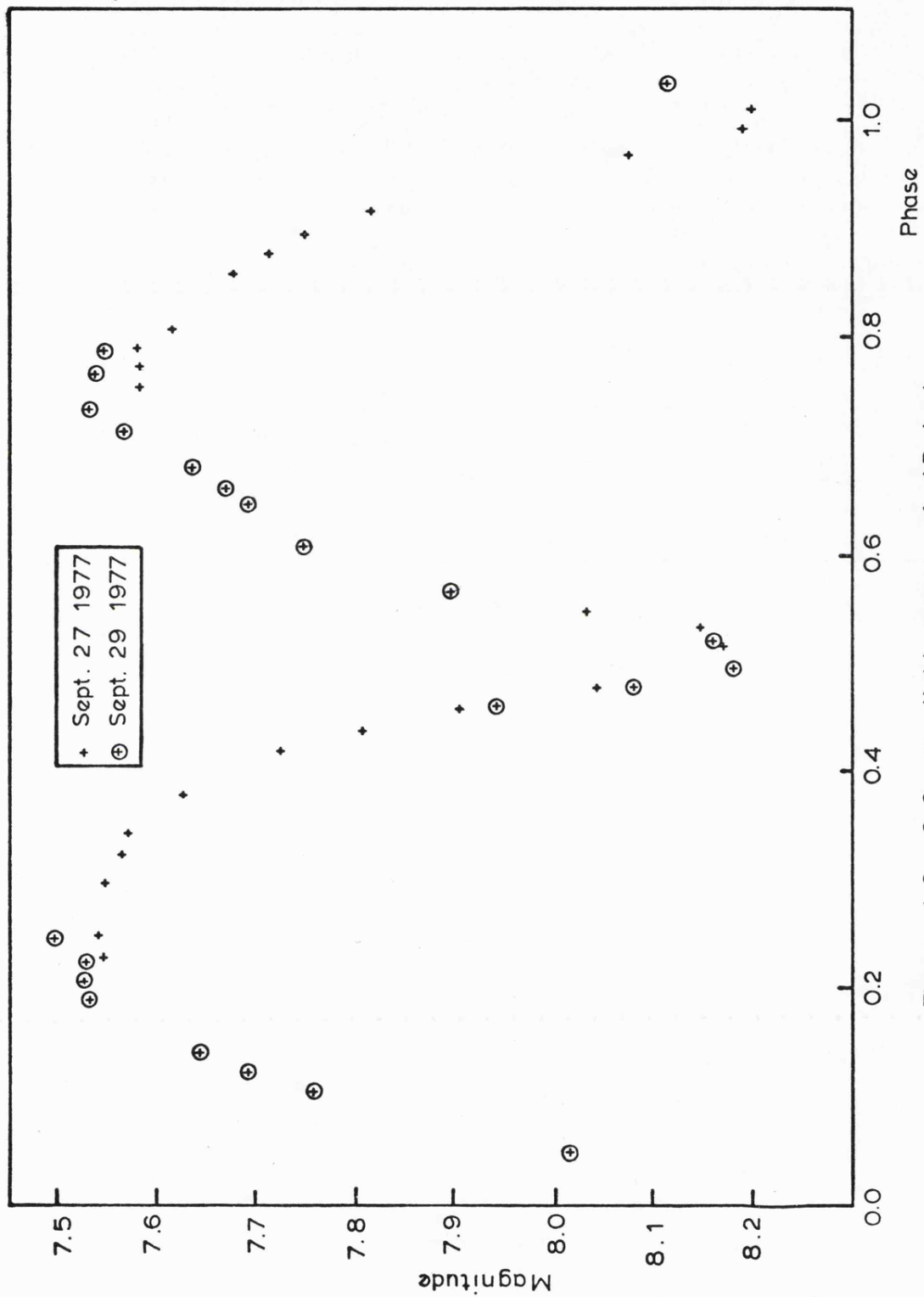


Figure 4.6 2.2  $\mu$ m light curve of AB And

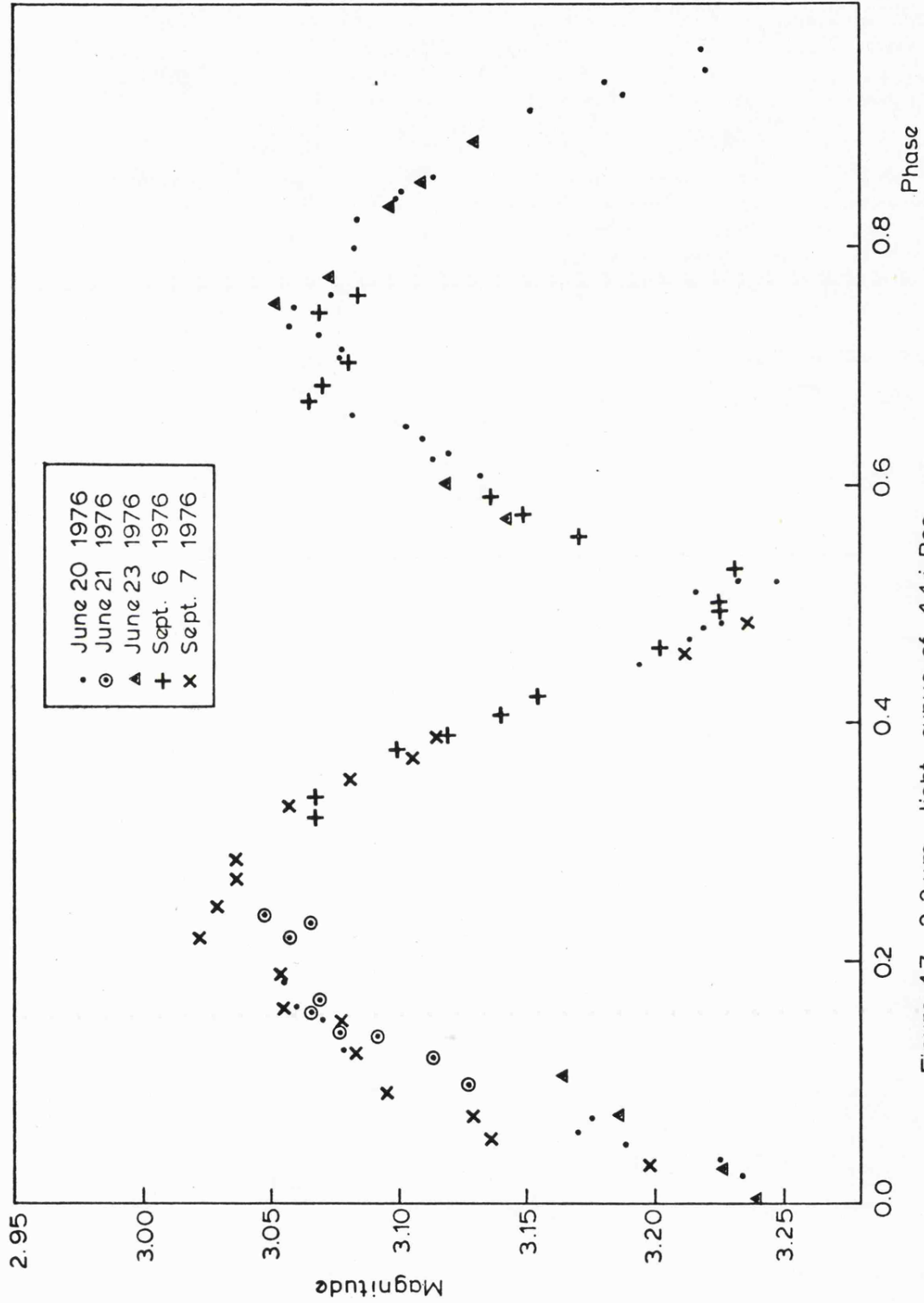
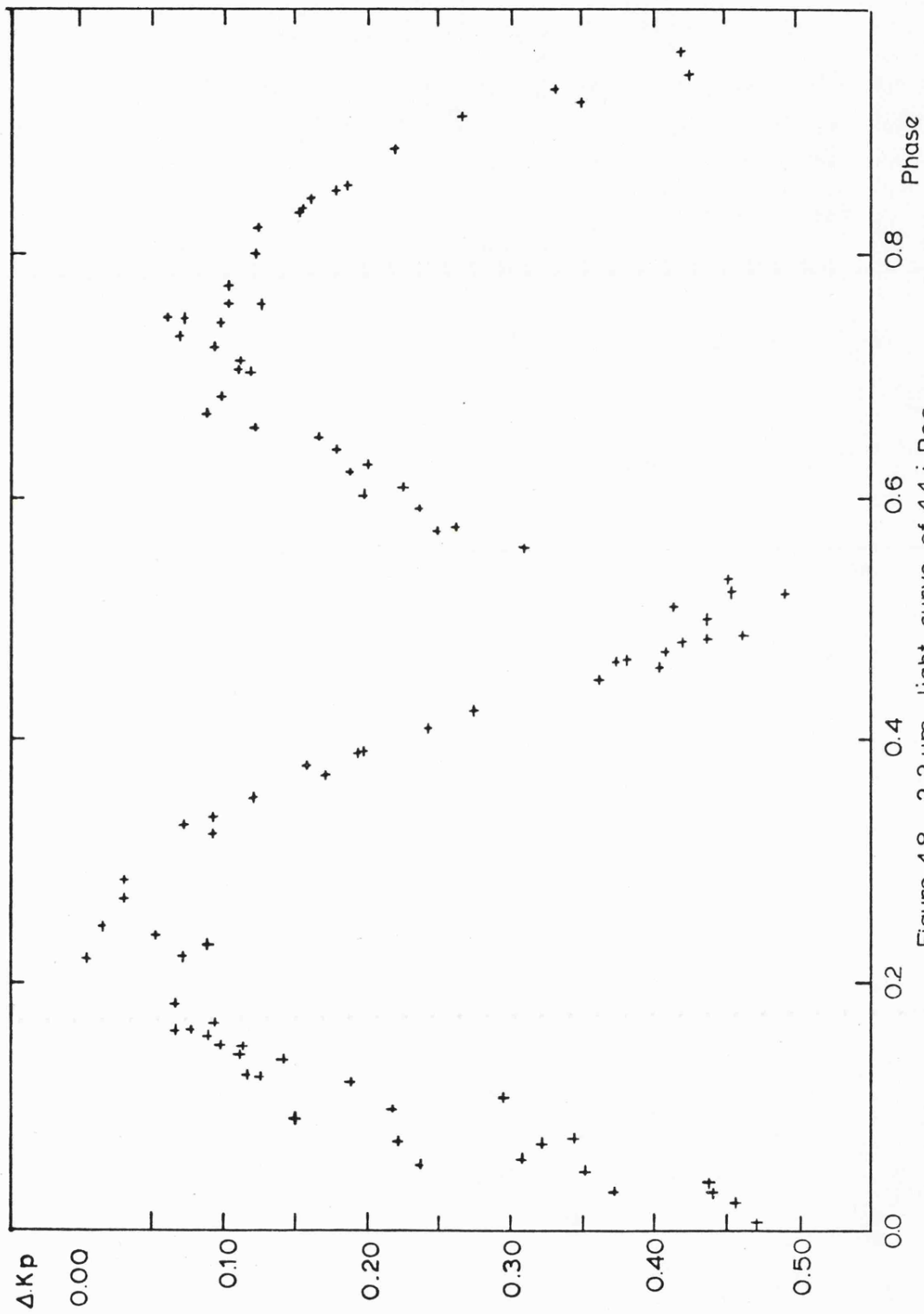


Figure 4.7 2.2  $\mu$ m light curve of 44 i Boo



**Figure 4.8** 2.2  $\mu$ m light curve of 44 i Boo  
(eclipsing binary only)

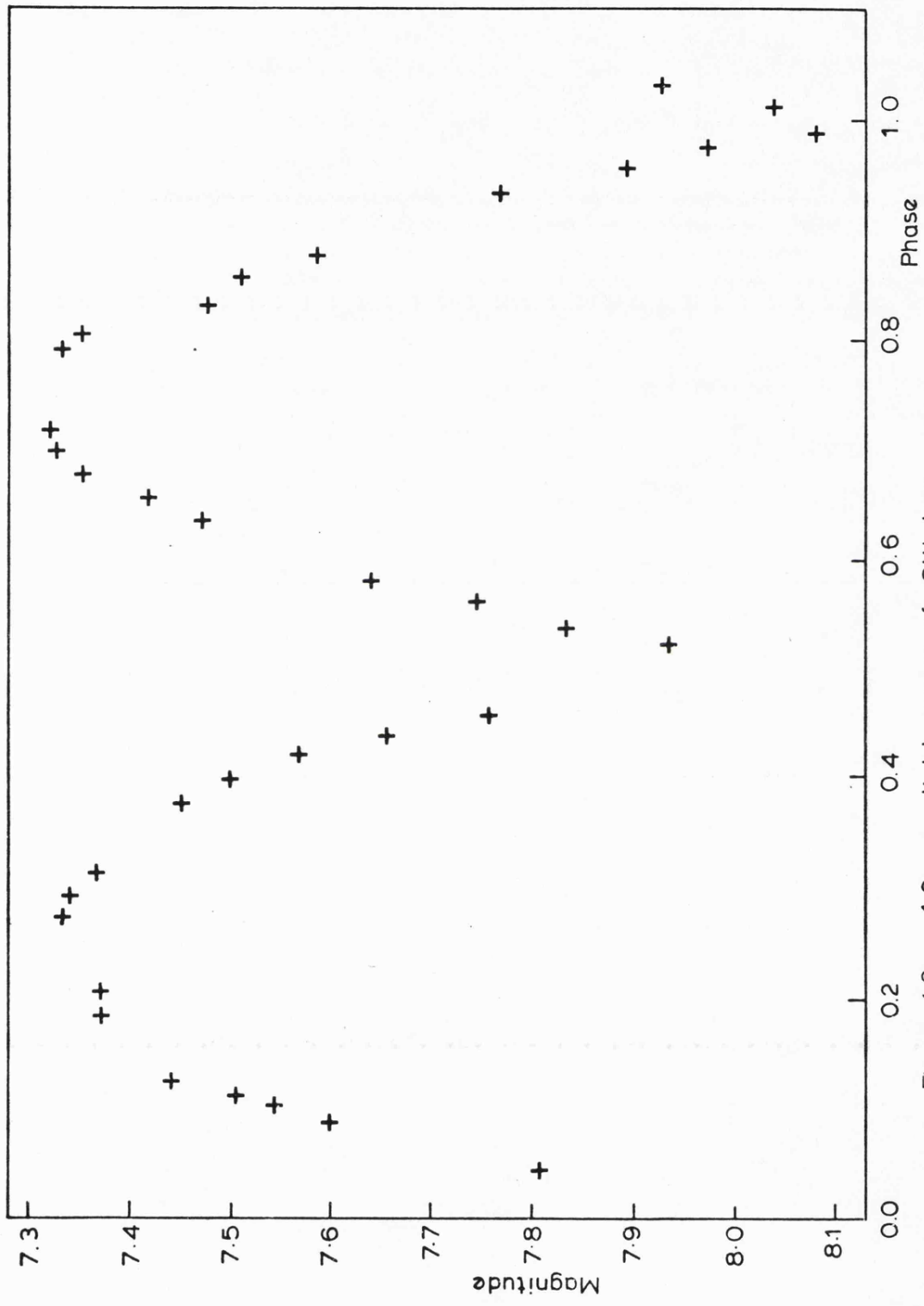


Figure 4.9 1.2  $\mu\text{m}$  light curve of SW Lac

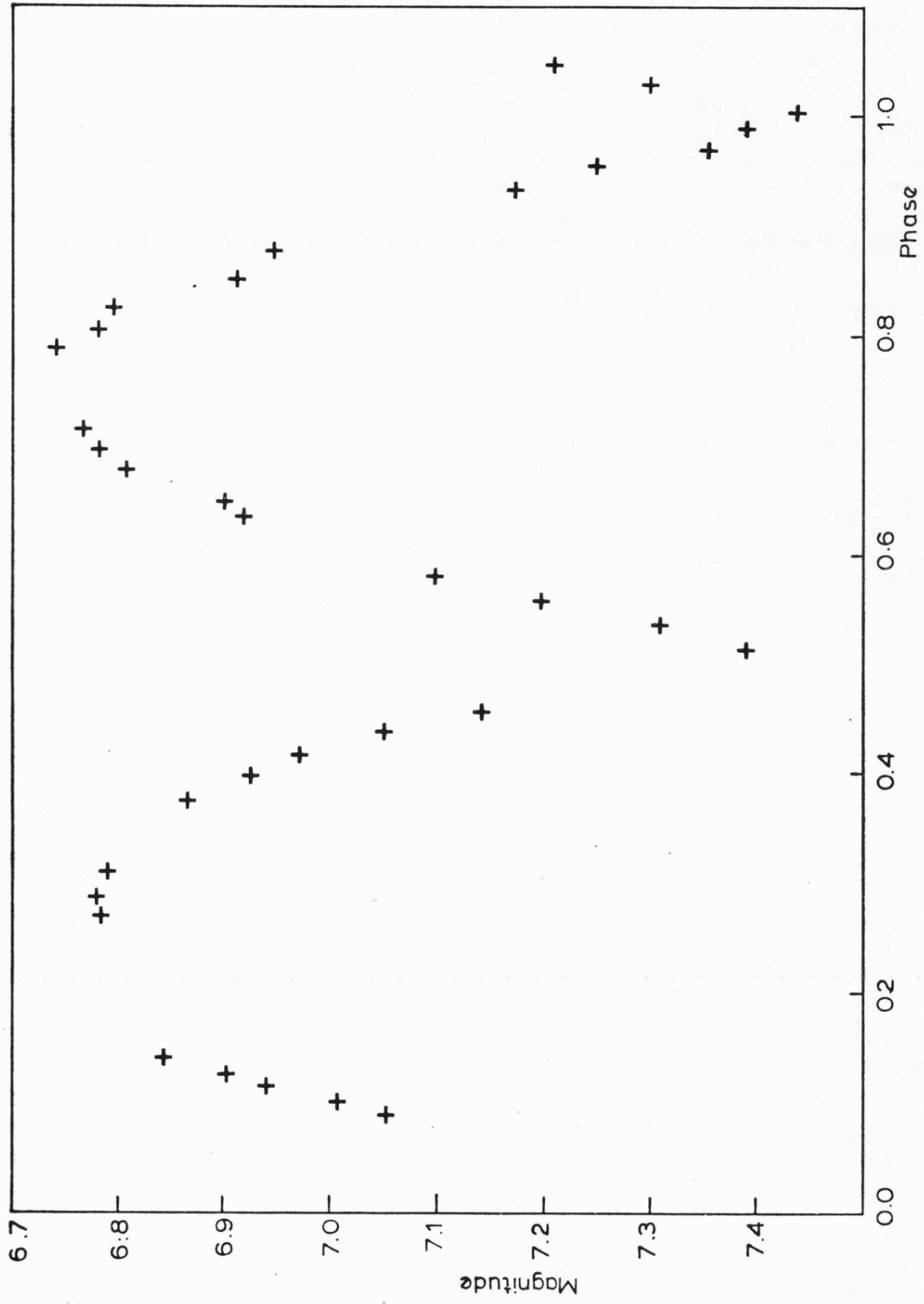


Figure 4.10  $2.2\ \mu\text{m}$  light curve of SW Lac

### Discussion

The infrared light curves presented show a number of features which are substantially different from the optical light curves of these systems. We do not feel that enough is known about these systems to attempt to construct a model which can completely describe all the features of the infrared light curves. We therefore propose to discuss the various features and offer some possible explanations for them individually. To assist this discussion the following table has been drawn up summarising the parameters of both infrared and optical light curves. Table 4.9 gives the spectral type, the visual and infrared magnitudes and the B - V and J - K colour indices for the systems at maximum light. This table also gives the depths of the minima for the optical and infrared light curves of the systems. The visual magnitudes and the B - V values are taken from Eggen (1967). A study of the optical data of SW Lac shows a variation of up to 0.3 of a magnitude at maxima in V. Such variations are also evident in the light curves of AB And and 44 i Boo. In view of the uncertainty in the visual magnitudes of the systems at maximum light a direct comparison between visual and infrared magnitudes cannot be made since the infrared and visual observations were not made at the same time. Inspection of Table V of Bookmyer (1965) shows that the depths of the minima in V, for SW Lac have been decreasing with time. These variations are due to changes in the heights of the maxima. The eclipse depths in V, for SW Lac are taken from Curve IV of Bookmyer (1965); the corresponding values for AB And and 44 i Boo were determined from the light curves obtained by Landolt (1969) and Binnendijk (1955) respectively.

Table 4.9

## Parameters of Infrared and Optical Light Curves

Star	AB And	44 1 Boo [eclipsing binary]	SW Lac
Spectral Type	G5V	G2V	G3V
V	9.6	5.85	8.5
J <sub>0.25</sub>	8.08	-	7.33
J <sub>0.75</sub>	8.13	-	7.33
K <sub>0.25</sub>	7.53	3.74	6.78
K <sub>0.75</sub>	7.56	3.80	6.75
B - V	+0.90	+0.85	+0.75
J - K	+0.56	-	+0.56
<u>Depths of Min. I</u>			
in V	0.82 (La)	0.61 (Bi)	0.78 (Bo)
in J	0.74	-	0.78
in K	0.68	0.47	0.66
<u>Depths of Min. II</u>			
in V	0.67 (La)	0.49 (Bi)	0.71 (Bo)
in J	0.71	-	0.72
in K	0.66	0.44	0.63

La = Landolt (1969)

Bi = Binnendijk (1955)

Bo = Bookmyer (1965)

(a) Infrared Colour Indices

On the basis of available photometric data for all three systems, V - K colours are determined, however they should be treated cautiously since V and K magnitudes were not observed simultaneously and the maximum of the light curves may vary with time. If we take the visual magnitudes of Eggen (1967) for AB And, 44 i Boo (eclipsing binary only) and SW Lac together with our corresponding values at K we find V - K colours of 2.05, 2.08 and 1.73 for AB And, 44 i Boo and SW Lac respectively. In addition, J - K colours for AB And and SW Lac are defined since J and K magnitudes were observed simultaneously for these systems. Using our observed J and K magnitudes we find a J - K colour of 0.56 for both AB And and SW Lac.

The V - K colour indices of all three stars and the J - K colours of AB And and SW Lac are very red for their spectral type. This was already known from the B - V colour indices. The spectral types of these stars do not correspond to their B - V colours. It should be noted that W Uma-type stars are classified as main sequence stars on the basis of their luminosities not on the appearance of their spectral lines which, due to rotation, are very broad. AB And (G5V) has B - V, V - K and J - K consistent with a G5III star. 44 i Boo (G2V) has  $B - V = + 0.85$  and  $V - K = + 2.08$ , these values are consistent with a G5III star. With SW Lac (G3V), J - K is fitted by G5III or K2V, but B - V requires G8V.

Since both components fill or nearly fill their Roche lobes surface-gravity will be small and low pressure atmospheres, which have large colour indices for their spectral type, can be expected. The narrow lines expected from such atmospheres will of course be masked by rapid rotation. The  $2.2 \mu\text{m H}^-$  absorption coefficient is less than its  $0.5 \mu\text{m}$  counterpart (Allen, 1973), and hence deeper and hotter

regions of the stars will be seen. This will also give a large  $V - K$ .

The possibility of reddening by circumstellar dust has also been considered. If the dust is sufficiently hot it will perhaps give additional  $2 \mu\text{m}$  radiation. However, this does not fit since  $B - V$  colours are too large for the observed  $J - K$ .

An infrared excess due to free-free emitting circumstellar envelope is also unlikely since temperatures over 7000 K are required if  $\text{H}^-$  free-free is not to be dominant. Using the formula for the absorption coefficient due to free-free emission for ionized hydrogen and the table for  $\text{H}^-$  free-free and bound-free, Allen (1973, page 102), together with the ionization table, Allen (page 36), it can be seen that with a temperature of 5770 K (temperature of a G2 main sequence star),  $\text{H}^-$  opacity dominates. If  $\text{H}^-$  opacity is dominant, optical emission by bound-free exceeds the infrared emission produced by  $\text{H}^-$  free-free.

(b) Eclipse Depths

Inspection of Table 4.9 clearly shows that primary and secondary eclipse depths are much more nearly equal at  $2.2 \mu\text{m}$  than in the optical light curves of these systems. From the optical light curves it is deduced that in W-type systems the secondary component is slightly hotter than the primary star. A deeper primary minimum occurs when the secondary component is eclipsed by the larger star. If one considers two Planck curves of slightly different temperatures, peaking at about  $0.6 \mu\text{m}$ , then the difference in brightness is very much greater at  $0.5 \mu\text{m}$  than at  $2.2 \mu\text{m}$ . This provides a simple explanation for the above effect.

A second noteworthy feature which is common to all three systems becomes apparent upon comparison of the optical light curves with those in the infrared. Namely that the depths of both primary and

secondary minima are smaller in the infrared than in the optical.

Again by considering Planck curves of slightly different temperatures, it can be seen that the reflection effect will be much less in the infrared. This means that the maxima of the light curves at phases 0.25 and 0.75 will be relatively less bright in the infrared than in the optical and the infrared eclipses will therefore be less deep.

(c) Variation of Colour Index with Phase

J - K colour index curves drawn from every 0.05 phase on the main light curves for AB And and SW Lac are illustrated in Figure 4.11. The variation of J - K with phase is such that  $C_{0.75} \leq C_{0.25} < C_{0.50} < C_{0.00}$  where C is the J - K colour index at the various phases. The B - V colour curve of all eclipsing binary systems with circular orbits shows a reddening during the primary minimum when the hotter component is eclipsed. For the W UMA-type systems, this reddening also appears during the secondary eclipse. This is caused by the reflection and gravity effects (Binnendijk, 1970). Comparing the B - V curves with the J - K curves it can be seen that similar phase-dependent variations are evident in B - V and J - K. However, the variations in J - K are smaller than the variation in spectral type implied by  $\Delta(B - V)$  would suggest. The variation of J - K colour is just as expected from the temperatures of different parts of the systems.

(d) Shape of the Light Curves

There are a number of differences in shape between the optical and infrared light curves. The infrared light curves of all three systems have a broader maximum at phase 0.25 than the maximum at phase 0.75. There may be a region of hot plasma, with an infrared excess due to free-free radiation, located near the inner Lagrangian point,

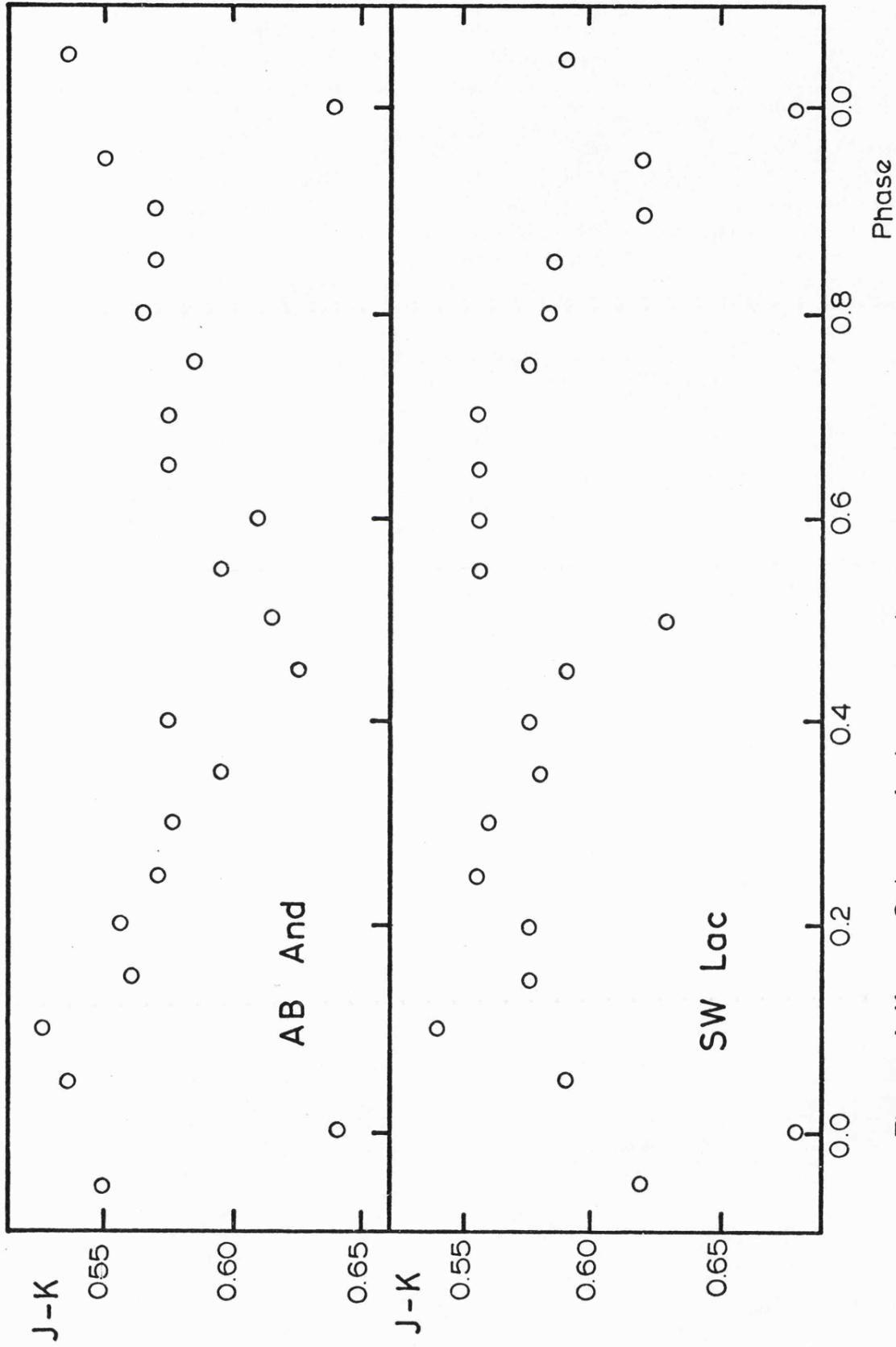


Figure 4.11 Colour index vs. phase curves

$L_1$ , but offset to the side seen at phase 0.25. This could be seen at both 0.25 and 0.75 phase but for a longer time around 0.25 phase. Hence the maxima would be of equal height but the maximum at phase 0.25 would be broader.

The infrared light curves of both AB And and 44 i Boo show a change of gradient at about 0.6 phase. A similar change, but not so obvious, occurs at 0.9 phase. This produces the narrow maximum at phase 0.75 and can be understood by the explanation above. It is strange however that the infrared light curves of SW Lac show a narrow maximum at phase 0.75 without the obvious gradient change.

The "O'Connell effect" which is used to refer to the phenomenon of unequal maxima (Milone, 1969) can be well seen in the infrared light curves of both AB And and 44 i Boo; this effect is not obvious with SW Lac. The brighter maximum occurs at phase 0.25.

Finally it should be remarked that the secondary minima for the  $2.2\mu\text{m}$  light curves of AB And and 44 i Boo are peculiar.

(e) Variations of the Maxima

When observations extend over more than one cycle there is evidence that the maxima of the light curves are variable. This is also observed in the optical light curves and could be explained by a variation in the gas streaming rate from the inner Lagrangian point causing a hot region of variable intensity.

Conclusion

If it were not for the complication of unequal maxima widths, infrared light curves would simplify the task of constructing models of W UMa-type systems since limb darkening and reflection effects appear to be less important than in the optical.

Further attention should be paid to the extreme red colour of these stars. It would be interesting to calculate a model atmosphere that could explain both the spectral type and the infrared colours of W UMa-type systems.

The infrared light curves can also be used for updating the ephemeris of these stars and determining period variations.

If this work is to be pursued further it is believed that it would be very desirable to make simultaneous visible and infrared observations of these systems.

## CHAPTER 5

## OBSERVATIONS AND DISCUSSION OF AM HERCULIS

AM Her ( $\alpha = 18^{\text{h}}14^{\text{m}}58^{\text{s}}.6$ ,  $\delta = 49^{\circ}50'55''$  (1950) ),

discovered in 1923 by M. Wolf at Heidelberg, Germany, was classified as a rapid irregular variable (Is) in the General Catalogue of Variable Stars (Kukarkin et al. 1969). A possible identification of AM Her as the optical counterpart of a weak unidentified X-ray source was first indicated by Berg and Duthie (1977). Independently, Hearn et al. (1976) have discovered a variable soft X-ray source, the error box of which contains the position of AM Her. This source has been detected with the SAS-3 satellite at a position near that of 3U 1809+50. The irregular variable AM Her has now been identified as the optical counterpart of the high-galactic-latitude X-ray source 3U 1809+50.

The brightness of the system has been shown to be variable over long time intervals from photographic observations made before 1974. A long term (130 to 176 days) variability of about 2 mag. was present in photographic data obtained in the years 1940 to 1960 (Meinunger, 1960). The photoelectric observations of AM Her made by Berg and Duthie (1977) indicated that the light curve shows rapid increases and decreases in intensity on time scales of minutes. Such flickering variability was present in both red and blue light curves.

A slit spectrogram ( $238 \text{ \AA mm}^{-1}$ ) of AM Her was obtained during a search for optically variable extragalactic objects by Bond and Tifft (1974). This showed emission lines of hydrogen and CaII K on a blue continuum, similar to cataclysmic variables of the U Gem type at minimum light. Cowley et al. (1976) and Priedhorsky (1977) have observed radial velocity variations in the emission lines. The observed radial velocity curves for the optical emission lines indicated

a low-mass binary system with a period of 3.1 hours.

Simultaneous spectroscopic (Cowley and Crampton, 1977) and photometric (Szkody and Brownlee, 1977) observations of AM Her made on 1976 August have both revealed a  $0^{\text{d}}.1289$  period for the system. Subsequent investigation by Hearn and Richardson (1976) showed that the soft X-ray flux of 3U 1809+50 is modulated with this period, confirming the identification of AM Her with the X-ray source. They found that the X-ray light curve of AM Her shows a deep minimum which coincides with a secondary minimum in the visible light curve.

Linear polarization observed in the V and I spectral bands and circular polarization observed in the V have been reported by Tapia (1977). Large variations were present in both polarization states. He has independently found a period of  $0^{\text{d}}.128918$  from the spikes of linear polarization. The maximum linear polarization occurs when the circular polarization changes sign. The maximum linear polarization observed by Tapia on JD 2443014.765 was chosen to be a standard epoch for calculating phases at the 1976 Ann Arbor symposium. Soon after Tapia's discovery of circular polarization in the optical flux, Stockman et al. (1977) made new polarimetric observations of AM Her in the red and UV bands. Their circular polarization measurements in the red band was in very good agreement with the visual photometric band measurements of Tapia. The UV measurements showed very little circular polarization. Linear and circular polarization observed in the optical emission indicate the presence of a magnetic white dwarf with a surface field of  $\sim 10^8$  gauss (Tapia, 1977; Stockman et al. 1977). The latter authors argued that AM Her is a binary system in which material is accreting onto a magnetic white dwarf. The rotation of the white dwarf is synchronised with the 3.1 hour binary period. Tapia (1977) suggested that the polarization observed in the optical

flux of AM Her is due to cyclotron emission of hot electrons in a magnetic field  $\sim 10^8$  gauss. Stockman et al. (1977) also suggested that cyclotron radiation from AM Her is produced in an accretion column close to the surface of the white dwarf.

The visual light curve of AM Her obtained by Szkody and Brownlee (1977) showed a broad, deep primary minimum of 0.7 magnitude, together with a possible secondary minimum. They also obtained U, B and R light curves, the primary minima of which were offset in phase from the visual light curve. They proposed a model for the system which includes a gas stream, hot spot, disk, primary and heated secondary. The primary minimum in V is due to the loss of light from a heated region of the secondary component facing the primary component when the back side of the secondary is in the line of sight.

Further multicolour observations of AM Her have been presented by Olson (1977) and Priedhorsky and Krzeminski (1978). The ephemeris for the visual and infrared eclipse:

$$J.D. \text{ Hel.Min.I} = 2443014.713 + 0.128924 E$$

has been derived by Olson (1977). Phases calculated with this ephemeris are denoted by  $\phi$  (phot). Therefore,  $\phi(\text{lin pol}) = \phi(\text{phot}) + 0.6$ , where  $\phi(\text{lin pol})$  denotes the phases calculated using the standard epoch of Tapia (1977). Deep and broad eclipses are well defined at visual and infrared wavelengths as shown in the work of Olson (1977). The period  $P = 0^d.128928 \pm 0^d.000001$  was determined by Priedhorsky and Krzeminski (1978). Their visual light curve of the system shows the same periodic variability with a deep and broad primary minimum centred at  $\phi(\text{lin pol}) = 0.56$  and a secondary minimum at  $\phi(\text{lin pol}) = 0.11$ . They concluded from these observations that an intense optical emission

region in the magnetic field near the surface of the degenerate dwarf is eclipsed by the dwarf itself during the primary minimum in the visual light curve.

In order to illustrate the periodic variation of several observed physical characteristics of this system, Crampton and Cowley (1977) collated phase diagrams for average Hydrogen radial velocities (from their data), smooth U and composite V light curves (Szkody and Brownlee, 1977), X-ray flux (Hearn and Richardson, 1976) and polarization variations, both linear and circular, (Tapia, 1976). These curves have been aligned relative to each other. Their schematic representation of these phase diagrams is reproduced in Figure 5.1.

Various models of AM Her which are based upon a binary system with a white dwarf, accretion disk, hot spot, and a gas stream from a companion star that fills its Roche lobe have been proposed by several investigators. Such a model by Fabian et al. (1977) will be discussed in more detail below.

#### Infrared Observations of AM Her

The infrared observations of AM Her were made with the 1.5 m Infrared Flux Collector at the Cabezón Observatory. The photometer with an InSb detector operating at 63 K was used. A total of 249 infrared measurements of the system at  $1.2 \mu\text{m}$  and  $2.2 \mu\text{m}$  was made on the nights of 1977 July 9 and 10. Each observation is the result of a 60 second integration, 30 seconds in each channel. The errors on each point are  $\pm 0.05$  mag. These were estimated from observations of a faint non-variable star. Observations covered one period only on both nights but there was a 15 minute break during the  $2.2 \mu\text{m}$  measurements.

$\alpha$  Lyr, used as the standard star was observed before and after the AM Her observations. This procedure was followed so that the

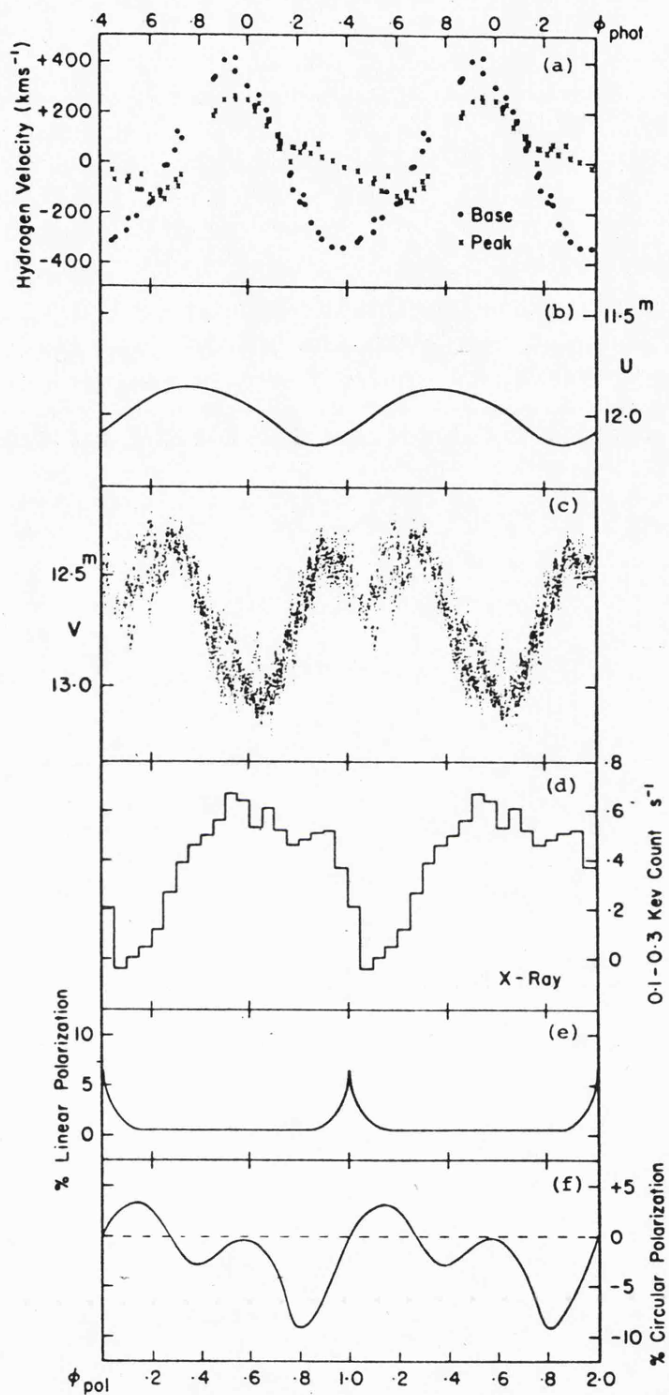


Figure 5.1 Schematic representation of phase diagrams for AM Her by Crampton and Cowley (1977)

light curves should be as complete as possible. The infrared magnitudes of  $\alpha$  Lyr given by Johnson et al. (1966) are  $J = 0.02$  and  $K = 0.02$ . Corrections were made for atmospheric extinction but these were very small. The heliocentric correction,  $dt = +0.0017$ , was applied to all observation times. The phases of the observations were calculated with the period,  $P = 0^d.128928$ , given by Priedhorsky and Krzeminski (1978). The epoch at the primary minimum of the visual light curve, J.D. Hel. 2443014.713 (Szkody and Brownlee, 1977), was used for these calculations.

The observations of AM Her at  $1.2 \mu\text{m}$  and  $2.2 \mu\text{m}$  are tabulated in Tables 5.1 and 5.2 respectively. The  $1.2 \mu\text{m}$  and  $2.2 \mu\text{m}$  light curves of the system are shown in Figures 5.2 and 5.3 respectively. These light curves have been published by Jameson et al. (1978), see Appendix 1A.

Table 5.1Infrared Observations of AM Her at 1.2  $\mu\text{m}$ 

JD2440000+	Phase	1.2 $\mu\text{m}$	JD2440000+	Phase	1.2 $\mu\text{m}$
3335.502	0.128	11.40	3335.534	0.370	11.41
3335.503	0.134	11.32	3335.534	0.376	11.31
3335.504	0.139	11.41	3335.535	0.381	11.41
3335.505	0.145	11.31	3335.536	0.387	11.59
3335.506	0.155	11.33	3335.537	0.397	11.53
3335.507	0.161	11.56	3335.538	0.403	11.59
3335.507	0.166	11.46	3335.539	0.408	11.58
3335.508	0.172	11.46	3335.541	0.425	11.36
3335.509	0.182	11.22	3335.541	0.430	11.48
3335.510	0.187	11.28	3335.542	0.435	11.54
3335.511	0.193	11.30	3335.544	0.452	11.54
3335.511	0.198	11.28	3335.545	0.457	11.59
3335.513	0.209	11.31	3335.546	0.463	11.52
3335.514	0.214	11.23	3335.546	0.467	11.58
3335.514	0.220	11.31	3335.547	0.473	11.59
3335.516	0.236	11.22	3335.548	0.478	11.54
3335.517	0.241	11.25	3335.548	0.483	11.62
3335.518	0.247	11.31	3335.549	0.489	11.44
3335.518	0.252	11.26	3335.550	0.494	11.45
3335.519	0.258	11.30	3335.551	0.505	11.53
3335.521	0.269	11.22	3335.552	0.511	11.34
3335.521	0.273	11.30	3335.555	0.538	11.54
3335.523	0.284	11.32	3335.557	0.549	11.37
3335.523	0.290	11.12	3335.557	0.554	11.31
3335.524	0.295	11.32	3335.558	0.560	11.28
3335.525	0.300	11.31	3335.559	0.564	11.36
3335.526	0.311	11.30	3335.559	0.570	11.24
3335.527	0.317	11.31	3335.561	0.586	11.24
3335.528	0.328	11.24	3335.562	0.591	11.30
3335.530	0.344	11.22	3335.563	0.597	11.26
3335.531	0.349	11.24	3335.565	0.613	11.17
3335.532	0.355	11.31	3335.566	0.618	11.27
3335.532	0.360	11.29	3335.566	0.624	11.32

Table 5.1 cont...

Table 5.1 cont..

JD2440000+	Phase	1.2 $\mu$ m	JD2440000+	Phase	1.2 $\mu$ m
3335.567	0.629	11.21	3335.600	0.888	11.66
3335.568	0.635	11.15	3335.601	0.893	11.62
3335.568	0.640	11.05	3335.602	0.898	11.51
3335.569	0.646	11.17	3335.603	0.909	11.44
3335.570	0.651	11.11	3335.604	0.915	11.61
3335.572	0.667	11.12	3335.605	0.920	11.59
3335.573	0.672	11.23	3335.607	0.936	11.52
3335.573	0.677	11.25	3335.607	0.942	11.56
3335.574	0.683	11.25	3335.608	0.947	11.56
3335.575	0.694	11.27	3335.609	0.952	11.64
3335.576	0.699	11.18	3335.610	0.963	11.56
3335.577	0.705	11.37	3335.611	0.968	11.46
3335.579	0.721	11.30	3335.611	0.974	11.69
3335.580	0.726	11.26	3335.612	0.979	11.62
3335.580	0.732	11.19	3335.614	0.990	11.47
3335.581	0.737	11.20	3335.614	0.995	11.41
3335.582	0.748	11.22	3335.615	0.001	11.66
3335.583	0.753	11.30	3335.617	0.017	11.62
3335.584	0.758	11.40	3335.618	0.023	11.57
3335.586	0.774	11.22	3335.618	0.028	11.43
3335.586	0.780	11.22	3335.619	0.033	11.51
3335.587	0.785	11.19	3335.621	0.044	11.62
3335.588	0.791	11.22	3335.621	0.049	11.52
3335.589	0.802	11.28	3335.622	0.054	11.47
3335.590	0.807	11.31	3335.623	0.060	11.37
3335.591	0.812	11.31	3335.623	0.065	11.48
3335.593	0.829	11.31	3335.624	0.071	11.30
3335.593	0.834	11.51	3335.628	0.103	11.34
3335.594	0.840	11.54	3335.629	0.109	11.32
3335.595	0.845	11.39	3335.630	0.114	11.30
3335.596	0.855	11.25	3335.630	0.120	11.41
3335.597	0.860	11.28	3335.632	0.130	11.37
3335.598	0.866	11.46	3335.632	0.136	11.45
3335.600	0.882	11.62	3335.633	0.141	11.42

Table 5.2Infrared Observations of AM Her at 2.2  $\mu$  m

JD2440000+	Phase	2.2 $\mu$ m	JD2440000+	Phase	2.2 $\mu$ m
3334.447	0.941	10.46	3334.481	0.205	10.65
3334.448	0.952	10.80	3334.482	0.211	10.90
3334.450	0.968	10.63	3334.483	0.222	10.77
3334.451	0.973	10.74	3334.484	0.232	10.69
3334.452	0.979	10.61	3334.485	0.237	10.64
3334.452	0.984	10.63	3334.486	0.242	10.66
3334.454	0.995	10.63	3334.486	0.248	10.58
3334.455	0.006	10.67	3334.489	0.264	10.60
3334.456	0.011	10.67	3334.490	0.275	10.58
3334.457	0.022	10.59	3334.491	0.280	10.81
3334.458	0.028	10.60	3334.492	0.291	10.85
3334.459	0.032	10.75	3334.493	0.297	10.78
3334.459	0.038	10.52	3334.493	0.302	10.70
3334.461	0.049	10.64	3334.494	0.308	10.65
3334.461	0.054	10.85	3334.495	0.312	10.64
3334.462	0.059	10.71	3334.496	0.323	10.76
3334.463	0.065	10.71	3334.497	0.329	10.73
3334.464	0.076	10.56	3334.498	0.334	10.84
3334.466	0.087	10.61	3334.499	0.345	10.54
3334.467	0.097	10.58	3334.500	0.350	10.59
3334.471	0.125	10.59	3334.500	0.356	10.62
3334.471	0.129	10.53	3334.502	0.372	10.86
3334.472	0.135	10.48	3334.503	0.377	10.86
3334.473	0.140	10.56	3334.504	0.382	11.11
3334.474	0.151	10.64	3334.505	0.388	11.11
3334.475	0.156	10.70	3334.506	0.399	10.74
3334.475	0.162	10.53	3334.507	0.405	10.93
3334.477	0.173	10.51	3334.508	0.415	10.84
3334.478	0.184	10.52	3334.509	0.426	10.98
3334.479	0.189	10.52	3334.510	0.431	11.13
3334.480	0.194	10.52	3334.523	0.533	10.75
3334.480	0.200	10.63	3334.524	0.539	11.46

Table 5.2 cont..

Table 5.2 cont..

JD2440000+	Phase	2.2 $\mu$ m	JD2440000+	Phase	2.2 $\mu$ m
3334.525	0.544	11.16	3334.550	0.738	11.00
3334.525	0.550	10.92	3334.551	0.749	10.79
3334.527	0.560	10.76	3334.552	0.754	10.83
3334.528	0.571	10.93	3334.552	0.760	10.64
3334.529	0.577	10.91	3334.553	0.765	10.54
3334.530	0.588	11.03	3334.555	0.776	10.72
3334.532	0.598	10.86	3334.555	0.782	10.58
3334.532	0.604	10.90	3334.556	0.787	10.58
3334.534	0.614	10.71	3334.558	0.803	10.53
3334.534	0.619	10.79	3334.559	0.808	10.50
3334.535	0.625	10.85	3334.559	0.813	10.53
3334.536	0.630	10.82	3334.560	0.819	10.74
3334.537	0.641	10.76	3334.561	0.830	10.60
3334.538	0.647	10.62	3334.562	0.835	10.74
3334.539	0.652	10.77	3334.563	0.840	10.63
3334.541	0.668	10.82	3334.565	0.857	10.72
3334.541	0.674	10.91	3334.566	0.862	10.71
3334.542	0.679	10.91	3334.566	0.868	10.76
3334.544	0.695	10.82	3334.568	0.878	10.70
3334.545	0.701	10.77	3334.568	0.884	10.61
3334.546	0.706	10.76	3334.569	0.889	10.74
3334.546	0.711	10.66	3334.570	0.895	10.74
3334.548	0.722	10.64	3334.572	0.910	10.54
3334.548	0.727	10.62	3334.573	0.916	10.63
3334.549	0.733	10.77	3334.573	0.921	10.78
			3334.575	0.932	10.62

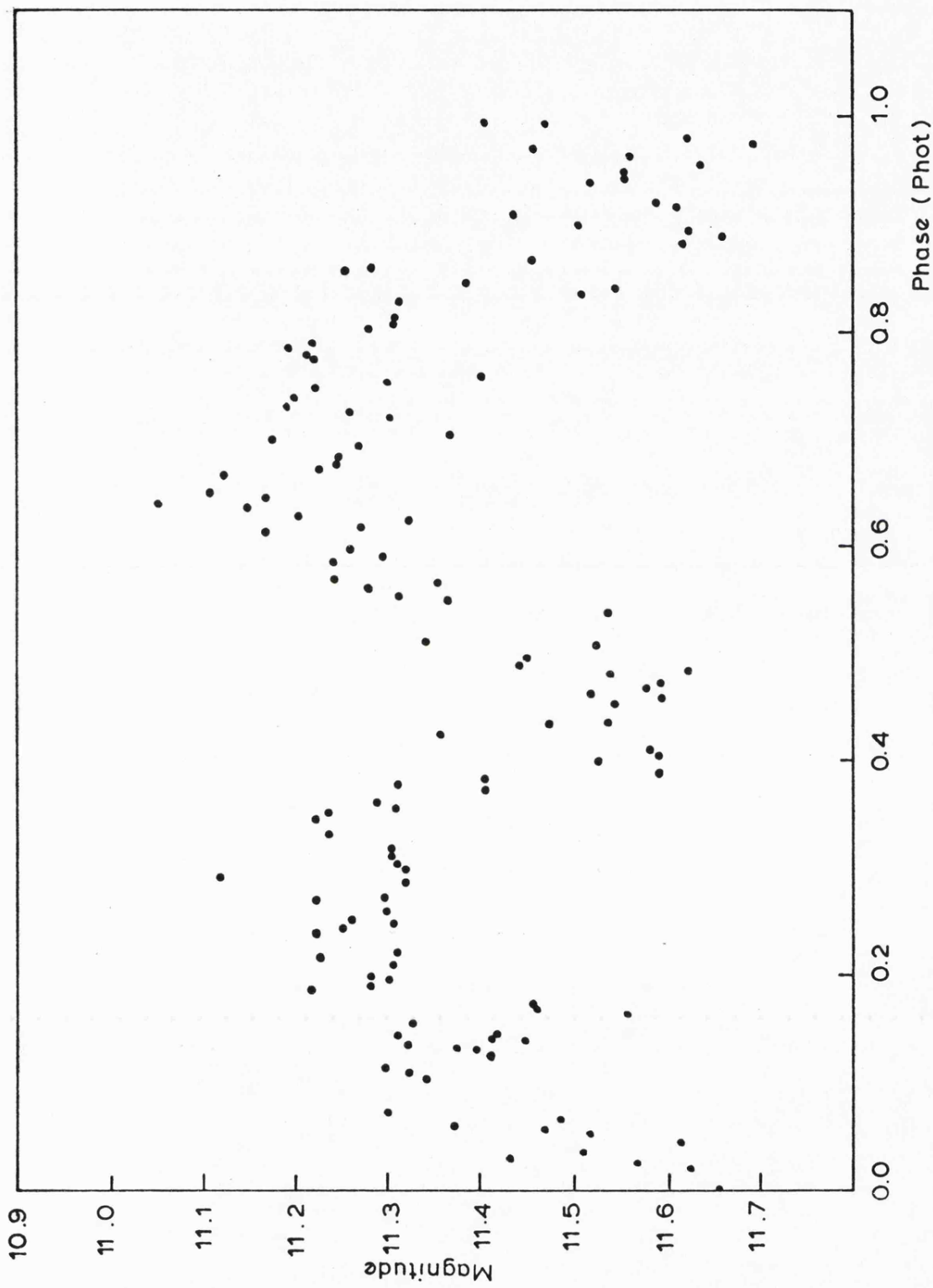


Figure 5.2 1.2  $\mu\text{m}$  light curve of AM Her

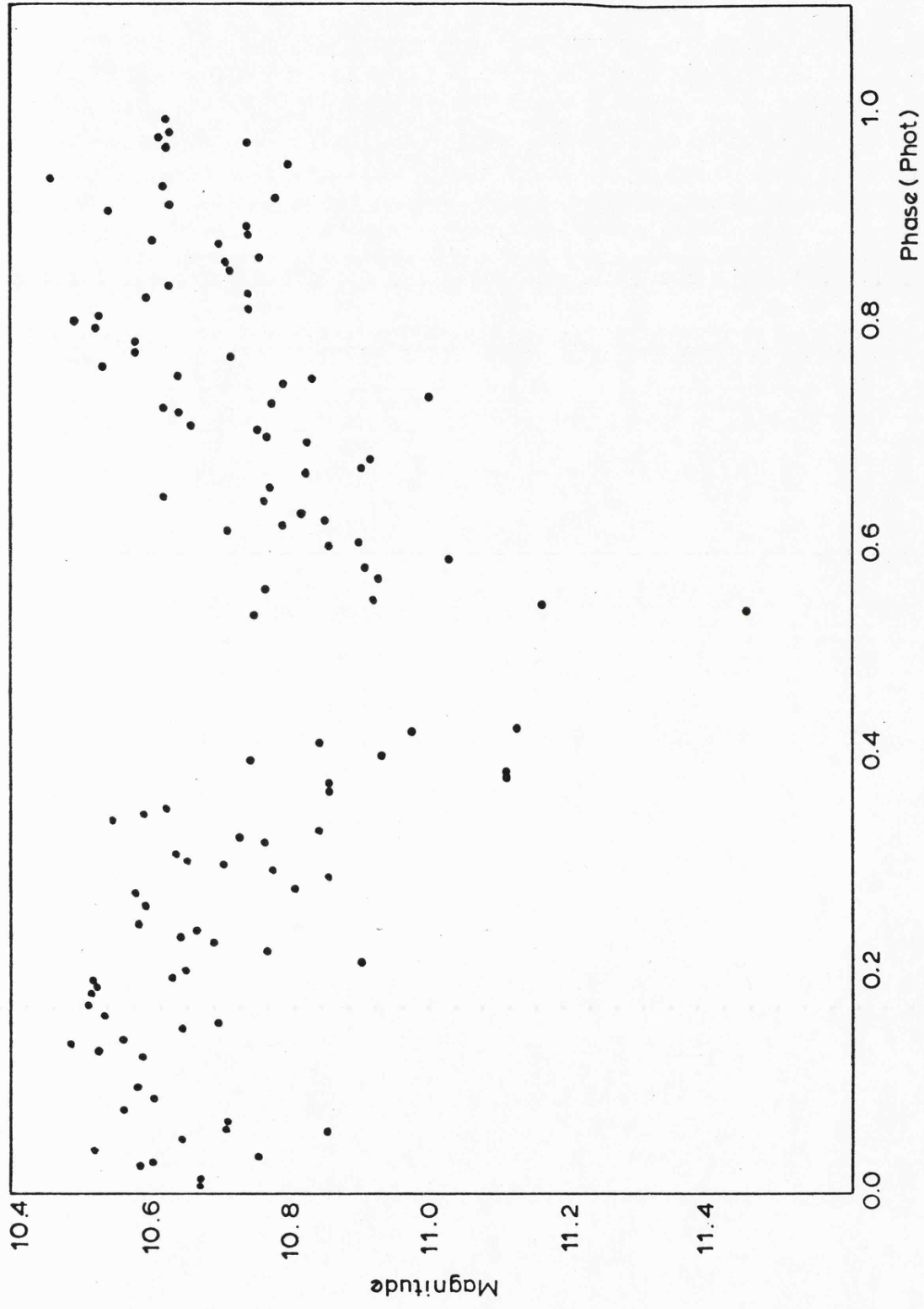


Figure 5.3 2.2 μm light curve of AM Her

### Features of the Infrared Light Curves

The most remarkable feature in the  $2.2 \mu\text{m}$  light curve is the absence of the primary eclipse at photometric phase 0.0. It is unfortunate that the bottom of the  $2.2 \mu\text{m}$  eclipse at phase 0.5 which corresponds to the secondary minimum in the visual light curve was not observed due to a short break during which it was thought the cryostat had run out of liquid nitrogen. However, this light curve shows a broad and very deep eclipse at photometric phase 0.5. Thus the  $2.2 \mu\text{m}$  light curve is similar to that observed in X-rays (Hearn and Richardson, 1976).

The primary and secondary eclipses are well defined at  $1.2 \mu\text{m}$ . Thus the  $1.2 \mu\text{m}$  light curve is similar to the optical light curve. However, the primary and secondary eclipse depths of the  $1.2 \mu\text{m}$  light curve are approximately equal ( $\Delta m \simeq 0.4$ ).

Large flickering activity from 0.1 to 0.3 mag. is seen throughout the cycle in both  $1.2$  and  $2.2 \mu\text{m}$  light curves. The error of each point was found to be  $\pm 0.05$ . Thus the spread of the points is genuine flickering of the system which is also seen in the optical light curves.

Finally, there may be a shallow  $2.2 \mu\text{m}$  primary eclipse, hidden by the flickering; if the data is smoothed a depth of 0.15 mag. would be consistent with the results.

### Discussion

Conclusions which can be drawn from the infrared light curves are:

(a) Any model which describes the optical light curve of this system could also explain the  $1.2 \mu\text{m}$  light curve. A dwarf nova like model of AM Her has been given by Fabian et al. (1977). In this model

the system consists of a cool companion (a faint red dwarf) transferring material through the inner Lagrangian point to an accretion disk around a highly magnetised white dwarf. The system is observed at a moderate inclination so that the white dwarf is not eclipsed by the secondary component. A high density hot spot is formed where the gas stream from the cool star meets the accretion disk. The radiation from the white dwarf will give rise to a reflection effect from the gas flow in the dwarf's Roche lobe and from the secondary component. Therefore, a combination of reflection effects and a partial eclipse of the disk and hot spot region by the secondary component produces the optical light curve of the system. Consequently, we suggest that at  $1.2 \mu\text{m}$  the flux is dominated by radiation from the disk and hot spot as in the optical.

(b) In the model of Fabian et al. (1977) the soft X-rays are produced by accretion of material onto the white dwarf. Electron scattering in the hot spot region produces the X-ray minimum. The similarity of the  $2.2 \mu\text{m}$  and X-ray light curves suggest that at  $2.2 \mu\text{m}$  the dominant emission must also arise near the white dwarf. Thus, electron scattering in the hot spot produces a minimum at phase 0.5 as for the X-rays.

(c) The infrared photometry yields a positive colour index,  $J - K \simeq 0.60$  for the system at maximum light. We therefore conclude that the system has an excess of radiation at  $2.2 \mu\text{m}$ . This excess must come from the vicinity of the white dwarf since the  $2.2 \mu\text{m}$  light curve is similar to X-ray curve. It is known that the white dwarf emits cyclotron radiation generated by its strong magnetic field ( $\sim 10^8$  gauss). Thus, the most likely cause of this  $2.2 \mu\text{m}$  excess is

cyclotron radiation. If this is the case then AM Her is the first star found to have an excess due to cyclotron radiation.

It may be noted that this excess of radiation cannot be due to the secondary component. Any star of reasonable temperature which emits at  $2.2 \mu\text{m}$  would also emit strongly at  $1.2 \mu\text{m}$ . The near equality of the eclipse depths at  $1.2 \mu\text{m}$  would then imply a temperature for the secondary component similar to that of the accretion disk and hot spot. This is clearly impossible. Therefore, the secondary component whose only function is to provide material which accretes onto the white dwarf makes an insignificant contribution to the infrared flux.

#### Interpretation of the infrared data and some parameters of the system

If we follow the model of Fabian et al. (1977) we now have three components to consider: accretion disk, hot spot or scattering wall and cyclotron radiation from the white dwarf. By considering relative eclipse depths and fluxes at  $1.2 \mu\text{m}$  and  $2.2 \mu\text{m}$  it is possible to derive some parameters of the system. This has been done by King et al. (1978) whose paper is reproduced in Appendix 1B.

They divide the radiation from AM Her into a number of components:  $C_1$  and  $C_2$  denote the eclipsed fluxes at phase 0.5 at  $1.2 \mu\text{m}$  and  $2.2 \mu\text{m}$  respectively, similarly  $F_1$  and  $F_2$  are the uneclipsed fluxes. At phase 0.0 the partially eclipsed fluxes are denoted by  $F_1'$  and  $F_2'$ .  $C_1$  and  $C_2$  then represent the cyclotron fluxes,  $F_1$  and  $F_2$  the fluxes of hot spot and disk, and  $F_1'$  and  $F_2'$  the fluxes of the disk alone. Consequently, the total fluxes from the system outside the eclipse at  $1.2 \mu\text{m}$  and  $2.2 \mu\text{m}$  are  $C_1 + F_1$  and  $C_2 + F_2$  respectively. Relations between these fluxes can be obtained from the observed light curves. In particular  $F_1'/F_2 = 1.7$ ,  $F_2'/F_2 = 0.73$  and  $F_1'/F_1 = 0.55$ . If  $T_d$ ,  $T_s$ ,  $A_d$ ,  $A_s$  represent the temperatures and surface areas of one

side of the disk and hot spot respectively and  $X = A_s T_s / A_d T_d$ , then assuming the hot spot to be optically thick one can solve for  $X$  and  $\tau_1$  and  $\tau_2$ , the free-free optical depths of the disk at  $1.2 \mu\text{m}$  and  $2.2 \mu\text{m}$  respectively. It is found that  $\tau_1 = 0.38$ ,  $\tau_2 = 3.36 \times 0.38$  and  $X = 0.31$ .

If reasonable dimensions are assumed for the system then the appropriate equations lead to values of  $T_s \geq 2 T_d$  and  $10^4 \leq T_d \leq 5 \times 10^4$  (in K). It is also found that the electron density of the disk must lie between  $4.4 \times 10^{12}$  and  $3.85 \times 10^{13} \text{ cm}^{-3}$ .

Finally, the ratio  $C_1/C_2 \leq 1.35$  is consistent with the cyclotron radiation from a dipole field although detailed formulae for cyclotron emission coefficients are not available in the literature.

### Conclusion

It would be useful to make further observations of this very interesting system. Clearly the  $2.2 \mu\text{m}$  light curve ought to be repeated to get the depth of secondary minimum. Observations of AM Her in its non flare state would also be valuable but would require a larger telescope. Finally since the  $2.2 \mu\text{m}$  flux is thought to be cyclotron one might expect to observe large  $2.2 \mu\text{m}$  polarizations and this could probably be done on UKIRT.

## CHAPTER 6

## OBSERVATIONS AND DISCUSSION OF RZ SCUTI

A brief description of RZ Sct has been given in the introduction. In this chapter previous work on this system will be reviewed and the results of our infrared observations presented.

RZ Sct (BD-9<sup>o</sup>4736;  $\alpha = 18^{\text{h}}21^{\text{m}}05^{\text{s}}$ ;  $\delta = -09^{\circ}15'.6$  (1900) ) is an Algol-type eclipsing binary with an orbital period of  $15^{\text{d}}.19070$ . It was discovered by Miss Cannon in 1908. Since then the system has been the subject of several photometric and spectroscopic investigations.

The orbital elements of the system were first derived by Shapley (1915) from the visual observations by Baker and Wylie (1913). He assumed partial eclipses at minimum light and his solution indicated that the inclination of the orbit was  $i = 76^{\circ}.8$  and that the radii of the brighter and fainter components (hereafter referred to as the primary and secondary components respectively) were  $r_1 = 0.150$  and  $r_2 = 0.306$  respectively. Therefore, the primary minimum was due to an occultation. Plaut (1950) determined the approximate photometric elements from the photographic light curve obtained by Gaposchkin (1943). His elements described a total eclipse at minimum light. In contrast his solution indicated that the primary minimum was due to a transit.

The radial velocity of this system was first observed by Neubauer (1943) at the Lick Observatory. A detailed spectroscopic work on RZ Sct was published by Neubauer and Struve (1945). They investigated the behaviour of the radial velocity of the system. A strong distortion of the radial velocity curve near eclipse was detected.

Further spectroscopic observations of RZ Sct have been obtained by Hansen and McNamara (1959) which showed that the system has

a gaseous envelope. Furthermore, they have investigated the stream trajectories in the system and found evidence for a stream circulating the whole system, and for a large eddy (or a countercurrent) behind the primary component. A schematic model of the gas streams which surround the components of the system has been developed from their observations. The counter-rotating eddy is proposed to explain changes in the asymmetry of the helium-line profiles observed during the phases between 0.6 and 0.9. Their observed velocity curve of RZ Sct is given in Figure 6.1. The velocities given by the H lines and those given by the He lines are plotted in this figure. A diagram of their model is also reproduced in the same figure.

Discussions of the spectra, luminosity classes and masses of the two components of RZ Sct have resulted in variant conclusions in the earlier investigations. According to Struve (1944) the spectral type of the primary component varies within type B (most likely peculiar B2). Morgan et al. (1955) determined the type as B3 Ib, and Roman (1956) as B0 V at phase 0.34. The spectrum of the secondary component has never been observed.

Kopal (1956) derived incredibly small masses ( $m_1 = 0.42 m_{\odot}$  and  $m_2 = 0.20 m_{\odot}$ ) for the components using Shapley's (1915) photometric elements. Neubauer and Struve (1945) found masses of  $m_1 = 0.70 m_{\odot}$  and  $m_2/m_1 = 0.38$ . The values  $m_1 = 1.73 m_{\odot}$  and  $m_2 = 0.81 m_{\odot}$  were derived by Hansen and McNamara (1959). Consequently, it was concluded that the luminosities of both components were considerably overluminous for their masses.

The study of this remarkable system has been extended by Kitamura and Sato (1967), Karetnikov (1967, 1973) and Wilcken et al. (1976). Kitamura and Sato (1967) have obtained a new photoelectric light curve. The transit nature of the primary minimum was confirmed

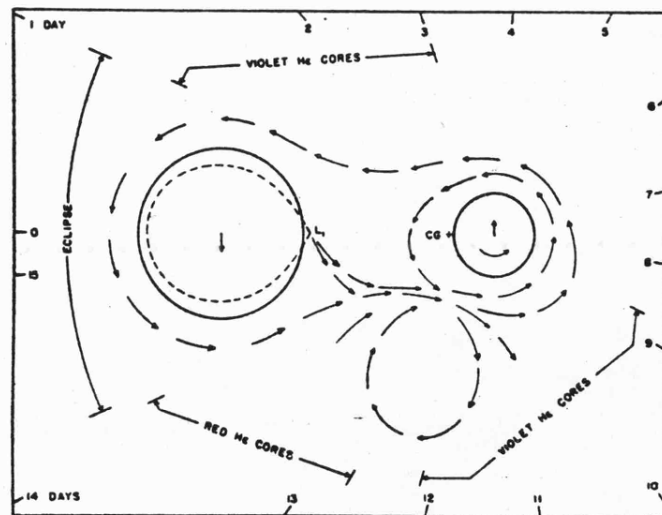
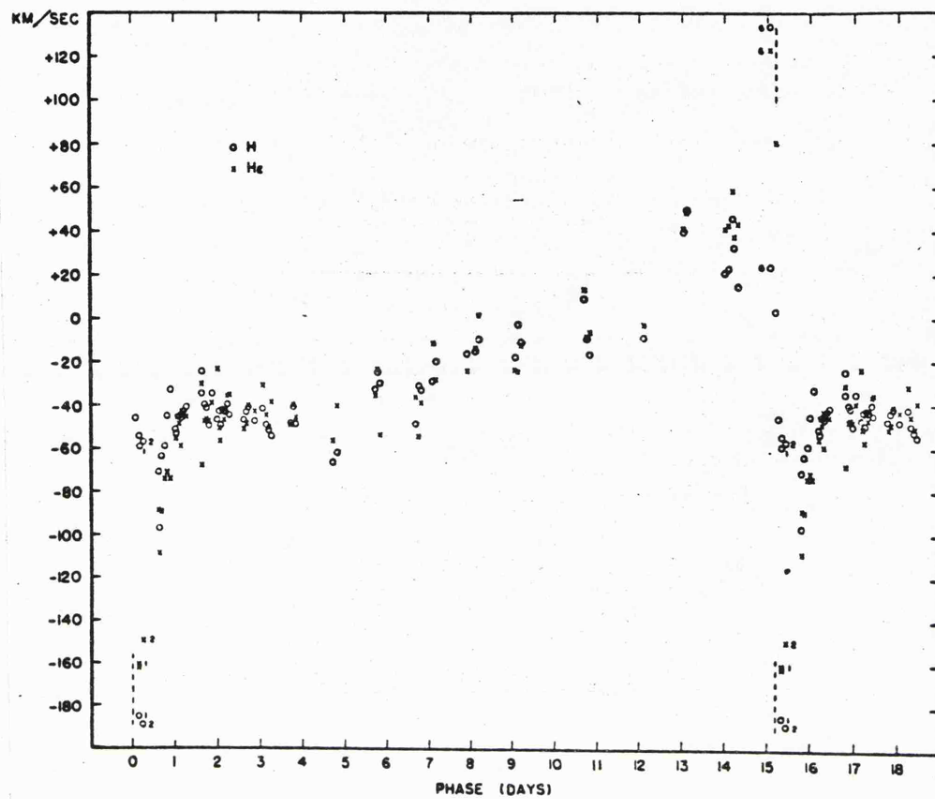


Figure 6.1 The observed velocity curve and a model of RZ Sct by Hansen and Mc Namara (1959)

with this photoelectric data. They combined the result of their photometric elements with the former spectrographic work by Hansen and McNamara and found masses of  $m_1 = 13.9 m_{\odot}$  and  $m_2 = 2.8 m_{\odot}$ . These observations then indicated that the luminosity of the primary component is normal for its mass as a supergiant star.

A qualitative model for RZ Sct has been constructed from the spectrophotometric observations by Karetnikov (1967). In this model the system consists of a primary star of spectral type B2 which is overluminous for its mass and a secondary component which is a subgiant whose spectrum is in the range F5 - G2. The secondary component fills up its Roche lobe transferring material through the inner contact point. Because of its high rotational velocity and nonstationary processes the primary component also ejects some of its material into surrounding space forming a disk around the star. Turbulent currents of material are formed where the gas stream from the secondary star collides with the material of the disk. A countercurrent is formed behind the primary star in an analogous way to that of Hansen and McNamara's proposal.

Some monochromatic light curves of RZ Sct have been constructed from the spectroscopic observations by Karetnikov (1973). These curves indicated that the depth and width of both the primary and secondary minima vary with wavelength. In his discussion it was concluded that the system consists of a supergiant of spectral type B3 and a subgiant of type F3. The brightness variation at eclipse provides further evidence for a gaseous envelope around the system.

A brief description of the photoelectric observations of RZ Sct has been published by Hansen (1969). The light curve of the system is peculiar. Between the primary and secondary eclipses the light curve is essentially normal and flat, but between secondary and primary minima

it is varying. Both minima, therefore, are asymmetric. He suggested that these asymmetries in the light curve are due to absorption occurring in the gas stream which surrounds the system. His preliminary calculations indicated that this absorption can probably be explained by electron scattering in the gas stream.

In 1976, Wilcken et al. (1976) have published the results of extensive photoelectric observations of RZ Sct in the U, B and V passbands obtained in the Brigham Young University. They presented complete U, B and V light curves of the system which are reproduced in Figure 6.2. Several interesting features of the light curves were discussed. The asymmetries and distortions in the light curves are evident. The ultraviolet observations show night-to-night variations. In all three light curves there is a long, gradual slope from phase 0.70 to phase 0.92. In the V light curve the secondary eclipse shows a relatively steep drop into eclipse and a much more gradual rise from phase 0.50 to phase 0.70. In view of these circumstances they made a number of solutions to obtain approximate photometric elements of the system. According to their conclusions the system is now thought to consist of a brighter primary component of spectral type B2 II and a secondary star of type AO II-III. Both components have radii  $\sim 14 R_{\odot}$ . The system has a large colour excess,  $E(B - V) \simeq 0.86$ .

Finally, a summary of the photometric elements of RZ Sct obtained by various investigators is presented in Table 6.1. The preceding review discussed the various conclusions reached by many investigators; those for which there is a strong consensus are summarised in the following list.

- (a) Gas streams are evident in the system RZ Sct.
- (b) The secondary component fills its Roche lobe transferring material through the inner Lagrangian point to a disk around

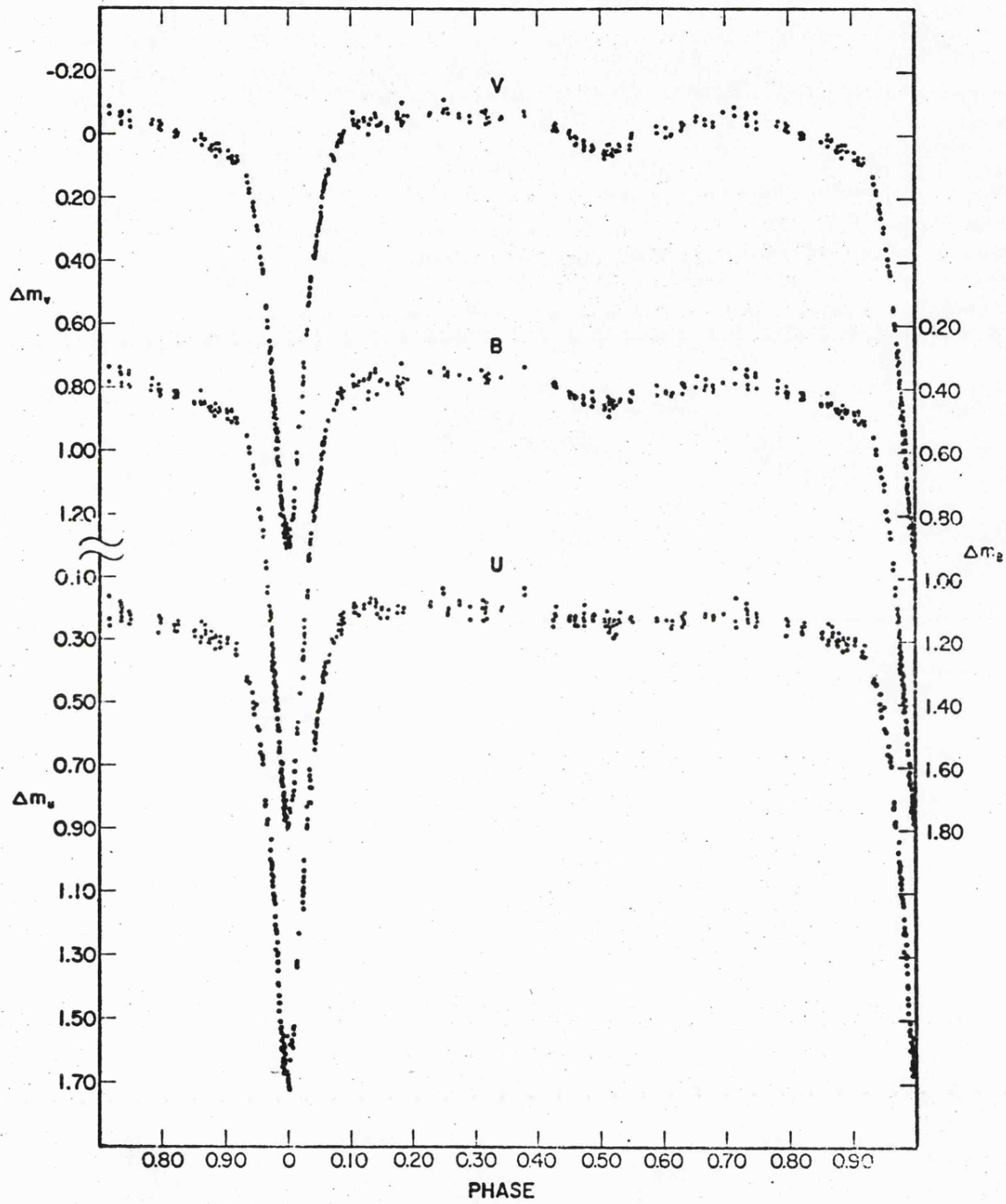


Figure 6.2    The V, B and U light curves of RZ Sct by  
Wilcken et al.(1976)

Table 6.1

Photometric elements of RZ Sct

Source	i	r <sub>1</sub>	r <sub>2</sub>	L <sub>1</sub>	L <sub>2</sub>
Shapley (1915)	76° .8	0.150	0.306	0.89	0.11
Kitamura and Sato (1967)	86°	0.30	0.24	0.90	0.10
Hansen (1969)	85° .4	0.290	0.276	0.91	0.09
Wilcken et al. (1976)	84°	0.26	0.26	0.89	0.11

the primary component.

- (c) The rotational velocity of the primary component is very high.
- (d) The B - V colour excess of the system is very large.
- (e) The asymmetries in the visual light curves are evident.

### Infrared Observations

The infrared observations of RZ Sct at 1.2, 2.2 and 3.6  $\mu\text{m}$  were made with the 1.5 m Infrared Flux Collector at the Cabezon Observatory in June 1974, June-July 1976 and August-September 1976. The standard Leicester photometer which was described in Chapter 2 was used for these observations. In the first observing session the PbS detector operating at 77 K was used. In 1976 the observations were made using the InSb detector operated at 63 K. Each observation is the average of a number (usually 9) of consecutive 10 second integrations in each channel. The error of each observation is taken as the standard deviation of the mean of the readings. The errors of all the readings are tabulated for each wavelength along with the magnitudes calculated for each observation in the appropriate tables. The error bars were drawn on the light curves for each point with an error greater than  $\pm 0.02$ .

$\alpha$  Lyr,  $\alpha$  Cyg and  $\beta$  Oph were used as the standard stars. The adopted magnitudes of  $\alpha$  Lyr and  $\alpha$  Cyg are given in Table 3.1. J, K and L magnitudes for  $\beta$  Oph (B.S. 6603) are given by Johnson et al. (1966) as 0.92, 0.23 and 0.13 respectively. Cross calibrations of these standards have been made in order to check the consistency of the given magnitudes. All observations were corrected for atmospheric extinction, and heliocentric corrections were applied to all observation times. The orbital phases were calculated from the equation given by

Wilcken et al. (1976),

$$\text{J.D.Hel.Min.I} = 2439676.8793 + 15.19070 \text{ E.}$$

The observations of RZ Sct at 1.2, 2.2 and 3.6  $\mu\text{m}$  are tabulated in Tables 6.2, 6.3 and 6.4 respectively. Figures 6.3, 6.4 and 6.5 illustrate the light curves of RZ Sct at 1.2, 2.2 and 3.6  $\mu\text{m}$  respectively.

Table 6.2Infrared Observations of RZ Sct at 1.2  $\mu$ m

JD 2440000+	Phase	1.2 $\mu$ m	$\sigma$
2213.549	0.988	6.59	$\pm$ 0.23
2214.515	0.052	6.39	0.27
2215.514	0.118	5.87	0.17
2218.510	0.315	5.81	0.11
2219.517	0.381	5.99	0.16
2220.552	0.449	5.93	0.13
2221.528	0.514	6.19	0.13
2221.599	0.518	6.16	0.20
2222.497	0.577	6.00	0.10
2222.569	0.582	5.93	0.06
2222.618	0.585	5.91	0.09
2223.462	0.641	6.03	0.07
2223.538	0.646	5.86	0.05
2942.639	0.984	7.08	0.04
2943.573	0.046	6.32	0.06
2944.590	0.113	5.82	0.03
2945.476	0.171	5.90	0.01
2946.479	0.237	5.87	0.03
2954.604	0.772	5.95	0.01
2955.515	0.832	6.00	0.01
2957.453	0.959	6.43	0.01
2963.470	0.355	6.94	0.01
2964.439	0.419	6.92	0.01
2965.426	0.484	6.14	0.004
2966.453	0.552	5.99	0.01
2967.467	0.619	5.93	0.01
3019.396	0.037	6.29	0.05
3019.462	0.041	6.31	0.07
3028.500	0.636	5.98	0.001
3029.493	0.702	5.96	0.03
3030.422	0.763	5.95	0.01
3031.438	0.830	5.99	0.01

Table 6.3Infrared Observations of RZ Sct at 2.2  $\mu\text{m}$ 

JD 2440000+	Phase	2.2 $\mu\text{m}$	$\sigma$
2212.618	0.927	5.97	$\pm 0.18$
2213.549	0.988	6.89	0.21
2214.515	0.052	6.03	0.20
2215.514	0.118	5.86	0.09
2217.549	0.252	5.53	0.07
2218.510	0.315	5.55	0.21
2219.517	0.381	5.49	0.11
2220.552	0.449	5.68	0.10
2221.528	0.514	5.72	0.07
2221.599	0.518	5.71	0.04
2222.497	0.577	5.57	0.09
2222.569	0.582	5.60	0.07
2222.618	0.585	5.61	0.08
2223.462	0.641	5.59	0.15
2223.538	0.646	5.55	0.06
2223.592	0.649	5.52	0.10
2224.629	0.718	5.54	0.12
2942.660	0.986	6.84	0.01
2943.566	0.045	6.15	0.02
2944.584	0.112	5.57	0.01
2945.483	0.171	5.57	0.03
2946.472	0.236	5.56	0.02
2951.490	0.567	5.54	0.01
2952.451	0.630	5.55	0.03

Table 6.3 continued

JD 2440000+	Phase	2.2 $\mu$ m	$\sigma$
2953.569	0.704	5.49	0.01
2954.611	0.772	5.57	0.004
2955.522	0.832	5.62	0.01
2957.458	0.960	6.04	0.004
2963.465	0.355	5.50	0.01
2964.445	0.420	5.55	0.004
2965.419	0.484	5.70	0.01
2966.448	0.552	5.57	0.01
2967.456	0.618	5.48	0.01
3019.465	0.042	5.98	0.05
3028.493	0.636	5.55	0.01
3029.489	0.701	5.50	0.04
3030.427	0.763	5.58	0.01
3031.442	0.830	5.61	0.01

Table 6.4Infrared Observations of RZ Sct at 3.6  $\mu\text{m}$ 

JD 2440000+	Phase	3.6 $\mu\text{m}$	$\sigma$
2944.576	0.112	5.48	$\pm 0.03$
2945.490	0.172	5.45	0.16
2946.487	0.237	5.29	0.05
2954.618	0.773	5.33	0.03
2955.528	0.833	5.69	0.05
2957.464	0.960	6.02	0.08
2963.475	0.356	5.48	0.04
2965.434	0.485	5.79	0.07
2966.460	0.552	5.40	0.11
2967.460	0.618	5.34	0.08
3030.434	0.764	5.45	0.03

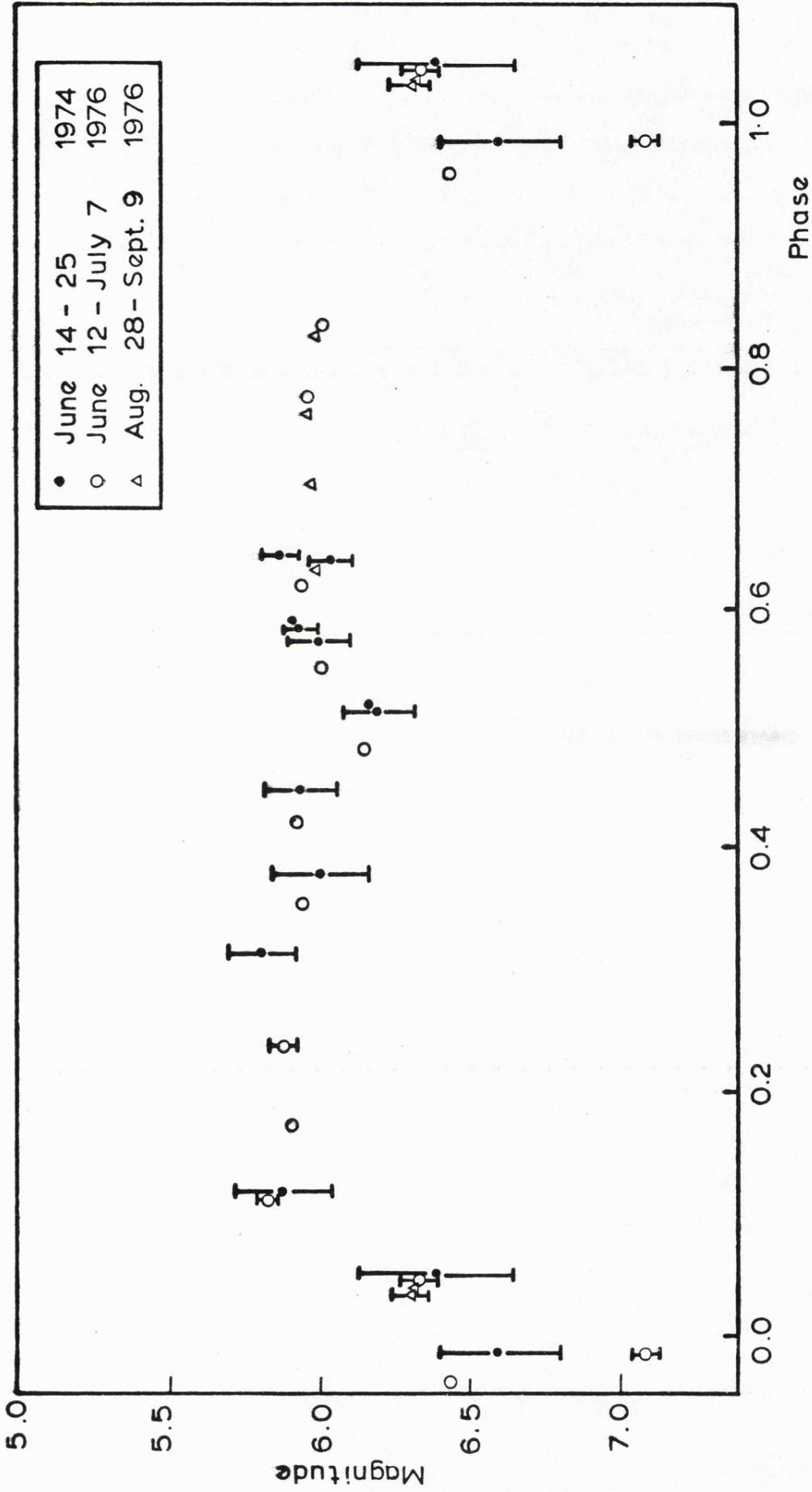


Figure 6.3 1.2  $\mu\text{m}$  light curve of RZ Sct

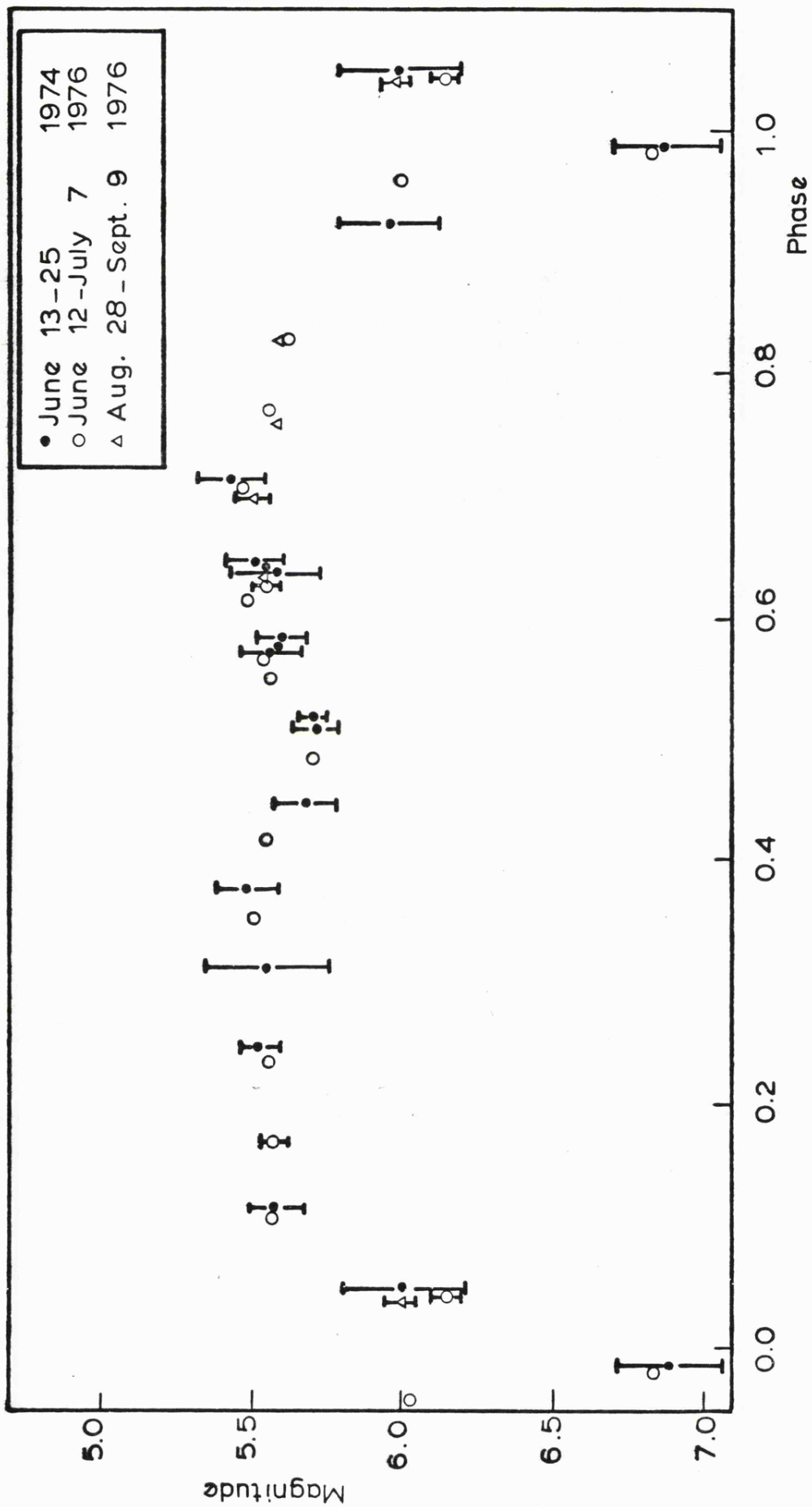


Figure 6.4 2.2  $\mu$ m light curve of RZ Sct

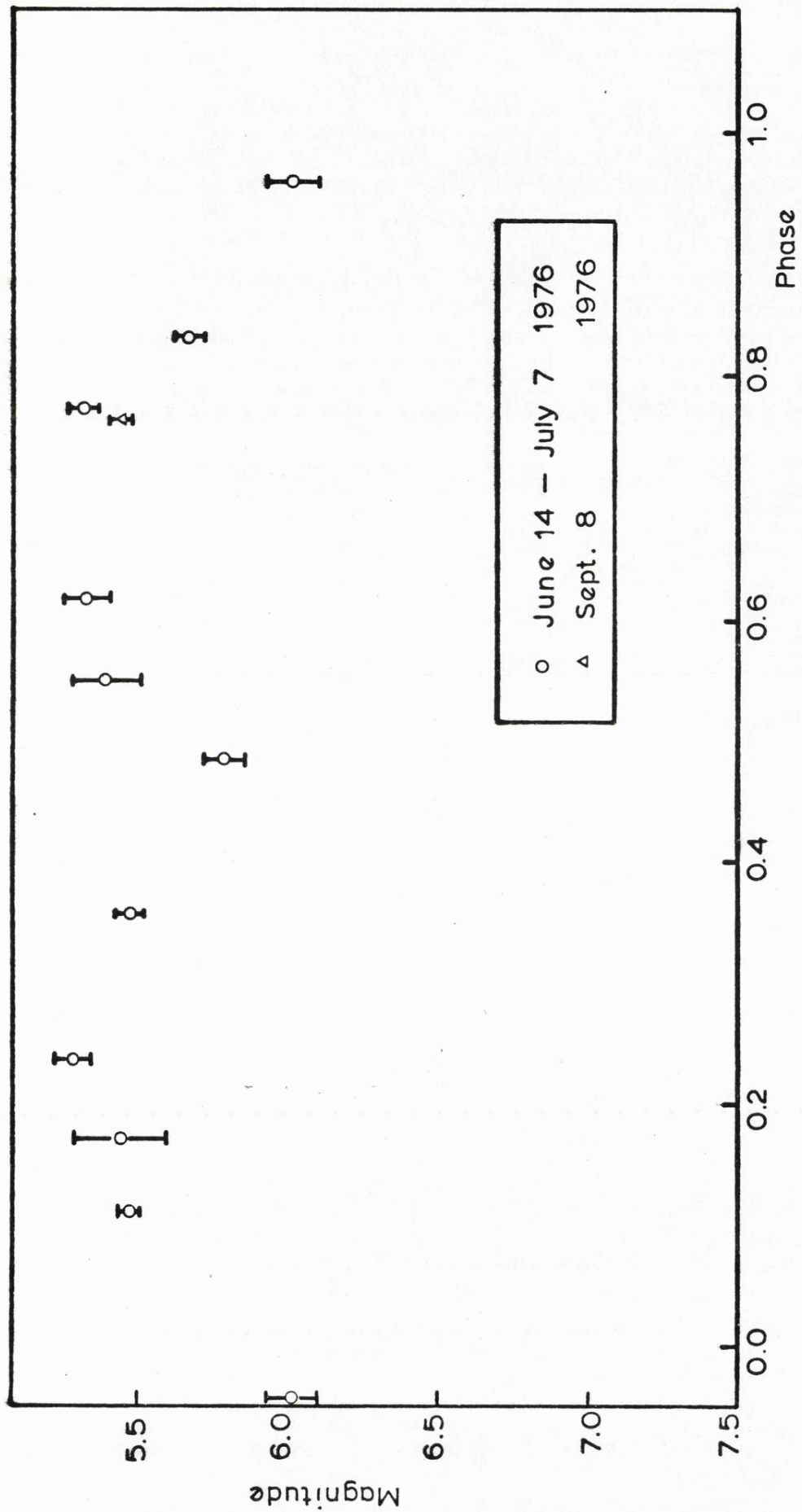


Figure 6.5 3.6  $\mu\text{m}$  light curve of RZ Sct

### Features of the Infrared Light Curves

An inspection of the infrared light curves of RZ Sct reveals several interesting features. Both the primary and secondary minima in all three light curves are asymmetric. Similar asymmetries are also evident in the optical light curves (see Figure 6.2). The most notable feature is the decrease in light shown in all three infrared light curves from approximately phase 0.75 to phase 0.95. It is nearly at this same phase interval that the radial velocity curve is distorted (Hansen and McNamara, 1959) and the optical light curves (U, B and V) show a definite decrease (Wilcken et al. 1976). As already mentioned (Hansen, 1969) the above feature can be explained by electron scattering in the gas stream and this, of course, applies also to the 1.2 and 2.2  $\mu\text{m}$  observations. However, the effect appears more pronounced at 3.6  $\mu\text{m}$  suggesting the stream may be optically thick to free-free radiation.

It is also shown from a comparison of the infrared and optical light curves that both eclipses are deeper in the infrared. This is due to the optically thick disk around the primary star which provides a larger eclipsed and eclipsing area.

### Discussion

It has already been noted that the system has a large B - V colour for its spectral type implying that the system suffers interstellar reddening. This is also evident in the infrared colours (for example,  $V - K = +1.93$  and  $J - K = +0.32$ ).

We must devise a method of separating the interstellar reddening from the intrinsic infrared excess. This can be done if one assumes no excess due to a gas stream seen at the primary minimum. This may ignore any gas around the secondary component; we return to

this point later. The  $V - J$ ,  $V - K$  and  $V - L$  colour curves (hereafter referred to as the S curves) for the component stars alone can be calculated from the appropriate colours for the spectral types of the stars. For these calculations we adopted the spectral types of the primary and secondary components to be B2 II and AO II-III respectively given by Wilcken et al. (1976). Using the appropriate tables for the mean colours of stars of different luminosity class by Johnson (1966a) we find  $(V - J)_{B2 II} \simeq -0.46$ ,  $(V - K)_{B2 II} \simeq -0.60$  and  $(V - L)_{B2 II} \simeq -0.62$ .

Since the depth of the primary minimum at V is 1.32 mag. (Figure 6.2) and the total intensity at maximum  $L_1 + L_2 = 1$ , it follows that the total intensity at the primary minimum is 0.30. From the solution of the visual light curve (Wilcken et al. 1976) it is known that at V the primary component contributes 89% of the light and the secondary component 11% of the light. Hence, at primary minimum the B2 component contributes 19% of the light. Using the colours of the B2 component it is now possible to derive the S curves for the component stars alone.

The difference between the S curves and the observed colour curves will then give the amount of infrared excess due to the gas around the system. Figures 6.6, 6.7 and 6.8 illustrate the  $V - J$ ,  $V - K$  and  $V - L$  curves (observed and calculated) respectively.

Thus, from Figures 6.6, 6.7 and 6.8, assuming that there is no gas around the AO star and AO star eclipses any gas (disk) around the B2 star at the primary minimum, it may be seen that  $X_J$  and  $X_K$  represent the colour difference  $V - J$  and  $V - K$  respectively due to interstellar reddening.  $X_L$  can not be measured since there are no  $3.6 \mu m$  measurements of the primary minimum. However, using the regional mean extinction data of Johnson (1965) it can be found that  $X_J$  leads to

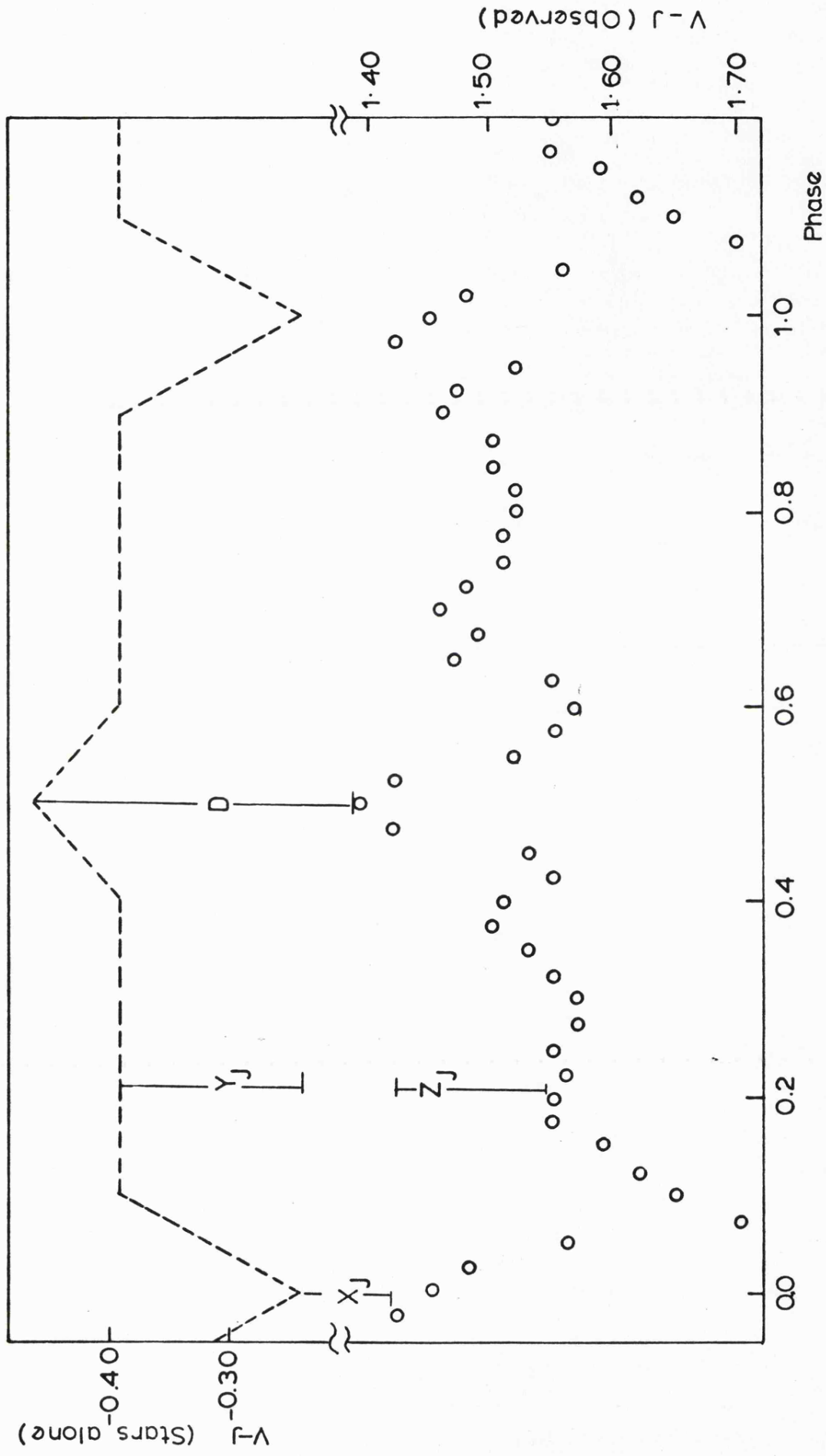


Figure 6.6 V-J Colour index vs. phase curves for RZ Sct

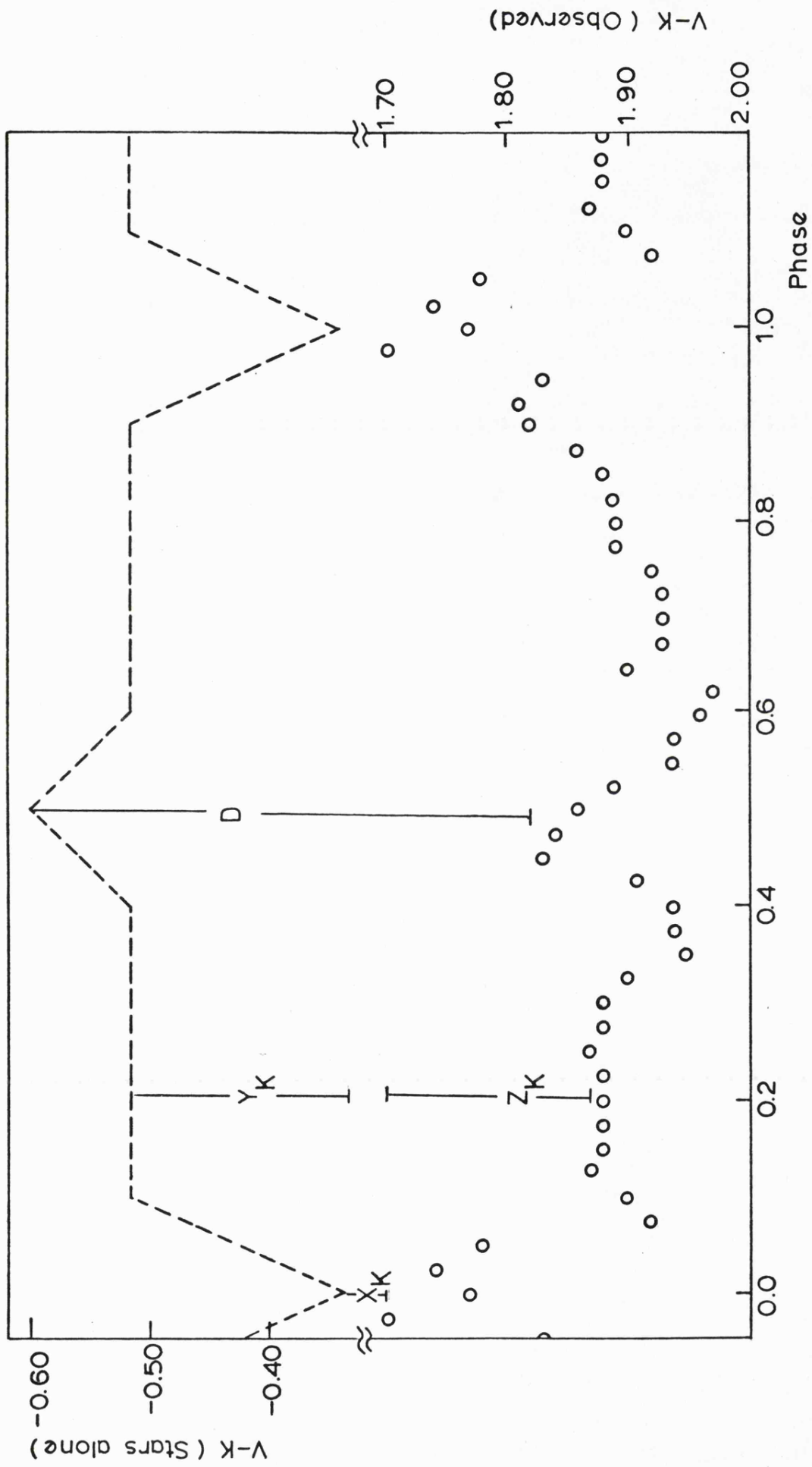


Figure 6.7 V-K Colour index vs. phase curves for RZ Sct.

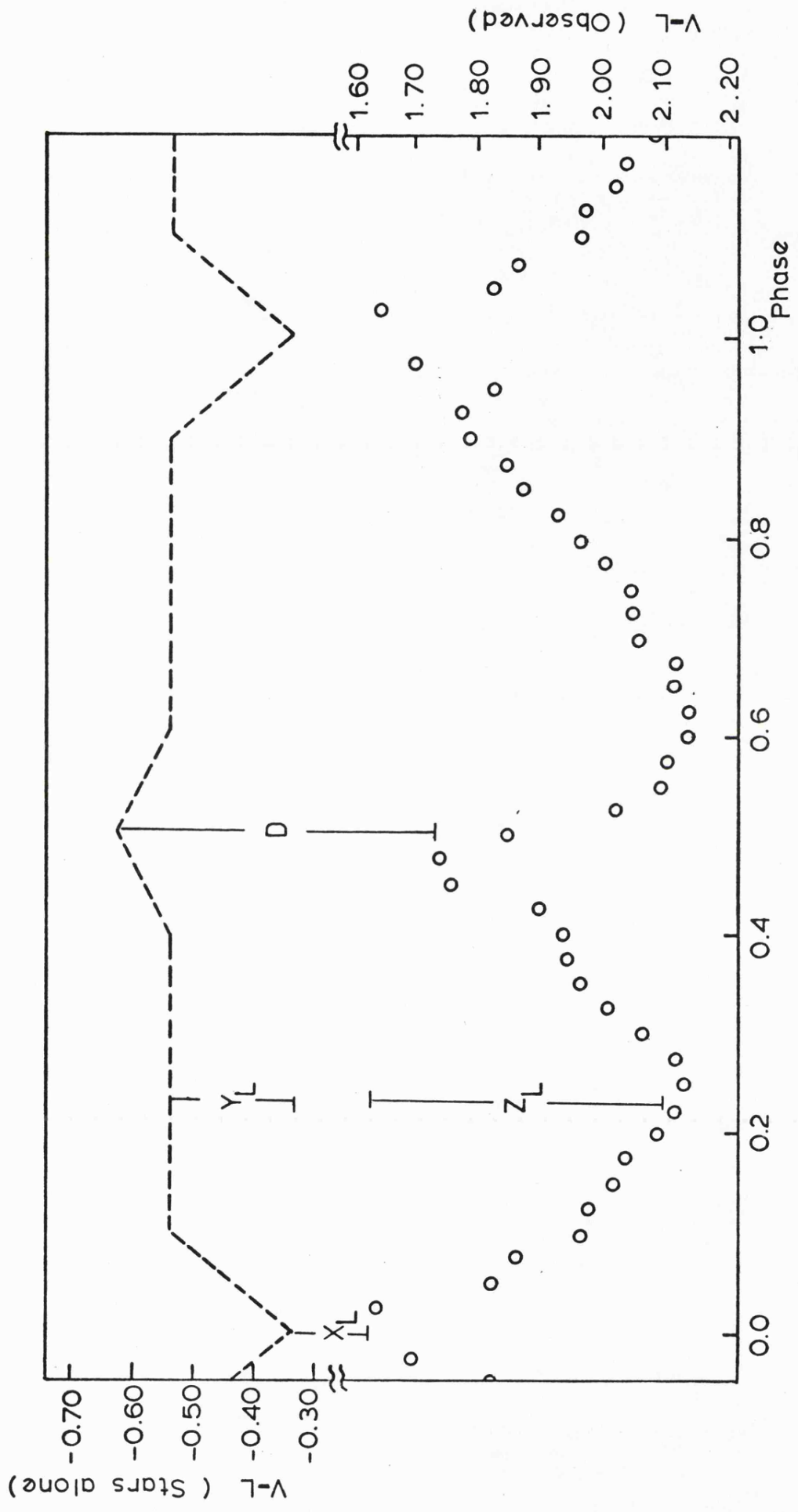


Figure 6.8 V-L Colour index vs. phase curves for RZ Sct

$A_v$  (visual absorption) =  $2^m .18$  and  $X_K$  leads to  $A_v = 2^m .24$ . These figures are in good agreement and suggest that the above assumption (i.e. no gas around AO star and the AO star is larger than the B2 star) is correct, at least sufficiently correct for the accuracy of our observations. Thus we do not rule out gas around the AO star as suggested by the spectroscopic observations, but we are unable to measure it. Furthermore using  $A_v = 2^m .24$  we can calculate  $X_L$  (V - L colour difference at primary minimum).

In Figures 6.6, 6.7 and 6.8, (Y + Z) represents the infrared excess seen at phase 0.25 or phase 0.75. Also at J and K,  $(X + Y + Z) \simeq D$ . Thus Y + Z also represents the infrared excess seen at phase 0.5. This implies that at 1.2 and  $2.2 \mu\text{m}$  we are seeing only a gas disk around the B2 star. However, at L the excess appears to peak at phase 0.25 and phase 0.75 suggesting that the gas stream is also contributing a significant amount of radiation. This agrees with the earlier conclusion that the gas stream is optically thick at  $3.6 \mu\text{m}$ .

From Figure 6.8 it can be found that  $(X + Y + Z)_L = 2.60$ . On the other hand, for  $A_v = 2.24$  we find  $X_L = V - L = 2.13$ . Hence  $(Y + Z)_L = 0.47$ . Thus, ignoring hopefully the gas stream it can be seen that  $V - L_{(Y+Z)} \equiv V - L_{\text{disk}} = 0.47$ . From Figures 6.6 and 6.7 it can also be found that  $V - J_{\text{disk}} = 0.27$  and  $V - K_{\text{disk}} = 0.40$ . Thus these colours imply that the disk is optically thin from J to K, but it is thick from K to L. Therefore we conclude that  $\tau_{\text{disk}} \simeq 1$  at K.

It is now possible to calculate the observed area of the disk.  $(D - X)_K = 0.40$  represents the infrared excess seen at the secondary minimum when the secondary component contributes virtually no light. Hence the system is  $10^{0.4 \times 0.4} = 1.45$  times brighter at K. Therefore, the protruding observed area of the disk seen edge on is 45% the area of the primary star. Here, it has been assumed that the disk temperature is the same as that of the primary star.

Estimating the disk and stream dimensions we can now calculate the electron density of the disk and stream. According to Wilcken et al. (1976) both components of the system have radii  $\sim 14 R_{\odot}$ . However, we assumed that the secondary component is larger than the primary B2 star. If we take the radius of the B2 component,  $R_1 = 14 R_{\odot}$ , then we can estimate the radius of the disk to be twice the radius of the B2 star implying a disk height of  $\sim 10.5 R_{\odot}$ . Thus the average observed physical depth of disk,  $d$ , is found to be  $37 R_{\odot}$ .

Therefore, if we take  $T_{\text{disk}} = 22700$  K and using

$$1 \simeq \tau_{\text{disk}} = k'_s d = 1.367 \times 10^{-35} \{1 - \exp(-h\nu/KT)\} Z^2 g T^{-\frac{1}{2}} \lambda^3 N_e^2 d,$$

we find  $N_{e_{\text{disk}}} \simeq 1.3 \times 10^{12} \text{ cm}^{-3}$ .

Similarly, estimating the stream depth as about  $7 R_{\odot}$ , the stream temperature of 15000 K and requiring  $\tau_{3.6} \simeq 1$  we find  $N_{e_{\text{stream}}} \simeq 1.3 \times 10^{12} \text{ cm}^{-3}$ . This gives an electron scattering optical depth for the stream of 0.42 which is about correct to produce the decline at phase  $\sim 0.8$ . It should be noted that the electron density only varies as  $T^{\frac{1}{2}}$  and  $d^{\frac{1}{2}}$ .

Any other streams (i.e. eddy or stream around the A0 star) do not show up very obviously from the infrared data and so it may be concluded that if they exist, they must have  $N_e < 10^{12} \text{ cm}^{-3}$ .

## CHAPTER 7

## CONCLUSIONS AND FUTURE WORK

Observations leading to the infrared light curves for several eclipsing binary stars have been presented and discussed in the preceding three chapters. As indicated in the introduction infrared observations provide valuable information about binary stars, particularly gas streams and disks. In certain cases e.g. AM Her, unsuspected properties such as cyclotron radiation may also be measured.

The infrared light curves have enabled us to define several new parameters for the systems, and this work can be summarised as follows.

The complete light curves at 1.2 and 2.2  $\mu\text{m}$  for both AB And and SW Lac, and that for 44 i Boo at 2.2  $\mu\text{m}$  were obtained. These curves have revealed several remarkable characteristics of the systems. The V - K colours of all three stars and J - K colours of AB And and SW Lac indicated that the spectral types of these systems do not correspond to their colours. The possibility of reddening by circumstellar dust and an infrared excess due to free-free emitting circumstellar envelope have been ruled out.

An exciting discovery in AM Her was the absence of the 2.2  $\mu\text{m}$  primary minimum. This together with a positive J - K colour index indicated that the system has an infrared excess at 2.2  $\mu\text{m}$  which must come from cyclotron radiation emitted close to the white dwarf.

The infrared excess found in RZ Sct was attributed to a gas disk around the primary component of this system with an electron density,  $N_e \simeq 10^{12} \text{ cm}^{-3}$ . A similar electron density was also found for the gas stream in the system.

The prospects for infrared studies of close binary stars in

the future are very exciting. The following observations would complement the work described in this thesis.

The observations of W UMa-type eclipsing binary stars have so far concentrated on those stars with large values of  $B - V$  for their spectral types. Clearly it would be desirable to make infrared observations of those systems whose  $B - V$  values are not so large. With larger telescopes,  $3.6 \mu\text{m}$  light curves should also be obtained to establish whether trends observed at  $1.2$  and  $2.2 \mu\text{m}$  are confirmed.

The exciting results on AM Her clearly suggest that  $1.2$  and  $2.2 \mu\text{m}$  light curves of other cataclysmic variables are likely to prove interesting. It would also be desirable to make UBV measurements simultaneously with the infrared observations. This would provide a more reliable visual to infrared comparison since these systems are intrinsically variable.

Finally there are a number of other Algol-type systems with emission lines which should prove interesting in the infrared.

The existing instrument has proved satisfactory and reliable, but there are a number of improvements which could still be made. As mentioned above it would be useful to incorporate a UBV photometer for simultaneous measurements. This could be located beneath the dichroic mirror and guiding would then be accomplished with the off-set guider.

The system could be more fully automated by using a computer or microprocessor to print both the readings and the observation times. It may even be possible to plot crude light curves in real time so that a quick look at the data is instantly available.

Clearly when the  $3.8 \text{ m}$  infrared telescope (UKIRT) is available greater sensitivities will be possible. Nevertheless, every effort should be made to keep updating detectors so that the most sensitive possible system is being used. For short period binary work

it is possible to conceive of a system using several detectors to make simultaneous infrared observations at different wavelengths e.g. 1.2 and 2.2  $\mu\text{m}$ .

**APPENDIX 1A**

## Infrared light curves of AM Herculis

AM HER has been identified as the optical counterpart of 3U 1809+50 by its common period of 3.1 h (refs 1, 2). The system shows strong emission lines, the radial velocities of which have been measured by Priedhorsky<sup>3</sup> and Cowley<sup>4</sup>. Tapia<sup>2</sup> has measured strong linear and circular polarisation which indicates that one component of the system is probably a white dwarf emitting strong cyclotron radiation. Photometric light curves have been observed<sup>5,6</sup> which show two minima, unlike the X-ray light curve which has only one; the system also has a red colour index. Models of the system which rely on a white dwarf, accretion disk, hot spot, and a gas stream from a companion star that fills its Roche Lobe have been proposed by Chanmugan<sup>7</sup> and Fabian<sup>8</sup>. In view of the red colour, strong emission lines and cyclotron radiation, we considered that infrared observations of this star would be of interest.

The 2.2  $\mu\text{m}$  light curve was observed on the night of the 9–10 July 1977 and the 1.2  $\mu\text{m}$  curve was observed the following night. The observations were made with the 1.5 m Infrared Flux Collector at the Cabezón Observatory, Tenerife. A standard infrared photometer with an InSb detector operated at 63 K was used. Observations covered one period only on both nights but there is a short break in the 2.2  $\mu\text{m}$  light curve when it was thought the cryostat had run out of liquid nitrogen. Both nights were of excellent photometric quality and  $\alpha$  Lyr, used as the standard star, was monitored throughout the night, but only before and after the AM Her observations. This procedure was followed so that the light curves should be as complete as possible. The magnitudes assumed for  $\alpha$  Lyr are  $J = 0.02$  and  $K = 0.02$  (ref. 9). Corrections were made for atmospheric extinction but these were very small. Each observation is the result of a 60-s integration, 30 s in each channel.

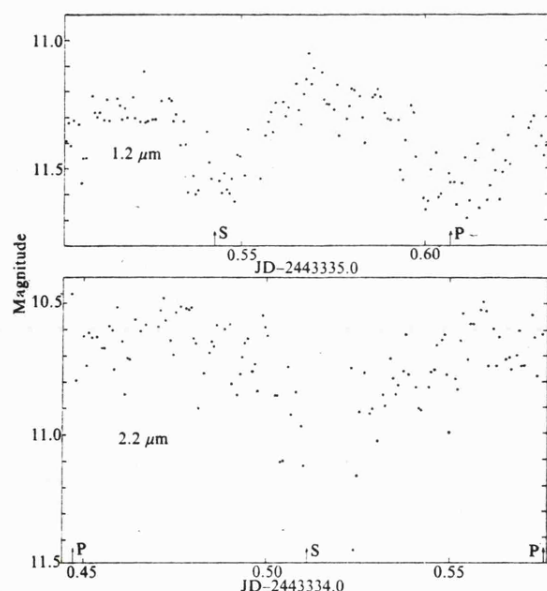


Fig. 1 1.2  $\mu\text{m}$  and 2.2  $\mu\text{m}$  light curves of AM Herculis

The errors on each point, estimated from observations of a similarly faint non-variable star, are  $\pm 0.05$  mag. Thus the spread of the points is thought to be genuine flickering of the star. Such flickering is also seen in the optical light curves<sup>5,6</sup>.

The light curves are shown in Fig. 1. The times shown are heliocentric Julian dates. Also shown are the positions of primary and secondary minima expected from the photometric ephemeris<sup>8</sup> H.J.D. 2,443,014.7133 + 0.128924  $\times$  E.

It is unfortunate that we did not observe the bottom of the 2.2  $\mu\text{m}$  secondary eclipse. However, the whole interest of these observations would seem to be the absence of the 2.2  $\mu\text{m}$  primary eclipse. Thus the 2.2  $\mu\text{m}$  light curve is similar to the X-ray light curve which also shows only a secondary minimum. In fact, there may be a shallow 2.2  $\mu\text{m}$  primary eclipse, hidden by the flickering; if the data is smoothed a depth of 0.15 mag would be consistent with the results.

The 1.2  $\mu\text{m}$  light curve is very similar to the optical light curve and so could be explained by any model which describes the optical light curve. The model of Fabian *et al.*<sup>8</sup> explains primary minimum as the eclipse of the hot spot by the companion star. This hot spot is formed where the gas stream meets the accretion disk; it is also a high density region. The secondary minimum is the eclipse of the white dwarf by this high density hot spot. X-rays are formed by accretion of material on to the white dwarf. The temperature of the hot spot is not sufficient to produce X-rays and thus the X-ray light curve shows only the secondary minimum. The similarity of the 2.2  $\mu\text{m}$  and X-ray light curves suggest that the dominant 2.2  $\mu\text{m}$  emission must also arise near the white dwarf stars.

We note, also, that the system has a positive colour index,  $J - K \approx 0.60$  at maximum light. This could be produced by the cool companion or free-free radiation from the accretion disk, however, it is difficult to see how either of these regions could be suitably eclipsed. It is known that the white dwarf emits cyclotron radiation generated by its strong magnetic field.

With cyclotron radiation, different frequencies are emitted at different magnetic fields and so in different volumes. This can lead to a flatter spectrum than black body emission, which might produce the observed colour index. We therefore propose that 2.2  $\mu\text{m}$  light curve is explained by strong cyclotron radiation produced near the white dwarf.

We are grateful to the SRC for travel funds to Tenerife. A.M. has an SRC studentship. We also thank Drs A. R. King and D. J. Raine for helpful discussions.

R. F. JAMESON  
 R. AKINCI  
 D. J. ADAMS  
 A. B. GILES

Department of Astronomy,  
 Leicester University, UK

A. MCCALL

Department of Astronomy,  
 Hatfield Polytechnic, UK

Received 15 August; accepted 23 November 1977.

- Hearn, D. R. & Richardson, J. A. *MIT preprint* CSR-P-76-36, (1976).
- Tapia, S. *Astrophys. J. Lett.* 212, L125 (1977).
- Priedhorsky, W. C. *Astrophys. J. Lett.* 212, L117 (1976).
- Cowley, A. P. & Crampton, D. *Astrophys. J. Lett.* 212, L121 (1976).
- Szkody, P. & Brownlee, D. E. *Astrophys. J. Lett.* 212, L113 (1976).
- Olson, E. C. *Astrophys. J.* 215, 166 (1976).
- Chanmugan, G. & Wagner, R. L. *Astrophys. J. Lett.* 213, L13 (1977).
- Fabian, A. C., Pringle, J. E., Rees, M. J. & Whelan, J. A. *J. Mon. Not. R. astr. Soc.* 179, 9P (1977).
- Johnson, H. L., Mitchell, R. I., Iriarte, B. & Wisneiwski, W. Z. *Commun. lunar planet. Lab. Univ. Arizona* 4, 99 (1966).

**APPENDIX 1B**

AM Herculis: Interpretation of the  $1.2\mu\text{m}$  and  $2.2\mu\text{m}$  light curves and  
model parameters for the system

A.R. King, D.J. Raine and R.F. Jameson

Astronomy Department, University of Leicester, Leicester LE1 7RH, England.

Summary

An explanation of the infrared light curves of AM Her is proposed in which the dominant flux at  $2.2\mu\text{m}$  is assumed to come from cyclotron emission near the white dwarf. This leads to an estimate of parameters for the accretion disc model.

Key words      binary stars, accretion discs, cataclysmic variables

For inclusion in main journal.

Section: Stars and Stellar Systems.

Running Title: Interpretation of IR Light Curves of AM Her.

Infrared observations at  $1.2\mu\text{m}$  and  $2.2\mu\text{m}$  of the nova-like variable AM Herculis have been reported recently by Jameson et al. (1977). A striking feature of the observations at  $2.2\mu\text{m}$  is the virtual absence of an eclipse at phase 0.0 corresponding to primary minimum in the optical, together with a very deep eclipse at the optical secondary minimum at phase 0.5. In this respect the  $2.2\mu\text{m}$  light curve is very similar to that observed in soft X-rays (Hearn et al. 1977). In contrast the  $1.2\mu\text{m}$  light curve is similar to the optical. This contrast enables us to place constraints on the system which are independent of a detailed model (assuming, of course, that we are dealing with a binary system in which mass is transferred from an optically unseen companion on to a white dwarf). We shall also be able to show that the model of Fabian et al. (1977) is quantitatively as well as qualitatively plausible; we do not rule out explanations using other models (e.g. Priedhersky and Krzeminski (1978), Stockman et al. (1977) ).

If the optically unseen companion were to be providing the dominant contribution to the infrared flux at  $2.2\mu\text{m}$  one might expect a single eclipse at around phase 0.4, (Fig. (i)), which is perhaps not entirely in contradiction with the observed eclipse at  $\Phi = 0.5$ , since the width of the eclipse might be dominated by the flickering. There are then two possibilities: either the cool star gives a negligible flux at  $1.2\mu\text{m}$ , or it provides a significant contribution. In the former case one could explain the observed similarity between the optical and  $1.2\mu\text{m}$  light curves by attributing them to the same mechanism provided that the flux from the cool star is less than the flickering ( $\leq 0.2^m$ ). However, this requires the cool star to have a (colour) temperature less than  $1800^\circ\text{K}$  which is untenable for a normal star. If we take a reasonable lower limit for the colour temperature of the cool star of, say,  $3000^\circ\text{K}$ , then we can show from the observed J and K magnitudes that the cool star must provide

virtually all the light at primary optical eclipse ( $\Phi = 0.0$ ) at  $1.2\mu\text{m}$ . The approximate equality of the eclipse depths at  $1.2\mu\text{m}$  then shows that the temperature of the cool star must in fact be the same as that of the optically emitting region. This is not only physically unreasonable, but contradicts the initial hypothesis that the optically unseen star dominates at  $2.2\mu\text{m}$  for any straightforward extrapolation of the spectrum of the optically emitting region into the infrared (see below).

Even if one could overcome these objections, the hypothesis that the cool star is important in the infrared requires that four different explanations must be provided for the  $2.2\mu\text{m}$ ,  $1.2\mu\text{m}$ , optical and X-ray light curves which just happen to be similar in pairs. This would therefore appear not to be the simplest assumption. Moreover, at the distance usually adopted for AM Her ( $\geq 50$  pc) there is no difficulty in assuming that the optically unseen companion is a late type dwarf which makes an insignificant contribution to the infrared flux. Henceforth, therefore, we shall assume that the observed similarity between the  $2.2\mu\text{m}$  and X-ray light curves implies that the flux eclipsed at  $\Phi = 0.5$  comes from the vicinity of the white dwarf.

#### Interpretation of the data

Let the eclipsed fluxes at  $\Phi = 0.5$  at  $1.2\mu\text{m}$  and  $2.2\mu\text{m}$  be  $C_1$  and  $C_2$  respectively, and let  $F_1$  and  $F_2$  be the uneclipsed fluxes. The minimum ( $\Delta_{m_1} \approx 0.4$ ) at phase 0.5 in the  $1.2\mu\text{m}$  light curve implies

$$F_1/(C_1 + F_1) = 10^{-0.16} \text{ giving } C_1/F_1 = 0.45 .$$

The ratio of fluxes at maximum light between  $1.2\mu\text{m}$  and  $2.2\mu\text{m}$  is 1.6 and hence

$$(C_1 + F_1)/(C_2 + F_2) = 1.6$$

The observed minimum in the  $2.2\mu\text{m}$  light curve at phase 0.5 is  $\Delta m_2 \geq 0.5$  and this leads to  $C_1 \leq 1.35 C_2$ . This shows that the flux eclipsed at  $\bar{\Phi} = 0.5$  has a relatively small variation with frequency, with a spectral index of no more than about 0.5. Furthermore, we find  $F_1/F_2 = 1.7$ .

At phase 0.0 let the (partially eclipsed) fluxes be  $F_1'$  and  $F_2'$ . The dip of 0.4 magnitudes in the  $1.2\mu\text{m}$  light curve leads to  $F_1'/F_1 = 0.55$ . The corresponding dip at  $2.2\mu\text{m}$  is very much shallower ( $\lesssim 0.15^m$ ) and because of the overall flickering could even be interpreted as no dip at all. This implies  $1 > F_2'/F_2 \gtrsim 0.73$ , and hence  $F_2'/F_2 > F_1'/F_1$ . Consequently, the flux which is not eclipsed at  $\bar{\Phi} = 0.5$  has two components: one of these has a fairly flat spectrum and emanates from an extended region; the other has a steeper spectrum and comes from a smaller region which is significantly eclipsed at  $\bar{\Phi} = 0.0$ . We shall later interpret the two components as due to an optically thin disc and a thick hot spot. This is consistent with the decreasing depth of the partial eclipse at longer wavelength which implies a decreasing importance for the latter component relative to the former. Note that these arguments depend essentially on the new infrared data since they follow from the dissimilarity between the light curves at  $1.2\mu\text{m}$  and  $2.2\mu\text{m}$ .

#### A Model for the System

A qualitative model of AM Her has been given by Fabian et al. (1977). In this model matter accretes on to a highly magnetised white dwarf from a cool companion via Roche lobe overflow. The X-rays are produced by matter cooling as it makes its way down the accretion columns near the poles of the white dwarf. The collision of the gas stream from the cool star and the accretion disc produces a higher density hot spot, and electron scattering in this region produces the

X-ray eclipse. The optical light curve is produced by a combination of reflection effects and a partial eclipse of the disc and hot spot by the cool star; the system is observed at moderate inclination so the white dwarf is not eclipsed. The strong phase-dependent linear and circular polarisations observed in the optical (Tapia 1977, Tapia and Angel 1976, Angel and Stockman 1977) are due to cyclotron radiation produced by the infalling material very close to the white dwarf and modulated by scattering in the hot spot. The geometry of the model is consistent with the variations of the spectroscopically determined radial velocities with phase (Cowley et al. 1976, Cowley and Crampton 1977, Friedhorsky 1977).

To explain the observed light curve at  $2.2 \mu\text{m}$  <sup>using this model</sup> we see that at this wavelength the flux is dominated by radiation from the vicinity of the white dwarf. Electron scattering in the hot spot is then supposed to produce a dip at  $\Phi = 0.5$  exactly as for the X-rays, while the partial eclipse of the disc and the hot spot at primary optical minimum gives only a very shallow dip in the  $2.2 \mu\text{m}$  light curve. This model provides also a natural explanation for the infrared excess of the system. In contrast, at  $1.2 \mu\text{m}$  the emission is dominated by the disc and hot spot as in the optical.

If we take the emission region of the infrared flux eclipsed at  $\Phi = 0.5$  to have a length scale of about the radius of the white dwarf (as is the case for the X-ray and polarised optical emission) then, with an assumed distance of  $\geq 50$  pc, we find a brightness temperature of  $\geq 10^8$  K. This suggests a non-thermal origin for the radiation, and it is natural to take this to be cyclotron emission. In general the prediction of a spectrum for this cyclotron flux is difficult (Masters et al. 1977), but at infrared wavelengths and for a non-relativistic plasma it is possible to make reasonable guesses. (Even this is not a severe restriction since at infrared wavelengths we shall be observing predominantly the lower cyclotron harmonics.)

For any acceptable density, temperature and magnetic field in the accretion columns the cyclotron radiation will be self-absorbed.

For a field strength which decreases monotonically outwards we can approximate the emission at any given frequency as a black-body flux from a radius at which the field is appropriate to the given Larmor frequency. This gives  $I_\nu \propto \nu^2 r^2$  where for a radial  $1/r^3$  field  $\nu \propto B \propto 1/r^3$  so  $I_\nu \propto \nu^{4/3}$  (Stockman et al. 1977) and for a true dipole field we get  $I_\nu \propto \nu$ . The main uncertainty appears to be the field geometry, but it is clear that the cyclotron hypothesis cannot be ruled out by these considerations even though it is not in good agreement with these naive estimates.

With the cyclotron assumption, we can attempt to fit plausible parameters to the model of Fabian et al. A priori there is no reason to believe that the consistency requirements can be satisfied for reasonable values of these parameters. In fact we shall find values in general agreement with those usually assumed for this type of system. We believe that this provides quantitative support for the model.

Model Parameters

Let us write  $T_d, T_s, A_d, A_s$  for the temperatures and surface areas of one side of the disc and hot spot respectively. If  $\tau_1, \tau_2 (= 3.36\tau_1)$  are the free-free optical depths along the disc at  $1.2\mu\text{m}$  and  $2.2\mu\text{m}$  the considerations of the previous section suggest  $\tau_1$  slightly smaller and  $\tau_2$  slightly greater than unity. Hence the total free-free radiation observed from the disc at  $1.2\mu\text{m}$  is

$$\pi A_d B_\nu(T_d)(1 - e^{-\tau_1}) \cos i \approx 2\pi k T_d A_d \tau_1 \cos i / (1.2\mu\text{m})^2 \text{ (erg s}^{-1} \text{ Hz}^{-1}\text{)}$$

where  $i$  is the inclination angle of the system. Similarly the flux at  $2.2\mu\text{m}$  is  $\approx 2\pi k T_d A_d \cos i / (2.2\mu\text{m})^2 \text{ (erg s}^{-1} \text{ Hz}^{-1}\text{)}$ .

The ratios  $F_1/F_2 = 1.7, F_2'/F_2 = 0.73, F_1'/F_1 = 0.55$  which we derived above now yield three equations if we take  $F$  as the total radiation from the disc and hot spot, and  $F'$  as approximately that of the disc alone; thus we are assuming that at  $\Phi = 0.5$  the hot spot is totally eclipsed but most of the disc is still visible, in agreement with the conclusions of the previous section. We find the three equations

$$\frac{\tau_1 + x}{1 + x} = 0.51, \quad \frac{1}{1 + x} = 0.73, \quad \frac{\tau_1}{1 + x} = 0.55,$$

where  $x = A_s T_s / A_d T_d$ . These are of course overdetermined, but give the consistent solution  $\tau_1 = 0.38, x = 0.31$ .

Thus our expectations about  $\tau_1, \tau_2$  are fulfilled and the approximations  $1 - e^{-\tau_1} \approx \tau_1, 1 - e^{-\tau_2} \approx 1$  justified, although one could iterate to improve the accuracy. We can now show that the parameters of the model are restricted to a fairly narrow range of values.

If  $R_s$  is the radial thickness of the hot spot (or "wall") and  $\theta$  the angle it subtends at the white dwarf we have  $A_s = \theta R_d R_s,$

where  $R_d$  is the radius of the disc. Thus the value of  $x$  we have found implies

$$\frac{\theta R_s T_s}{\pi R_d T_d} = 0.31 \quad (1)$$

Writing  $R_d = 10^{10} R_{10}(d)$  (cm) and  $N_{12}(d)$ ,  $T_4(d)$  for the electron density and temperature of the disc in units of  $10^{12} \text{ cm}^{-3}$  and  $10^4 \text{ }^\circ\text{K}$  respectively, the value  $\tau_1 = 0.38$  yields

$$N_{12}^2(d) R_{10}(d) T_4^{-3/2}(d) = 132 \quad (2)$$

We can get one more equation by comparing the predicted and observed

$1.2 \mu\text{m}$  fluxes at maximum light. (This determines  $F_1, F_2, F_1', F_2'$  in turn uniquely.) The total flux in the line of sight at  $1.2 \mu\text{m}$  is

$2(C_1 + F_1) \cos i / 4\pi D^2 = 2.9 F_1 \cos i / 4\pi D^2$  where  $D$  is the distance to the system and we have used the relation  $C_1 =$

$0.45 F_1$  found earlier. Replacing  $F_1$  as before by the sum of contributions from the disc and hot spot we find a flux

$$3.39 \times 10^{-26} R_{10}^2(d) T_4(d) D_{100}^{-2} \quad \text{ergs}^{-1} \text{cm}^{-2} \text{Hz}^{-1}$$

where we have taken  $\cos i = 0.1$ , which is consistent with the light curves, and  $D_{100}$  is  $D$  in units of 100pc. The apparent magnitude  $J = 11$  at  $1.2 \mu\text{m}$  means an observed flux of  $7 \times 10^{-25} \text{ ergs}^{-1} \text{cm}^{-2} \text{Hz}^{-1}$ ; equating these two expressions gives the further relation

$$R_{10}^2(d) T_4(d) D_{100}^{-2} = 20.6 \quad (3)$$

In (1) the length of X-ray eclipse implies  $\theta \leq 1$ , and the thickness of the spot is unlikely to exceed half the disc's radius, so  $R_s < 0.5 R_d$ . From (1) we now find  $T_s / T_d \geq 2$ . Since both temperatures probably lie in the range  $10^4 - 10^5 \text{ }^\circ\text{K}$  this yields  $10^4 \leq T_d \leq 5 \times 10^4$ ;  $T_s \geq 2 T_d$ . The expected distance to the system should be between about 50 to 150pc.

Thus with  $0.5 \leq D_{100} \leq 1.5$ ,  $1 \leq T_4(d) \leq 5$ ,  
 (3) implies  $1.0 \leq R_{10}(d) \leq 6.8$ , or

$$1.0 \times 10^{10} \leq R_d \leq 6.8 \times 10^{10}$$

The binary separation is  $(7.0-9.1) \times 10^{10}$  cm and the likely radius of the secondary  $2.8 \times 10^{10}$  cm (Priedhorsky and Krzeminski (1978)), so this estimate of  $R_d$  is highly reasonable.

From (2) we now get

$$4.4 \leq N_{12}(d) \leq 38.5$$

a range of disc densities close to what is usually found for such systems. For a given  $R_{10}(d)$ , the upper limit on  $N_{12}(d)$  is

$N_{12}(d) \leq 38.5 R_{10}^{-1/2}(d)$ . Thus an upper limit to the electron scattering optical depth in the disc is

$$\tau_{es} \leq 6.7 \times 10^{-25} \times 10^{10} R_{10}^{1/2}(d) \times 3.85 \times 10^{13} \leq 0.67$$

Hence for any possible parameters the disc will always be thin to electron scattering. This is of course required for internal consistency of the model of Fabian et al.. Two final requirements for consistency of the model are that the hot spot ("wall") should be thick to electron scattering and that its free-free radiation should be self-absorbed, producing a blackbody spectrum. It is easily seen that both requirements are satisfied for any electron density in the spot greater than about  $10^{16} \text{ cm}^{-3}$ , again agreeing with the usual estimates for such systems.

We can also work out what fraction of the total optical emission is cyclotron radiation by using the analysis given above. If we extrapolate the cyclotron emission into the optical with a spectral index 0.5, and assume that the disc flux is constant while the hot spot has a Rayleigh-Jeans spectrum in the  $1.2 \mu\text{m}-5000 \text{ \AA}$  range, we find that cyclotron emission is certainly more than 15% of the total light in the optical continuum. A steeper cyclotron spectral index would raise this estimate; all of this suggests that the model can explain the observed polarisation data.

Acknowledgments

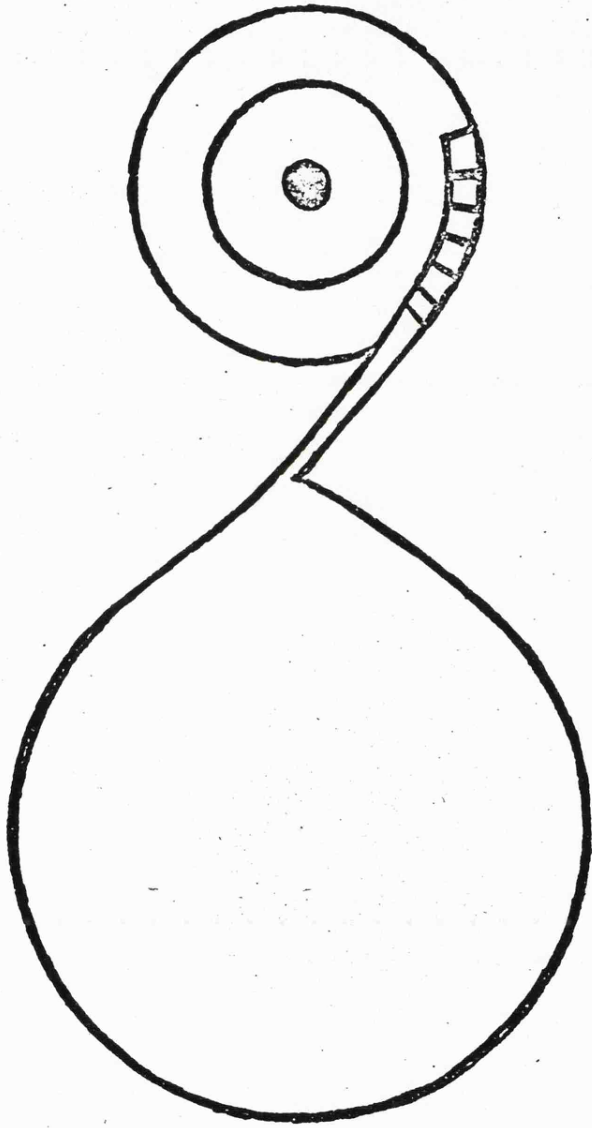
We should like to thank Dr. A.C. Fabian for helpful criticism and the referee for suggesting improvements in presentation.

References

- Angel, J.R.P. and Stockman, H., preprint (1977).
- Cowley, A.P. and Crampton, D., *Astrophys. J.* 212, L121, 28-B4 (1977).
- Cowley, A.P., Crampton, D., Szkody, P. and Brownlee, D. *I.A.U. Circ.* 2984 (1976).
- Fabian, A.C., Pringle, J.E., Rees, M.J. and Whelan, J.A.J., *Mon. Not. R.A.S.* 179, 9p (1977).
- Hearn, D.R., Richardson, J.A. and Clark, G.W., *Astrophys. J.* 213, L115, 44-D8 (1977).
- Jameson, R.F., Akinici, R., Adams, D.J., Giles, A.B. and McCall, A., *Nature* (in press).
- Masters, A.R., Pringle, J.E., Fabian, A.C., Rees, M.J., *Mon. Not. R.A.S.* 178, 501 (1977).
- Priedhorsky, W.C., *Astrophys. J.* 212, L117, 28-B4 (1977).
- Priedhorsky W.C. and Krzeminski W. *Astrophys J.* 219, 597, (1978).
- Stockman, H.S., Schmidt, G.D., Angel, J.R.P., Liebert, J., Tapia, S. and Beaver, E.A., *Astrophys. J.* 217, 815, 99-D4 (1977).
- Tapia, S., *Astrophys. J. Lett.* 212, L125 (1977).
- Tapia, S. and Angel, J.R.P. *I.A.U. Circ.* 2994 (1976).

0.0

0.25



0.75

0.5

## REFERENCES

- Alexander, J.B., Andrews, P.J., Catchpole, R.M., Feast, M.W., Evans, T.L., Menzies, J.W., Wisse, P.N.J. and Wisse, M., 1972. Mon. Not. R. astr. Soc., 158, 305.
- Allen, C.W., 1973. Astrophysical Quantities, Athlone Press, London.
- Allen, D.A., 1973. Mon. Not. R. astr. Soc., 161, 145.
- Allen, D.A., 1975. Infrared The New Astronomy, Keith Reid Ltd., Devon.
- Allen, D.A., Swings, J.P. and Harvey, P.M., 1972. Astr. Astrophys., 20, 333.
- Avery, D.G., Goodwin, D.W. and Rennie, A.E., 1957. J. Sci. Instrum., 34, 394.
- Bachman, R., Kirsch, H.D. and Geballe, T.H., 1970. Rev. Sci. Insts., 41, 547.
- Baker, M.L. and Yen, V.L., 1967. Appd. Optics, 6, 1343.
- Baker, R.H. and Wylie, C.C., 1913. Laws Obs. Bull., No. 20.
- Batten, A.H., 1973. Binary and Multiple Systems of Stars, Pergamon Press, Oxford.
- Berg, R.A. and Duthie, J.G., 1977. Astrophys. J., 211, 859.
- Bergeat, J., Lunel, M., Sibille, F. and van't Veer, F., 1972. Astr. Astrophys., 17, 215.
- Berthier, E., 1975. Astr. Astrophys., 40, 237.
- Biermann, P. and Thomas, H.C., 1972. Astr. Astrophys., 16, 60.
- Biermann, P. and Thomas, H.C., 1973. Astr. Astrophys., 23, 55.
- Binnendijk, L., 1955. Astr. J., 60, 355.
- Binnendijk, L., 1959. Astr. J., 64, 65.
- Binnendijk, L., 1967. Publ. Dom. Ap. Obs., 13, 27.
- Binnendijk, L., 1970. Vistas in Astronomy, Pergamon Press, Oxford, 12, 217.
- Blouke, M.M., Burgett, C.B. and Williams, R.L., 1973. Infrared Phys.

13, 61.

Bond, H.E. and Tifft, W.G., 1974. Publ. astr. Soc. Pacific, 86, 981.

Bookmyer, B.B., 1965. Astr. J., 70, 415.

Bratt, P., Engeler, W., Levinstein, H., Mac Rae, A. and Pehek, J.,

1961. Infrared Phys., 1, 27.

Brogia, P., 1962. Mem. Soc. Astr. Italia, 33, 43.

Brown, D.A. and Huang, S.S., 1977. Astrophys. J., 218, 461.

Brownlee, R.R., 1957. Astrophys. J., 125, 372.

Chen, K. and Reuning, E.G., 1966. Astr. J., 71, 283.

Chou, K.C., 1963. Astr. J., 68, 342.

Cowley, A.P. and Crampton, D., 1977. Astrophys. J. Letts., 212, L121.

Cowley, A.P., Crampton, D., Szkody, P. and Brownlee, D., 1976. IAU

Circ., No. 2984.

Cox, J.T., Hass, G. and Jacobus, G.F., 1961. J. Opt. Soc. Am., 51, 714.

Crampton, D. and Cowley, A.P., 1977. Publ. astr. Soc. Pacific, 89, 374.

Eggen, O.J., 1948. Astrophys. J., 108, 15.

Eggen, O.J., 1967. Mem. R. astr. Soc., 70, 111.

Fabian, A.C., Pringle, J.E., Rees, M.J. and Whelan, J.A.J., 1977. Mon.

Not. R. astr. Soc., 179, 9p.

Fawley, W.M., 1977. Astrophys. J., 218, 181.

Feast, M.W. and Glass, I.S., 1973. Mon. Not. R. astr. Soc., 161, 293.

Ford, W.K. and Rubin, V.C., 1965. Astrophys. J., 142, 1303.

Forrest, W.J., Gillett, F.C. and Stein, W.A., 1971. Astrophys. J.

Letts., 170, L29.

Forrest, W.J., Gillett, F.C. and Stein, W.A., 1972. Astrophys. J.

Letts., 178, L129.

Gaposchkin, S., 1943. Harvard Bull., No. 917, 15.

Gehrz, R.D., Hackwell, J.A. and Jones, T.W., 1974. Astrophys. J., 191,

675.

- Geisel, S.L., 1970. *Astrophys. J. Letts.*, 161, L105.
- Geisel, S.L., Kleinmann, D.E. and Low, F.J., 1970. *Astrophys. J. Letts.*, 161, L101.
- Gillett, F.C., Low, F.J. and Stein, W.A., 1968. *Astrophys. J.*, 154, 667.
- Gillett, F.C., Merrill, K.M. and Stein, W.A., 1971. *Astrophys. J.*, 164, 83.
- Goodwin, D.W., 1957. *J. Sci. Instrum.*, 34, 367.
- Guthnick, P. and Prager, R., 1927. *Astr. Nachr.*, 229, 455.
- Hall, D.N.B., Aikens, R.S., Joyce, R. and McCurnin, T.W., 1975. *Appd. Optics*, 14, 450.
- Hansen, H.K., 1969. *Publ. astr. Soc. Pacific*, 81, 540.
- Hansen, H.K. and McNamara, D.H., 1959. *Astrophys. J.*, 130, 791.
- Hartmann, L., 1977. *Bull. Am. astr. Soc.*, 9, 367.
- Hazlehurst, J., 1970. *Mon. Not. R. astr. Soc.*, 149, 129.
- Hearn, D.R. and Richardson, J.A., 1976. MIT preprint, CSR-P-76-36.
- Hearn, D.R., Richardson, J.A. and Clark, G.W., 1976. *Astrophys. J. Letts.*, 210, L23.
- Herbig, G.H., 1974. *Astrophys. J.*, 189, 75.
- Herbig, G.H. and Lorre, J., 1974. *Astrophys. J.*, 189, 73.
- Herbig, G.H. and Zappala, R.R., 1970. *Astrophys. J. Letts.*, 162, L15.
- Hill, G., Barnes, J.V., Hutchings, J.B. and Pearce, J.A., 1971. *Astrophys. J.*, 168, 443.
- Hilsum, C. and Ross, I.M., 1957. *Nature*, 179, 146.
- Hinderer, F., 1960. *J. Obs.*, 43, 161.
- Huang, S.-S., 1965. *Astrophys. J.*, 141, 976.
- Hudson, R.D., 1969. *Infrared Systems Engineering*, Wiley.
- Humphrey, J.N., 1965. *Appd. Optics*, 4, 665.
- Humphreys, R.M., 1974. *Astrophys. J.*, 188, 75.
- Humphreys, R.M. and Ney, E.P., 1974a. *Astrophys. J. Letts.*, 187, L75.

- Humphreys, R.M. and Ney, E.P., 1974b. *Astrophys. J.*, 190, 339.
- Hyland, A.R. and Neugebauer, G., 1970. *Astrophys. J. Letts.*, 160, L177.
- Jameson, R.F. and Longmore, A.J., 1976. *Mon. Not. R. astr. Soc.*, 174,  
217.
- Jameson, R.F., Longmore, A.J. and Crawford, B., 1973. *Nature*, 242, 107.
- Jameson, R.F., Akinici, R., Adams, D.J., Giles, A.B. and McCall, A., 1978.  
*Nature*, 271, 334.
- Jamieson, J.A., McFee, R.H., Plass, G.N., Grube, R.H. and Richards, R.G.,  
1963. *Infrared Phys. and Engineering*, McGraw-Hill, Ch. 7.
- Johnson, H.L., 1965. *Astrophys. J.*, 141, 923.
- Johnson, H.L., 1966. *Sky and Telescope*, 32, 73.
- Johnson, H.L., 1966a. *Ann. Rev. astr. Astrophys.*, 4, 193.
- Johnson, H.L., 1967. *Astrophys. J. Letts.*, 150, L39.
- Johnson, H.L., 1968. *Astrophys. J. Letts.*, 154, L125.
- Johnson, H.L., Low, F.J. and Steinmetz, D., 1965. *Astrophys. J.*, 142,  
808.
- Johnson, H.L., Mitchell, R.I., Iriarte, B. and Wisniewski, W.Z., 1966.  
*Comm. Lunar Planetary Lab.*, 4, 99.
- Johnson, J.B., 1928. *Physical Rev.*, 32, 97.
- Jones, R.C., 1953a. *Nature*, 170, 937.
- Jones, R.C., 1953b. *Advances in Electronics*, Academic Press, New York,  
5, 1.
- Kalchaev, K. and Truste, Y.L., 1968. *Perem. Zvezdy*, 16, 454.
- Karetnikov, V.G., 1967. *Sov. Astr.*, 11, 16.
- Karetnikov, V.G., 1973. *Sov. Astr.*, 16, 965.
- King, A.R., Raine, D.J. and Jameson, R.F., 1978. *Astr. Astrophys.*, in  
press.
- Kitamura, M. and Sato, K., 1967. *Publ. astr. Soc. Japan*, 19, 575.
- Kopal, Z., 1956. *Ann. d'Astrophys.*, 19, 298.

- Kopal, Z., 1959. Close Binary Systems, Chapman and Hall, London, Ch.7.
- Kuiper, G.P., 1929. B.A.N., 5, 29.
- Kukarkin, B.V. et al., 1969. General Catalogue of Variable Stars,  
Academy of Sci. USSR, Moskow.
- Kurpinska, M. and van't Veer, F., 1970. Astr. Astrophys., 4, 253.
- Lambert, D.L. and Snell, R.L., 1975. Mon. Not. R. astr. Soc., 172, 277.
- Landolt, A.U., 1969. Astr. J., 74, 1078.
- Landolt, A.U. and Blondeau, K.L., 1972. Publ. astr. Soc. Pacific, 84,  
784.
- Lee, T.A. and Nariai, K., 1967. Astrophys. J. Letts., 149, L93.
- Levinstein, H., 1965. Appd. Optics, 4, 639.
- Longmore, A.J., 1975. Ph.D. thesis, Leicester University.
- Longmore, A.J. and Jameson, R.F., 1975. Mon. Not. R. astr. Soc., 173,  
271.
- Low, F.J., 1961. J. opt. Soc. Am., 51, 1300.
- Low, F.J. and Swamy, K.S.K., 1970. Nature, 227, 1333.
- Low, F.J., Johnson, H.L., Kleinmann, D.E., Latham, A.S. and Geisel, S.L.,  
1970. Astrophys. J., 160, 531.
- Lucy, L.B., 1968a. Astrophys. J., 151, 1123.
- Lucy, L.B., 1968b. Astrophys. J., 153, 877.
- Lucy, L.B., 1973. Astrophys. Space Sci., 22, 381.
- Meinunger, L., 1960. Mitte. über, veränderliche Sterne, 12, No. 523.
- Merrill, P.W., 1928. Astrophys. J., 67, 405.
- Milone, E.F., 1969. Non-Periodic Phenomena in Variable Stars, IAU  
Colloquium, Academic Press, Budapest, page 457.
- Milone, E.F., 1976. Astrophys. J. Suppl., 31, 93.
- Morgan, W.W., Code, A.D. and Whitford, A.E., 1955. Astrophys. J.  
Suppl., 2, 41.
- Morten, F.D. and King, R.E., 1965. Appd. Optics, 4, 659.

- Moss, D.L. and Whelan, J.A.J., 1970. *Mon. Not. R. astr. Soc.*, 149, 147.
- Mumford, G.S., 1967. *Publ. astr. Soc. Pacific*, 79, 283.
- Nayar, P.S., 1974. *Infrared Phys.* 14, 31.
- Neubauer, F.J., 1943. *Astrophys. J.*, 97, 300.
- Neubauer, F.J. and Struve, O., 1945. *Astrophys. J.*, 101, 240.
- Neugebauer, G. and Leighton, R.B., 1969. *Two-Micron Sky Survey*, NASA, SP 3047.
- Neugebauer, G., Martz, D.E. and Leighton, R.B., 1965. *Astrophys. J.*, 142, 399.
- Neugebauer, G., Becklin, E. and Hyland, A.R., 1971. *Ann. Rev. astr. Astrophys.*, 9, 67.
- Nyquist, H., 1928. *Physical Rev.*, 32, 110.
- Olson, E.C., 1977. *Astrophys. J.*, 215, 166.
- Piotrowski, S.L., Ruciński, S.M. and Semeniuk, I., 1974. *Acta. astr.* 24, 389.
- Plaut, L., 1950. *Publ. Groningen*, No. 54, 66.
- Pohl, E., 1967. *Inform. Bull. Variable Stars*, No. 209.
- Popper, D.M., 1943. *Astrophys. J.*, 97, 394.
- Priedhorsky, W.C., 1977. *Astrophys. J. Letts.*, 212, L117.
- Priedhorsky, W.C. and Krzeminski, W., 1978. *Astrophys. J.*, 219, 597.
- Purgathofer, A. and Prochazka, F., 1967. *Mitt. Univ. Sternw. Wien.*, 13, 151.
- Rahunen, T. and Vilhu, Q., 1977. *Astr. Astrophys.*, 56, 99.
- Rigtering, P.V., 1973. *Astr. Astrophys. Suppl.*, 12, 313.
- Robertson, J.A. and Eggleton, P.P., 1977. *Mon. Not. R. astr. Soc.*, 179, 359.
- Robinson, E.L., 1976. *Ann. Rev. astr. Astrophys.*, 14, 119.
- Roman, N.G., 1956. *Astrophys. J.*, 123, 246.
- Sahade, J., 1969. *Mass Loss From Stars*, D. Reidel Publ. Dordrecht.

Sánchez Magro, C., Needham, J.D., Phillips, J.P. and Selby, M.J., 1977.

Mon. Not. R. astr. Soc., 180, 461.

Schilt, J., 1926. Astrophys. J., 64, 215.

Shapley, H., 1915. Contr. Princeton Univ. Obs., No. 3.

Smith, R.A., Jones, F.E., and Chasmar, R.P., 1957. The detection and  
Measurement of Infrared Radiation, Clarendon Press, Oxford,  
Ch. V.

Smyth, M.J., Dow, M.J. and Napier, W. Mcd., 1975. Mon. Not. R. astr.  
Soc., 172, 235.

Spinrad, H. and Wing, R.F., 1969. Ann. Rev. astr. Astrophys., 7, 249.

Stein, W.A., Gaustad, J.E., Gillett, F.C. and Knacke, R.F., 1969.

Astrophys. J. Letts., 155, L3.

Stockman, H.S., Schmidt, G.D., Angel, J.R.P., Liebert, J., Tapia, S.  
and Beaver, E.A., 1977. Astrophys. J., 217, 815.

Strand, K. Aa., 1937. Ann. Stw. Leiden, 18, 98.

Struve, O., 1944. Astr. J., 51, 3.

Struve, O., 1949. Astrophys. J., 109, 436.

Struve, O., Horak, H.G., Canavaggia, R., Kourganoff, V. and Colacevich,  
A., 1950. Astrophys. J., 111, 658.

Swings, J.P., 1973. Astr. Astrophys., 26, 443.

Swings, J.P. and Allen, D.A., 1971. Astrophys. J. Letts., 167, L41.

Szkody, P. and Brownlee, D.E., 1977. Astrophys. J. Letts., 212, L113.

Tapia, S., 1976. IAU Circ. No. 2987.

Tapia, S., 1977. Astrophys. J. Letts., 212, L125.

van't Veer, P., 1972. Astr. Astrophys., 20, 131.

Wilcken, S.K., McNamara, D.H. and Hansen, H.K., 1976. Publ. astr. Soc.  
Pacific, 88, 262.

Wildey, R.L. and Murray, B.C., 1964. Astrophys. J., 139, 435.

Williams, P.M., Beattie, D.H. and Stewart, J.M., 1977. Observatory,

97, 76.

Wilson, R.E. and Devinney, E.J., 1971. *Astrophys. J.*, 166, 605.

Wilson, W.J. and Barrett, A.H., 1968. *Science*, 161, 778.

Wilson, W.J., Barrett, A.H. and Moran, J.M., 1970. *Astrophys. J.*, 160,  
545.

Wing, R.F., Spinrad, H. and Kuhl, L.V., 1967. *Astrophys. J.*, 147, 117.

Wolf, N.J., 1973. *Astrophys. J.*, 185, 229.

Wolf, N.J. and Ney, E.P., 1969. *Astrophys. J. Letts.*, 155, L181.

Wolf, N.J., Stein, W.A. and Strittmatter, P.A., 1970. *Astr. Astrophys.*,  
9, 252.

Wyse, A.B., 1934. *Lick Obs. Bull.*, 17, 37.

Zwerdling, S., Smith, R.A. and Theriault, J.P., 1968. *Infrared Phys.*,  
8, 271.



INFRARED PHOTOMETRY OF ECLIPSING BINARY STARS

R. AKINCI

A B S T R A C T

The infrared observations of several eclipsing binary stars are presented and discussed. Initially a brief review of the relevant literature is given together with a description of binary systems, in particular eclipsing binary stars. This is followed by an outline of the instrumentation and techniques used in making infrared observations of these systems.

1.2 and 2.2  $\mu\text{m}$  observations of AB And and SW Lac, together with 2.2  $\mu\text{m}$  observations of 44 i Boo are presented. These stars are all of the W Uma-type. The infrared light curves show a number of features not found optically and these features are discussed. All three systems appear to be very red for their spectral types.

Observations are given of the cataclysmic variable AM Her at 1.2 and 2.2  $\mu\text{m}$ . The 1.2  $\mu\text{m}$  light curve is very similar to the optical light curves. However, the 2.2  $\mu\text{m}$  light curve shows only a secondary eclipse, in this respect it is similar to the X-ray light curve. The system has a J - K colour of +0.60 at maximum light. These facts indicate that at 2.2  $\mu\text{m}$  the system is emitting strong cyclotron radiation from near the white dwarf component.

Finally, 1.2, 2.2 and 3.6  $\mu\text{m}$  light curves of the Algol-type eclipsing binary RZ Sct are presented. The infrared excess found is attributed to a gas stream and disk around the primary component of the system. The electron density in both the stream and the disk is  $\sim 10^{12} \text{ cm}^{-3}$ .